VISCOUS EFFECTS ON PERIPHERAL JET FLUID SUSPENSIONS

by

YUCEL ERCAN

M.S., Dept. of M.E., June 1968

VISCOUS EFFECTS ON PERIPHERAL JET FLUID SUSPENSIONS

by

YUCEL ERCAN

S.B., Massachusetts Institute of Technology
(1966)

SUBMITTED IN PARTIAL FULFILLMENT

OF THE REQUIREMENTS FOR THE

DEGREE OF MASTER OF

SCIENCE

at the

MASSACHUSETTS INSTITUTE OF

TECHNOLOGY

June, 1968

Signature of Author ..... Yucel Ercan .....
Department of Mechanical Engineering, May 6, 1968

Certified by ..... Herbert H. Richardson .....
Thesis Supervisor

Accepted by .....
Chairman, Departmental Committee on Graduate Students

ABSTRACT

VISCOUS EFFECTS ON
PERIPHERAL JET FLUID SUSPENSIONS

by

YUCEL ERCAN

Submitted to the Department of Mechanical Engineering on May 6, 1968 in partial fulfillment of the requirements for the Degree of Master of Science.

A viscous analysis which is capable of predicting the static and quasi-static behavior of peripheral jets is performed. The theory accounts for the large differences between data and the previous inviscid theories by the effects of entrainment and turbulent mixing. It predicts the equilibrium behavior within 3 - 4% (while the best of the inviscid theories, Barratt Theory, has errors up to 40%). Solutions of the unbalanced jet which the viscous theory yields give continuous curves around the equilibrium point. This makes the prediction of the dynamic behavior of the peripheral jet fluid suspensions possible. The calculated sensitivities for Reynolds number of 2×10^4 predict the data within 8% (the Barratt Theory on the other hand gives errors up to 100%). The use of the theory is simplified by the computer programs presented in the appendices and solutions for various Reynolds numbers can be obtained easily by use of these programs.

Thesis Adviser: Herbert H. Richardson

Title: Professor of Mechanical Engineering

ACKNOWLEDGEMENTS

The author would like to express his appreciation to Professor Herbert H. Richardson for his guidance and encouragement for without his help this work would have been impossible.

The author is also grateful to William A. Ribich for his assistance during every phase of this thesis.

The thesis was supported in part by the Department of Transportation, Office of High Speed Ground Transport under contract C-85-65 and sponsored by the Division of Sponsored Research of M.I.T.

TABLE OF CONTENTS

LIST OF FIGURES

NOMENCLATURE

a_c	Dimensionless cushion flow-cushion pressure sensitivity
a_s	Dimensionless cushion flow-supply pressure sensitivity
f	Dimensionless mass flow
f'	Dimensionless velocity
h	Nozzle height
$\bar{h}$	$(h/t)/(1 + \sin \theta)$
k,l	Scaling factors
m	Mass flux
M	Momentum flux
p	Pressure
Q	Volume flux
Re_w	Wall jet Reynolds number
Re_j	Jet exit Reynolds number
t	Nozzle thickness
t'	Downstream jet thickness for inviscid flow
T	Temperature
v, V	Velocity
x	Distance along the wall
y	Distance from the wall
z	Distance across the nozzle
α	Fractional cushion flow, m_c/m_a
ρ	Density

η	Dimensionless distance from wall
β	Wall jet Reynolds number parameter
δ_t	Wall jet thickness
η_t	Dimensionless wall jet thickness
ν	Kinematic viscosity
θ	Nozzle angle
λ	A parameter for inviscid flow defined by $\lambda = \sqrt{1-p_{cg}/p_{sg}}$
ξ	A parameter for viscous flow defined by $\xi = \sqrt{1-p_{cg}/p_{sg}}$

Subscripts

c	Cushion
a	Atmosphere (except that m_a means nozzle flow)
s	Fluid source
g	Gage pressure
m	Maximum value
$\beta=g$	Value of a term when the parameter $\beta=g$

I. INTRODUCTION

Fluid suspensions, especially those which use air as working fluid, have certain merits when compared with mechanical suspensions at high speeds. With a fluid suspension system the weight of the vehicle can be supported over large areas on the guideway. This eliminates the concentrated loads minimizing wear and deformations on the guideway. Unsprung mass can be made almost negligible and this gives a soft coupling between the vehicle and road. As a result, a vehicle which is equipped with fluid suspensions can operate on rougher guideways than if it were using mechanical suspensions and still give the same or lower levels of accelerations as mechanically suspended vehicles. At high speeds catastrophic failures of mechanical suspensions may be hazardeous. Such a failure can take place at bearings, at a shaft or at some other part where stress concentrations exist. The use of fluid suspensions minimizes the chances of such unfortunate incidents which may result in loss of lives and money.

There are several types of fluid suspensions. In these systems lift is maintained by viscous effects as in the case of air bearings or momentum effects of a fluid stream or by quasistatic pressure of the fluid pumped beneath the vehicle as in plenums or peripheral jets. The fluid suspensions which are used today in transport vehicles are of the latter two types with some additional features such as flexible skirts, etc. For relatively large ground-to-cushion clearances the peripheral jet requires less power for maintaining a static hovering

height than the plenum; because of this reason most of the past research on fluid suspensions has dealt with peripheral jets.

A peripheral jet fluid suspension is basically an annular jet directed towards a flat plate; i.e. the ground beneath the vehicle. When the jet is initially started, it impinges on the plate, and fluid flows into the so-called cushion area beneath the suspension, increasing the pressure in the cushion area until the jet is forced to bend outward. Once steady flow conditions are maintained, the jet acts as a "jet curtain" and confines the static pressure in the large cushion area. The pressure within this area supports the vehicle and the lift obtained is many times the lift due to the jet reaction itself. This shows that a peripheral jet suspension is a device which employs "ground effect" to magnify jet momentum effects.

A diagram of a peripheral jet suspension, with the important system parameters shown, is presented in Figure 1. After the flow conditions assume steady-state, the vehicle is supported at an equilibrium height above the ground and there is no net flow into or out of the cushion. This equilibrium case is referred to in the peripheral jet literature as the "balanced jet". If the vehicle height from the ground is somehow disturbed, the flow patterns also change. When the vehicle moves up from its equilibrium height, the cushion volume increases and some net flow takes place into the cushion. The net flow into or out of the cushion is called "cushion flow" and the case in which the cushion flow is into the cushion is called the "overfed jet". In an overfed jet the annular jet splits into two

portions one of which supplies the net flow into the cushion (Figure 2a).

If the vehicle moves down from its equilibrium height while operating under the steady-state balanced condition some net flow out of the cushion occurs (Figure 2b). A peripheral jet operating under these conditions is called an "underfed jet". The overfed and underfed jets are both called "unbalanced jets". The pressure-flow and displacement-flow sensitivities of unbalanced jets are used to determine the dynamic behavior of the suspension system as explained by Richardson and Ribich (1)*.

During recent years several theories were proposed by various authors to predict the performance of a peripheral jet type fluid suspension system. Almost all of the present theories assume inviscid and incompressible flow conditions. Strand (2) developed an exact theory for the two-dimensional incompressible, inviscid irrotational flow based on potential flow theory. The Stanton-Jones Theory (3), commonly called the exponential theory, considers a differential element on the two dimensional cross section of a constant curvature jet, then equates the pressures to the centrifugal force per unit area and integrates over the jet thickness to obtain an expression for the cushion pressure as a function of the h/t ratio and angle θ. The Velocity Distribution Theory**assumes a potential vortex at the

---

* Numbers refer to the list of references at the end of the thesis.

** Presented later in this thesis.

nozzle exit and uniform flow along the ground and then applies the momentum balance equation for a control volume ABCD (Figure 1) which includes the cushion and the part of the jet before it becomes parallel to the ground. The Barratt Theory (4) considers the adjacent streamlines down-stream of the jet exit to have a common center of curvature (the curvature need not be constant along the jet). It takes the total head to be constant across the jet thickness and assumes that the magnitude of the total momentum of the jet after it is deflected is equal to the jet momentum just down-stream of the jet. The total jet momentum is calculated by using these assumptions. Then the momentum balance in the horizontal direction applied to the control volume of Figure 1 yields an expression for the cushion pressure in terms of h/t ratio. The Thin Jet Theory (5) which was proposed by Chaplin assumes a thin and non-mixing jet of circular arc cross section of radius $h/(1+\sin\theta)$ where h is the height of the nozzle from the ground. Then the cushion pressure is determined by balancing the static pressure to the centrifugal force density. These theories are plotted in Figure 3 which shows the cushion pressures as a function of h/t for a balanced jet.

An experimental program for the investigation of the pressure-flow-displacement characteristics of peripheral jet fluid suspensions has been carried cut over the last three years at M.I.T. The data which has been obtained by using the "2-D Fluid Suspension Test Apparatus" (Figure 4) is adequate to describe the performance

characteristics of a peripheral jet suspension for different nozzle thicknesses and heights at different Reynold's numbers. (See Figures 10 through 17.) The dimensional analysis performed by Richardson and Ribich (6) shows that the dynamic similarity for a constant geometry suspension (h/t fixed) is maintained if dimensionless pressures and flows are used and the product $p_a \cdot t$ is kept constant, where p_a is the ambient pressure and t the characteristic dimension (taken to be nozzle thickness) of the suspension. It is also shown by Richardson and Ribich that the dynamic similarity can also be maintained if the jet exit Mach and Reynolds numbers of a fixed geometry system are kept constant. Therefore, the data taken and published by M.I.T (7) is shown in terms of these dimensionless parameters (Figure 10 through 17.) The interpolation of these data curves would yield curves of Pcg/Psg vs h/t. This is done for jet thickness Reynolds number, $Re_j = 2 \times 10^3$ and 4.1×10^4 in Figure 5. The data at a specific Reynolds number for the cases $p_a \cdot t \geq .2$ atm-in practically fall on the same curve. For the case when $p_a \cdot t = .1$ atm-in, the data is somewhat lower than the rest probably due to some effects such as nozzle losses which become pronounced when the jet thickness is small; therefore, this degenerate case will be neglected in comparing the data with the theories.

The comparison of data with the inviscid theories shows that these theories overestimate equilibrium cushion pressures from 40% at high h/t ratios and low Reynolds numbers to 5% at low h/t ratios and high Reynolds numbers (Figure 5). Increasing Reynolds number shifts the curve upward and makes it closer to the inviscid theories, but this shift is never enough to bring the data on the curves which represent the inviscid theories.

The theories of unbalanced jets make the assumption that the problem can be treated quasistatically. The known theories, however, are inadequate for predicting the pressure flow and displacement flow sensitivities around the equilibrium point (balanced jet) which are needed to determine the dynamic behavior of the suspension. The Barratt Theory for an unbalanced jet is shown in Figure 6. It predicts a discontinuity in slope of the curves of cushion pressure vs. cushion flow m_c at the equilibrium point ($m_c = 0$) whereas the experiments show that the sensitivities around the zero cushion flow line are continuous as shown in the same figure. The same problem is also encountered in the other inviscid theories. The results of inviscid Velocity Distribution Theory are also shown in the same figure. This critical deficiency in the inviscid unbalanced jet solutions makes them of limited value in predicting the dynamic behavior of the system.

The purpose of this thesis is to develop a new theory which will yield more accurate results in predicting equilibrium and non-equilibrium behavior of peripheral jet suspensions. The large differences between the data and the inviscid theories will be explained by the viscous interactions which take place between the jet and the surrounding fluid

medium. The flow patterns observed by Ben-Chie Yen (8) are similar to that of diffusing jets. Although there are standing vortices under the nozzle on both sides of the jet, they are weak enough not to contribute anything significant to the cushion pressure. The fact that the effect of the standing vortices is unimportant compared with the effects of the jet mixing is also proved by Hsu (9). As a result in the following analysis the effect of the standing vortices will be neglected and only the entrainment effects will be considered. As the jet emerges from the nozzle the high velocity gradients at the boundaries of the jet cause high shear forces in the fluid. As a result turbulence is generated in the flow and the eddies which are formed at the boundaries result in lateral mixing. The fluid within the jet is decelerated and the fluid in the surrounding region is accelerated or entrained. The diffusion process which takes place here is similar to the process which takes place in a submerged jet as described by Albertson et. al (10). When the jet hits the ground and becomes horizontal a 1/7th velocity profile prevails along the wall while the entrainment of stationary fluid from the surroundings continue along the other boundary of the jet. In the subsequent sections of this thesis the velocity profile along the wall will be described by using the fully developed wall jet velocity profile described by Glauert (11) along with some considerations derived from the diffusion of jets in unbounded space as described by Albertson.

To obtain a better understanding of the jet-interaction phenomenon a water table was set up to simulate a peripheral jet suspension. The experiments conducted by using this table consisted of measuring velocity profiles across the nozzle and the wall jet at various Reynolds numbers.

These results are presented in Chapter 2 in greater detail. Figure 7 shows some of the pictures taken from the water table for the purpose of flow visualization. The generation of eddies and lateral mixing along the boundaries of the jet are seen very clearly from these pictures. The velocity profiles were measured by following the ends of dye streaks for low Reynolds numbers or small plastic beads for high Reynolds numbers. The forms of the velocity profiles (Figure 8 and 9) obtained from these experiments are similar in shape to those obtained by Ben-Chie Yen. They will be used for comparison with the theoretically derived velocity profiles in the subsequent sections.

2. EXPERIMENTAL STUDIES

In this chapter the experimental results which were obtained from the broad study of fluid suspensions conducted at M.I.T. will be reviewed. These results can be considered in two main groups. The first one of these consists of the data which were taken over the last three years from the 2-D Fluid Suspension Test Apparatus. Most of the data have already been published by M.I.T. (7). The results in the second group were obtained from the experiments which were done by using a water table especially set up to visualize the flow patterns in peripheral jets and to demonstrate the validity of some of the assumptions of the viscous analysis which will be presented in the next chapter.

2.1. 2-D Fluid Suspension Test Apparatus

In order to determine the behavior of a full size vehicle

suspension from the data obtained by using a smaller model, dynamic similarity parameters must be determined and dynamically similar experiments conducted. The dimensionless analysis of peripheral jets performed by Richardson and Ribich (6) shows that dimensionless cushion pressure is a function of the jet exit Mach number, Reynolds number and geometry or,

$$\frac{P_c}{P_a} = f\,(M_e,\ Rey_e,\ \text{geometry})$$

and the geometric scaling is provided if the product $p_a \cdot t$ is kept constant.

The 2-D Fluid Suspension Test Apparatus was designed and developed to test the dynamic similarity conditions and to investigate the equilibrium and non-equilibrium pressure-displacement-flow characteristics of fluid suspensions. The design and instrumentation of the apparatus is explained thoroughly in the the report by Richardson and Ribich (6). A diagram of the device is shown in Figure 4.

The jet width in the apparatus can be adjusted by using different size spacers. The cushion volume can be changed by modifying the height of the base plate and the hovering height h of the nozzle can be set by placing auxiliary plates on the ground board. The non-equilibrium conditions may be tested by introducing or removing fluid from the cushion region through the cushion orifices. The jet exhaust region can be pressurized or subjected to vacuum so that a wide range of ambient pressures can be maintained.

The device can be used to obtain both quantitative results and qualitative flow visualization pictures by introducing smoke into the flow. The pressure taps on the base plate are connected to U-manometers and give the pressure distribution in the cushion. There are also probes to measure the upstream pressure and the ambient pressure. The mass flows through the nozzle as well as through the cushion orifices are measured by using orifice plates.

The results are presented in Figures 10 through 17 for equilibrium and non-equilibrium cases at one, two and five atmospheres ambient pressures for jet thicknesses .1 and .2 inches. As one can see from the figures, the tests cover a wide range of Reynolds numbers. The data are shown along with the Barratt Theory which gives the closest prediction among the inviscid theories. Figures show that the equilibrium performance is overestimated by the best of the inviscid theories by 5% to 40% depending on the Reynolds number and the ratio h/t.

Some of the runs for non-equilibrium cases are shown in Figure 6. The data curves of pressure ratio vs. cushion flow in these figures do not show the discontinuity of slope at the equilibrium point as predicted by the inviscid theories. The slopes of pressure-flow curves for underfed jet are predicted quite closely although the data curves are shifted with respect to the inviscid theory.

2.2. Water Table Experiments

Now we turn our attention to the water table experiments. The main purpose of these experiments were to set up a large model of a

peripheral jet on a plexiglas, horizontal, closed water table and observe the flow patterns and the entrainment effects more clearly and if possible obtain some quantitative results. The top view of the table which was used for the tests is shown in Figure 18. The water was supplied to the nozzle from a reservoir as shown on the left hand side of the figure. Before the water was introduced to the nozzle it was strained by a layer of glass fibers which prevented the small air bubbles to enter the test section. The tube bundles which are placed right upstream of the nozzle served two purposes. They prevented the secondary vortex which is caused by the turning of the flow between sections A and B before the nozzle. They also kept the flow entering the nozzle laminar at relatively low Reynolds numbers at which a dye* was injected into the fluid to visualize the flow pattern. The nozzle thickness was set to 1.0 inches during the experiments and the ratio h/t was changed by placing additional plates on the ground plate. The unbalanced jet flow patterns were achieved by introducing fluid into the cushion through C or removing fluid through D. The mass flow per unit time was measured by using a bucket-scale placed at the far down-stream of the flow and the Reynolds number was based on the average mass flow per unit time.

The water table experiments can be examined in two groups. The first consists of the experiments which were conducted for the purpose of visualizing the flow patterns. Visualization was achieved by injecting basic phenolphthalein solution into the flow. At relatively

---

* Basic solution of phenolphthalein.

low Reynolds numbers this dye gave excellent results. Some of the pictures taken at Reynolds numbers of 1200 and 500 are shown in Figure 7a and 7b. At high Reynolds numbers, however, the dye diffused into the water very fast. The flow pattern was not so clear but the pictures still showed the boundaries of the jet.

The second set of water table experiments was conducted for the purpose of determining the velocity profiles across the jet at the nozzle exit and at a section after it impinges on the ground plate and becomes horizontal. At relatively low Reynolds numbers the velocities were measured by taking successive pictures of the flow with a movie camera and then by following the ends of the dye streaks and irregularities on the dye lines on these pictures. The profiles for the h/t ratios of 4.0 and 5.0 at Reynolds numbers of the order of 2×10^3 are shown in Figure 8. At high Reynolds numbers the dye diffused very fast; therefore, pellets made out of a plastic* whose density is very close to the density of water was used. The pellets were followed in succesively taken pictures to determine the velocities. The results of this experiment showed a wide range of scattering probably due to the unsteadiness which results from the highly turbulent flow or from the irregularity of the shapes of the pellets. The results are shown in Figure 9 along with the calculated wall jet profile which will be developed in chapter 3. The calculated wall jet profiles are also shown in Figures 8a and 8b.

---

* A product called Cycolac by Morbon Chemical Co. in Washington, West Virginia.

The immediate and important conclusion from the water table experiments is that the viscous effects play an important role; there are clear indications of entrainment and turbulent mixing along the boundaries of the jet. The formations of eddies at the boundaries are recognizable from the dye patterns. These results show that the momentum dissipation due to turbulent mixing has to be accounted for in the theories which predict the suspension behavior. This we will do in the following chapters.

It was also observed during the water table experiments that the standing vortices are very weak and carry negligible momentum when compared with the momentum carried by the main jet itself.

3. VISCOUS THEORY FOR BALANCED PERIPHERAL JET

In this thesis the technique which will be used to find a solution to the problem will be quite straightforward. The general method of approach will simply be the application of an x-direction momentum balance applied to the control volume ABCD of Figure 1, and most of our efforts will be given to the evaluation of the forces on the control volume and the momentum fluxes which pass through the control surface.

Now let us consider the control volume ABCD in Figure 1. In general, the cushion pressure can be expressed by balancing momentum fluxes in and out of the control volume with the forces on the boundary. The x-direction momentum balance gives

$$h \cdot p_c - h \cdot p_a - \tau = M_I \sin\theta + M_{II} \qquad (1)$$

where M_I and M_{II} are the momentum fluxes across the boundary at the sections I and II respectively and τ is the total shear force on the control surface. However, the shear force on the control surface is small compared to the pressure forces as demonstrated in Appendix I; therefore, it can be neglected. As a result, the momentum equation takes the form

$$h(p_a - p_c) = M_I \sin\theta + M_{II} \tag{2}$$

From here on our efforts will be directed toward the evaluation of the momentum fluxes M_I and M_{II}. The approach to the problem is similar to the inviscid velocity distribution theory which is presented in the following section for the purpose of clarifying the method of approach to the problem; moreover, some of the results from this inviscid theory will be used in the subsequent sections.

3.1. Inviscid Velocity Distribution Theory

Consider the peripheral jet model as depicted in Figure 19 and consider the control surface ABCD.

Assume the following conditions:

a) Flow leaving the nozzle is irrotational

b) Flow is incompressible

c) Pressure and velocity along the free streamlines are constant

d) Velocity across the exit jet is uniform

e) Shear forces are neglected.

The velocity profile at the nozzle exit can be found by using the irrotationality condition. For a potential vortex

$$v(z)\ (z + a) = v_o a \qquad \text{or} \qquad v(z) = \frac{av_o}{z + a} \tag{3}$$

where "a" is a constant yet to be determined. But the boundary conditions along the outer and inner streamlines give

$$v(o) = v_o = \sqrt{\frac{2(p_s - p_a)}{\rho}} \tag{4a}$$

and $$v(t) = v_1 = \sqrt{\frac{2(p_s - p_c)}{\rho}} \tag{4b}$$

If these conditions are substituted into expression for velocity, the constant "a" can be shown to be

$$a = \frac{\lambda t}{t + \lambda} \tag{5}$$

where

$$\lambda = \sqrt{1 - \frac{p_c - p_a}{p_s - p_a}} = \sqrt{1 - \frac{p_{cg}}{p_{sg}}} \tag{6}$$

Now the following quantities can be calculated directly:

$$m_I = \rho \int_o^t v(z)\, dz = \rho a v_o \ln\left(\frac{t+a}{a}\right) = \rho v_o \frac{\lambda t}{1-\lambda} \ln\left(\frac{1}{\lambda}\right) \tag{7}$$

and

$$M_I = \rho \int_o^t [v(z)]^2\, dz = \rho v_o^2 \frac{at}{t+a} = \rho v_o^2\, t\lambda \tag{8}$$

where m_I is the mass flux and M_I is the momentum flux across Section I.

Now the thickness t' of the exit jet can be determined by using the continuity relation $m_I = m_{II}$,

$$m_I = \rho v_o \frac{\lambda t}{1-\lambda} \ln\left(\frac{1}{\lambda}\right) = m_{II} = \rho v_o t'$$

$$\text{or} \quad t' = \frac{\lambda t}{1-\lambda} \ln\left(\frac{1}{\lambda}\right) \tag{9}$$

The momentum flux across section II is then,

$$M_{II} = \rho v_o^2 t' = \rho v_o^2 \frac{\lambda t}{1-\lambda} \ln\left(\frac{1}{\lambda}\right) \tag{10}$$

Now substituting M_I and M_{II} into the momentum equation

$$h\, p_{cg} = \rho v_o^2\, t\, \lambda \sin\theta + \rho v_o^2 \frac{\lambda t}{1-\lambda} \ln\left(\frac{1}{\lambda}\right) \tag{11}$$

but $\rho v_o^2 = 2\, p_{sg}$ and $\frac{p_{cg}}{p_{sg}} = 1 - \lambda^2$; therefore,

$$\frac{h}{t}(1-\lambda^2) - 2\lambda \sin\theta - \frac{2\lambda}{1-\lambda} \ln\left(\frac{1}{\lambda}\right) = 0 \tag{12}$$

from which λ or $\frac{p_{cg}}{p_{sg}} = 1 - \lambda^2$ can be solved for given values of h/t and θ.

The solution is plotted in Figure 20 in terms of h/t and p_{cg}/p_{sg} for θ's of 0^o, 30^o, 45^o and 60^o. The computer program No. 1 in Appendix III gives the solutions for balanced and unbalanced cases of the velocity distribution theory. Results for the unbalanced cases are presented in Figure 38.

3.2. Viscous Theory

3.2-1 Incoming Momentum Flux

Here the assumption will be made that the viscous losses in the nozzle are negligible and the flow is irrotational; therefore, the velocity profile is of the same form as described in the inviscid theory. However, the boundary condition along the innermost streamline is now replaced by $v_1 = \sqrt{\frac{2(p_s - p_c)}{\rho}}$ where p_c is the cushion pressure for the viscous model. Then the mass and momentum fluxes across the nozzle are given by

$$m_1 = \rho\, v_o \frac{\xi\, t}{1-\xi} \ln\left(\frac{1}{\xi}\right) \tag{13}$$

and

$$M_I = \rho\, v_o^2\, t\, \xi \tag{14}$$

where

$$\xi = \sqrt{1 - \frac{p_{cg}}{p_{sg}}} \tag{15}$$

3.2-2 Submerged Jets in Unbounded Space

Earlier in the thesis, the water table experiments indicated that turbulence is created along the boundaries of the peripheral jet and the mixing zone diffuses into the core of the jet and into the surrounding medium. It was also suggested that the basic mechanism which causes the cushion pressure to deviate from the theoretically predicted values is the mixing process. The same kind of turbulent mixing process takes place in a submerged jet in a much simpler

fashion since the jet is straight in the later case. Therefore, review of some of the results obtained from the theories of the submerged jets* would be useful since they are used in the calculation to define the velocity profile across the exit jet.

When a jet emerges from an opening into a stationary fluid medium, the eddies generated in the region of discontinuity between the jet and the surrounding medium will result in lateral mixing. A submerged jet can be investigated in two regions as shown in Figure 21. The first region starts from the nozzle and ends at the point where the turbulent mixing zone penetrates the centerline of the jet. It is called the zone of flow establishment. The zone of flow establishment ends at a distance $x_o = 5.2\ t$ from the nozzle where t is the nozzle width. Once the entire central part of the jet becomes turbulent then the diffusion continues without changing its character. This second region is called the zone of established flow. In this region, the flow is dynamically similar and the velocity profile is described by the Gaussian distribution function $\frac{v_x}{v_{max}} = \exp\left(-\frac{y^2}{\sigma^2}\right)$ where the constant σ can be determined empirically.

In the zone of flow establishment

$$\frac{v_x}{v_1} = \exp\left(-\frac{(y+\sqrt{\pi}\, C_o \frac{x}{2} - \frac{t}{2})^2}{2(C_o x)^2}\right) \qquad (16)$$

---

* See reference (10) for a detailed analysis of submerged jets.

$$\frac{v_{max}}{v_1} = 1.0 \tag{17}$$

and

$$\frac{Q}{Q_1} = 1 + \sqrt{\pi}\ (\sqrt{2} - 1)\ C_o \frac{x}{t} \tag{18}$$

where the subscript "1" denotes the conditions right at the exit of the nozzle and C_o is an empirically determined constant equal to 0.109.*

In the zone of established flow

$$\frac{v_{max}}{v_1} = \sqrt{\frac{1}{\sqrt{\pi}\ C_o}\ \frac{t}{x}} \tag{19}$$

$$\frac{v_{max}}{v_1} = \sqrt{\frac{1}{\sqrt{\pi}\ C_o}\ \frac{t}{x}}\ \exp\left(-\frac{1}{2(C_o)^2}\ \frac{y^2}{x^2}\right) \tag{20}$$

and

$$\frac{Q}{Q_1} = \sqrt{2\sqrt{\pi}\ C_o \frac{x}{t}}$$

Notice that these results are independent of Reynolds number. The above equations will be used to calculate the magnitude of the maximum velocity and the total mass flux in the exit jet.

3.2-3 Semicontained Jet

When the peripheral jet hits the ground plate it spreads over it. In a balanced jet the flow is directed into one direction after it impinges on the ground and the surrounding medium is of the same fluid as the fluid coming through the nozzle. Such a jet is described as a

---

* See reference (10).

semi-contained jet or simply a wall jet. After the wall jet flows along the wall for a certain distance, the flow becomes fully developed and dynamically similar. A numerical solution can be found for a fully developed wall jet even though it is quite cumbersome. The procedure was first proposed by Glauert (11). In reference (11) a more detailed analysis of the problem is given. Here we simply lay out the procedure.

The boundary layer equations for turbulent flow are

$$u \frac{\partial u}{\partial x} + v \frac{\partial u}{\partial y} = \frac{\partial}{\partial y} \left(\varepsilon \frac{\partial u}{\partial y} \right) \tag{21}$$

$$\frac{\partial (xu)}{\partial x} + \frac{\partial (xv)}{\partial y} = 0 \tag{22}$$

with the boundary conditions $u = v = 0$ at $y = 0$ and $u \to 0$ as $y \to \infty$; another boundary condition arises from the assumption that near the wall the dimensionless velocity profile changes as the 1/7th power of the distance. This last condition will be expressed more clearly once the above equations are nondimensionalized. In the above equations x-distance is measured along the wall and y-distance is measured perpendicularly from the wall with u and v the respective velocity components in these directions; ε is the eddy viscosity.

The wall jet can be analyzed in two portions. The first is the inner layer which is between the wall and the point of maximum velocity. In this region, the effect of the wall on the flow is dominant.

Therefore, it has the 1/7th profile of a turbulent boundary layer which implies that the eddy viscosity is proportional to $y^{6/7}$ and $Re^{3/4}$. The second region is the outer layer which starts at the point of maximum velocity. The eddy viscosity in this region will be assumed to vary in the same way as in a free turbulent boundary layer flow and it will be taken to be a constant which is proportional to the Reynold's number.* Since in the inner portion $\varepsilon \alpha Re^{3/4}$ and in the outer section $\varepsilon \alpha Re$, a complete similarity is no longer possible. However, ε is taken proportional to $Re^{3/4}$ rather than to R also in the outer layer for the sake of a dynamically similar solution.

It can be shown that the boundary layer equations for the inner and the outer layers can be written as follows in terms of the dimensionless quantities η and f_1'. Here η is the dimensionless distance from the wall and f_1' is the dimensionless velocity function. For the inner layer

$$\frac{d}{d\eta}\left(A\, f_1'^{6}\, f_1''\right) + f_1\, f_1'' + \beta\, f_1'^{2} = 0 \qquad (23)$$

or writing $f_1(\eta) = A^{-1/5}\, X^{7}\, f_2\,(X^{-5}\,\eta)$ we get

$$\frac{d}{d\eta}\left(f_2'^{6}\, f_2''\right) + f_2 f_2'' + \beta\, f_2'^{2} = 0 \qquad (24)$$

---

*See the section on Prandtl's hypothesis in Glauert (11).

For the outer layer

$$f_o''' + f_o f_o'' + \beta f_o'^2 = 0 \tag{25}$$

The boundary conditions are $f_1' \eta^{-1/7} \rightarrow$ constant as $\eta \rightarrow 0$ and $f_o'(\infty) = 0$. β is a parameter which is determined by Reynolds number* as shown in Table I. The conditions to be satisfied at the junction between the inner and the outer layers also impose some restrictions. Here the interface is taken to be at the velocity maximum; therefore, at this point

$$f_o'' = f_1'' = f_2'' = 0;\ f_o = f_1 = A^{-1/5} X^7 f_2;\ f_o' = f_1' = A^{-1/5} X^2 f_2' \tag{26}$$

If the solutions for f_2 and f_o are known A and X can be found. The solutions for f_2 and f_o are given by the following expressions. For the inner layer

$$\gamma = \int_o^g \frac{dy}{(1-g^{9/7})^{1/7}} \tag{27}$$

where $g(\gamma) = f_2^{7/8}$ and $\gamma = \frac{7}{8}\left(\frac{56}{9}\right)^{1/7} \eta$. The solution for the outer layer for large values of η is determined by a series expansion of the form

$$f_o(\eta) = 1 + a_1 e^{-\eta} + \sum_{k=2}^{k=\infty} \left[\frac{1}{k^2(k-1)} \sum_{i=1}^{i=k-1} a_i a_{k-i} (k-i)[(k-i)+i\beta]] \right] e^{-k\eta} \tag{28}$$

where $a_1 = -1$. Taking the coefficient a_i of $e^{-\eta}$ is equivalent

*The Reynolds number here is determined with respect to the thickness of the wall jet. The distance between the point of maximum velocity and the point where velocity is half the maximum velocity is taken as a measure of the thickness.

TABLE 1

β	Re
1.0	∞
1.1	1.4×10^6
1.2	4.1×10^4
1.3	5200
1.4	1200
1.5	380
1.6	150
1.8	33
2.0	10

to making a suitable choice of zero of η. The above solution also assumes arbitrarily that $f_o(\infty) = 1.0$ which is the dimensionless mass flow. A computer program which calculates f_o and its derivatives for large values of η is given in Appendix 2.

From the series solution, f_o and its derivatives can be calculated at a suitably large value of η, then the solution can be extended to smaller values of η by numerical integration of the differential equation (25). Then the values of $f_o = f_{om}$, $f'_o = f'_{om}$ and the dimensionless jet thickness η_t can be found at the point when $f''_{om} = 0$. Here η_t is defined as the interval between the point where the velocity is maximum and the point where $f'_o = \frac{1}{2} f'_{om}$.

Another computer program in Appendix 2 calculates the inner and the outer layers for a certain value of β, then matches them at the maximum velocity point and prints out η, total mass flux, total momentum flux and some other useful quantities.

The special cases for $\beta = 1.0$ and $\beta = 2.0$ can be solved in closed forms. For the case $\beta = 1.0$

$$f_o(\eta) = \tanh \frac{\eta}{2} \tag{29}$$

which gives $f'_{om} = .5$ and $\int_o^\infty [f'_o(\eta)]^2 \, d\eta = .333$

The solution for $\beta = 2.0$ is

$$\eta = \ln \frac{\sqrt{(1+g+g^2)}}{1-g} + \sqrt{3} \tan^{-1} \frac{\sqrt{3}\, g}{2+g} \tag{30}$$

where $f_o = g^2$.

The results of the closed form solution are used for the case when $\beta = 1.0$ to avoid the numerical error which might be introduced into the solution of the program No.2 of Appendix 2. Figure 22 shows the final result as a function of β. Figure 22 along with Table 1 describes the important parameters of a dimensionless wall jet velocity profile at a given Reynolds number. The results are also presented in analytical form in Appendix 2. Figure 23 shows a typical dimensionless velocity profile for $\beta = 1.4$.

In the wall jet calculations, Reynolds number is defined as $\frac{v_{max}\delta_t}{\nu}$ whereas all experimental data is plotted in terms of the jet exit Reynolds number $\frac{v_o t}{\nu}$. Here δ_t is the physical distance between the point of maximum velocity and the point at which velocity is half the maximum velocity. For a meaningful comparison of the data and the viscous theory which will use the wall jet results, one of these Reynolds numbers has to be expressed in terms of the other. The relation between them will be given in the following sections.

3.2-4 Momentum Flux Across Section II, M_{II}

Consider one of the solutions of the wall jet as presented in Figure 23. As one can see, the results we have from the wall jet analysis are in nondimensional form. If the actual velocity profile is needed, the vertical and the horizontal scaling of the graph has to be determined. Two expressions are required to determine the two

scaling factors by which the vertical and the horizontal axes have to be multiplied.

One of these expressions which can be used for this purpose is the continuity relation; the other expression is the one which determines the magnitude of the maximum velocity with respect to the initial jet exit velocity v_o from the nozzle. This initial velocity is taken to be v_o since under inviscid flow conditions the uniform flow along the wall would have the magnitude v_o.

The wall jet analysis shows that the solution is dependent on the wall jet Reynolds number; however, this dependency becomes less important as the Reynolds number increases. On the other hand the submerged jet theory as proposed by Albertson (10) is not dependent on Reynolds number. As a result, if an expression derived from the submerged jet theory is going to be used to correlate the maximum velocity of the wall jet to v_o, this has to be done for the cases when the Reynolds number dependency is weak. This means that the results of Albertson can only be used for the wall jet when Reynolds number is infinite.

Submerged jet theory gives:

$$\frac{v_{max}}{v_o} = 1.0; \qquad \frac{x}{t} < 5.2 \tag{31.a}$$

$$\frac{v_{max}}{v_o} = \sqrt{\frac{1}{\sqrt{\pi} C_1} \frac{t}{x}} \quad ; \quad \frac{x}{t} > 5.2 \tag{31.b}$$

Now a characteristic length x must be defined. Since the entrainment occurs mostly along the outer streamline the length of the outer boundary of the jet can be taken as an approximate measure of x. Here we will define x as the length of the outer streamline between the nozzle and the point N where the streamlines become parallel to the wall at inviscid flow conditions (Figure 19). Moreover, we shall assume that the streamlines are circular with points of tangency at the nozzle and at the Section II. Then $h-t' = R\,(1+\sin\theta)$ or

$$R = \frac{(h-t')}{1+\sin\theta}\,, \text{ but } \quad x = 2\pi R\,\frac{90^\circ+\theta}{360^\circ} = \frac{2\pi\,(90^\circ+\theta)}{360^\circ(1+\sin\theta)}\,(h-t')$$

$$\frac{x}{t} = \frac{2\,\pi(90^\circ+\theta)}{360^\circ(1+\sin\theta)}\left(\frac{h}{t} - \frac{t'}{t}\right) \tag{32}$$

where $\frac{t'}{t} = \frac{\lambda}{1-\lambda}\,\ln\left(\frac{1}{\lambda}\right)$ given by the inviscid velocity distribution theory. If the value of $\frac{x}{t}$ from this expression is substituted into equation (31) we get an expression which relates the maximum velocity of a wall jet at infinite Reynolds number to v_o.

In balanced flow, there is no net flow out of or into the cushion; therefore, the inner streamline is the stagnation streamline and touches the wall. This means that the mass flow across section II is equal to the sum of the mass flow coming through the

nozzle and the entrained flow along the outer streamline. Assuming that this entrainment flow is of the same amount as in a submerged jet at x/t dimensionless distance from the nozzle, we can write

$$\frac{Q_{IIv}}{Q_I} = 1 + \frac{\sqrt{\pi}}{2} \left(\sqrt{2} - 1 \right) C_o \frac{x}{t} \quad ; \quad \frac{x}{t} < 5.2 \tag{33.a}$$

$$\frac{Q_{IIv}}{Q_I} = \frac{1}{2} + \frac{1}{2} \sqrt{2\sqrt{\pi}\, C_o \frac{x}{t}} \qquad \frac{x}{t} > 5.2 \tag{33.b}$$

where x/t is as defined in equation (32) and Q_{IIv} is the total volume flow across section II. Notice that these expressions are different from the ones given by the submerged jet theory because entrainment only on one side of the jet is assumed here. The net entrainment here is only half of the net entrainment which takes place in a submerged jet.

The values for $\frac{v_{m\beta=1.0}}{v_o}$ and $\frac{Q_{IIv}}{Q_{Iv}}$ are given in Table II for the range of h/t ratios between 1 and 6 for $\theta = 30°$.

Now, we have the two conditions which determine the scaling factors of Figure 23. Define the factors "k" and "l" as follows:

$$k = \frac{\eta}{y} \qquad\qquad l = \frac{v_{m\beta=g}}{V_{m\beta=g}} \tag{34}$$

where y is the distance from the wall, $v_{m\beta=g}$ is the actual physical maximum velocity which a velocity measuring device would measure in the flow and $V_{m\beta=g}$ is the maximum dimensionless velocity

as obtained from the Glauerts theory for wall jet. The parameter g varies between 1.0 and 2.0. For the case $\beta = g = 1.0$, ie $Re = \infty$, we have

$$1.V_{m\beta=1.0} = v_{m\beta=1.0} = \frac{v_{m\beta=1.0}}{v_o} \; v_o$$

As a result

$$1 = \left(\frac{v_{m\beta=1.0}}{v_o} \right) \frac{v_o}{V_{m\beta=1.0}} \tag{35}$$

where $V_{m\beta=1.0} = .5$ and $\frac{v_{m\beta=1.0}}{v_o}$ is given by equation (31). If the horizontal and vertical axes of Figure 23 are multiplied by 1/k and 1 respectively then the horizontal axis reads y and the maximum velocity is equal to the physical maximum velocity. The expression for the mass flux becomes

$$m_{II} = \rho \; \frac{m_{\beta=g}}{k} \cdot 1 = \rho \; \frac{m_{\beta=g}}{V_{m\beta=1.0}} \left(\frac{v_{m\beta=1.0}}{v_o} \right) \frac{v_o}{k} \tag{36}$$

where $m_{\beta=g}$ is the dimensionless mass flux from Glauerts solution of wall jet. However, the continuity relation gives $m_{II} = \rho(Q_{IIv}) = \rho \left(\frac{Q_{IIv}}{Q_{Iv}} \right) Q_{Iv}$. From this k can be determined

$$k = \frac{\frac{m_{\beta=g}}{V_{m\beta=1.0}} \left(\frac{v_{m\beta=1.0}}{v_o} \right) v_o}{\left(\frac{Q_{IIv}}{Q_{Iv}} \right) Q_{Iv}} \tag{37}$$

TABLE II

h/t	λ	t'/t	x/t	$\frac{v_{m\beta=1.0}}{v_o}$	$\frac{Q_{IIv}}{Q_{Iv}}$
1	.223	.431	.794	1.0	1.0319
2	.412	.621	1.925	1.0	1.0775
3	.565	.742	3.152	1.0	1.1269
4	.663	.808	4.456	1.0	1.1794
5	.721	.845	5.801	.944	1.250
6	.768	.873	7.158	.850	1.333

When the axes of Figure 23 are multiplied by 1 and 1/k, the momentum flux expression becomes

$$M_{II} = \rho \frac{M_{\beta=g} \cdot 1^2}{k} = \rho v_o \frac{M_{\beta=g}}{(V_{m\beta=1.0})(m_{\beta=g})} \left(\frac{v_{m\beta=1.0}}{v_o}\right)\left(\frac{Q_{IIv}}{Q_{Iv}}\right) Q_{Iv} \qquad (38)$$

where $M_{\beta=g}$ is the dimensionless momentum flux from the Glauert solution. But $Q_{Iv} = v_o \frac{\xi t}{1-\xi} \ln\left(\frac{1}{\xi}\right)$ and $\rho v_o^2 = 2p_{sg}$; therefore,

$$\frac{M_{II}}{p_{sg} \cdot t} = \frac{2\, M_{\beta=g}}{(V_{m\beta=1.0})(m_{\beta=g})} \left(\frac{v_{m\beta=1.0}}{v_o}\right)\left(\frac{Q_{IIv}}{Q_{Iv}}\right) \frac{\xi}{1-\xi} \ln\left(\frac{1}{\xi}\right) \qquad (39)$$

Since from the wall jet solution $m_{\beta=g} = 1.0$ and $V_{m\beta=1.0} = 5$, we obtain

$$\frac{M_{II}}{p_{sg} \cdot t} = 4.0\, (M_{\beta=g}) \left(\frac{v_{m\beta=1.0}}{v_o}\right) \left(\frac{Q_{IIv}}{Q_{Iv}}\right) \frac{\xi}{1-\xi} \ln\left(\frac{1}{\xi}\right) \qquad (40)$$

The x-direction momentum balance applied to the control volume ABCD of Figure 24 gives

$$h \cdot p_{cg} = \rho\, v_o^2 t \sin\theta + M_{II}$$

Since $\rho\, v_o^2 = 2\, p_{sg}$ and $p_{cg}/p_{sg} = 1 - \xi^2$, the final form of the momentum balance is given by

$$\frac{h}{t}(1 - \xi^2) - 2\xi\sin\theta - \frac{M_{II}}{p_{sg} \cdot t} = 0 \qquad (41)$$

Here $M_{II}/p_{sg} \cdot t$ has to be substituted from equation (40). All of the terms in equation (40) are defined for a given wall jet

Reynolds number and a given h/t ratio with the exception of ξ. This means that for given values of θ and h/t, the only unknown in expression (41) is ξ. This equation can be solved for ξ numerically by using a computer and then p_{cg}/p_{sg} can be determined by using the fact that $\frac{p_{cg}}{p_{sg}} = 1 - \xi^2$. The computer program no.2 in Appendix 3 does this for a given β, i.e. Re_w.

The final step for the complete solution of the problem is finding a relation between the wall jet Reynolds number

$Re_w = \frac{v_{m\beta=g} \cdot \delta_t}{\nu}$ which is used above and the jet exit Reynolds number $Re_j = \frac{v_o t}{\nu}$ which is used to plot the data. Here we will make an assumption only for the calculations relating the two Reynolds numbers to each other. Namely, that

$$\frac{v_{m\beta=g}}{v_o} \cong \frac{v_{m\beta=1.0}}{v_0} .$$

This assumption is quite good for relatively high Reynolds numbers. Although, for low Reynolds numbers, it introduces an error of up to 25% into the values Reynolds numbers, it simplifies the calculations enourmously. However, this will not effect our calculations much, because the quantities which are calculated by using these Reynolds numbers are quite insensitive to these small changes of Reynolds number.

We now have

$$Re_w = \frac{v_{m\beta=g} \cdot \delta_t}{\nu} = \frac{(\frac{v_{m\beta=g}}{v_o}) v_o \cdot \eta_t}{\nu k} \simeq \frac{(\frac{v_{m\beta=1.0}}{v_o}) v_o \cdot \eta_t}{\nu k} \qquad (42.a)$$

Substituting the relation for k from equation (37)

$$\frac{Re_w}{Re_j} = .5 \, (\frac{Q_{IIv}}{Q_{Iv}}) \, \eta_t \cdot \frac{\xi}{1-\xi} \ln (\frac{1}{\xi}) \qquad (42.b)$$

Figure 25 shows the data interpolated for the jet exit Reynolds numbers which correspond to $Re_w = 1.2 \times 10^3$ and $Re_w = 4 \times 10^4$ for a nozzle angle $\theta = 30°$.

The same figure also shows the results of the calculations of the viscous theory we just developed for $Re_w = 1.2 \times 10^3$ and $Re_w = \infty$. and the results of some of the earlier inviscid theories. Our results are better than any of the inviscid theories and predict the dimensionless cushion pressure within a few percent.

The results of the same procedure for given Re_j of ∞, $2x10^4$ and $2x10^3$ are shown in Figure 26, These results are obtained by using the program no.3 in Appendix 3 which gives the solution for a fixed jet exit Reynolds number Re_j. This program finds the corresponding Re_w's by iteration. The effect of the nozzle angle θ on the solution is shown in Figure 27. This figure shows the solutions for $Re_j = 2x10^4$ for θ's of 0°, 30°, 45° and 60°.

4. UNBALANCED JET VISCOUS THEORY

While a peripheral jet is operating under equilibrium conditions as described until now, if the cushion pressure drops below the equilibrium value, the jet splits and some net flow takes place into the cushion. Similarly, if the cushion pressure rises above the equilibrium value some net flow occurs out of the cushion. These two conditions are called overfeeding and underfeeding respectively. In order to describe the dynamic characteristics of the suspension system, the flow-pressure-displacement characteristics of the system must be determined while operating under these non-equilibrium conditions. In other words, a relation between the cushion pressure, total mass flow and the cushion flow has to be found. Moreover, it is desired that this relation follow the data closely, especially around the equilibrium value, since it is used in a linearized solution around this point. Figure 6 shows the results from the Barratt theory and velocity distribution theory for overfed and underfed jets along with data taken at M.I.T. The theories show discontinuities in slope around the equilibrium value while the data goes smoothly through this point. This shows that they are inadequate to describe the dynamic behavior of the suspension. In the following sections of this thesis, a new approach which takes viscous effects into account will be used to predict the suspension behavior under nonequilibrium conditions.

4.1 Overfed Jet

A split jet is shown in Figure 28, together with its important parameters. If the flow were completely inviscid then the velocity profiles across the sections II and III would be uniform. Their magnitudes would have been determined by the respective values of $p_s - p_a$ and $p_s - p_c$. When viscosity exists lateral mixing would result from the eddies formed along the boundaries due to high magnitude shear forces between the jet and the surrounding fluid. When the jet hits the wall and starts to flow parallel to it the effect of the wall becomes dominant near the ground plate. Therefore, the inner layer of the flow obeys the "1/7 th law" while the outer layer satisfies the conditions of free turbulent flow. These facts strongly indicate that the velocity profiles across the sections II and III will be in the form of a wall jet profile as described in the balanced case in the previous chapter. The results of the wall jet apply unchanged with the exception that the profiles have to be scaled again so that they satisfy the conservation of mass principle. The maximum velocities of the wall jets are also to be determined again.

The momentum equation in its general form applied to the control volume PSTU would give

$$h \cdot p_s - h \cdot p_c = M_I \sin\theta + M_{II} - M_{III}$$

where M_I, M_{II} and M_{III} stand for the momentum fluxes across the section I, II, and III. In the following sections of this chapter these momentum fluxes will be evaluated.

4.1-1 Estimation of Momentum Fluxes

The assumptions which were made about the enterance section for the balanced case still continue to hold true; therefore, the mass and momentum fluxes across section I are given by

$$m_1 = \rho v_o \frac{\xi t}{1-\xi} \ln\left(\frac{1}{\xi}\right) ; \qquad M_I = \rho v_o^2 t \xi \tag{44}$$

where $$\xi = \sqrt{1 - \frac{p_{cg}}{p_{sg}}} .$$

Let us define α as the ratio of the cushion flow to the total flow coming through the nozzle. That is,

$$\alpha = \frac{m_3}{m_1} \tag{45}$$

then $$m_3 = \alpha m_1 = \alpha \rho v_o \frac{\xi t}{1-\xi} \ln\left(\frac{1}{\xi}\right) \tag{46}$$

$$m_2 = (1 - \alpha) m_1 = (1 - \alpha) \rho v_o \frac{\xi t}{1-\xi} \ln\left(\frac{1}{\xi}\right) \tag{47}$$

By using a similar argument presented for the balanced flow, the 1-factor at section II is given by

$$1_2 = \frac{v_{m\beta=1.0}}{V_{m\beta=1.0}} = \left(\frac{v_{m\beta=1.0}}{v_o}\right) \frac{v_o}{V_{m\beta=1.0}} \tag{48}$$

and by using continuity, the k-factor is

$$k_2 = \frac{(\frac{m_{\beta=g}}{v_{m\beta=1.0}})(\frac{v_{m\beta=1.0}}{v_o})v_o}{(\frac{Q'_{IIv}}{Q'_{Iv}})Q'_{Iv}}$$

$$\text{or } M_{II} = \rho\frac{M_{\beta=g}\cdot 1_2^2}{k_2} = v_o \frac{M_{\beta=g}}{(V_{m\beta=1.0})(m_{\beta=g})}(\frac{v_{m\beta=1.0}}{v_o})(\frac{Q'_{IIv}}{Q'_{Iv}})Q'_{Iv} \quad (50)$$

Here Q'_{IIv} is the total volume flow going across section II; Q'_{Iv} is the portion of the incoming flow which is due to the part of the jet at the right side of the stagnation streamline. In terms of α it is given by

$$Q'_{Iv} = (1 - \alpha)v_o \frac{\xi t}{1-\xi} \ln (\frac{1}{\xi})$$

Notice that Q'_{IIv} is the sum of Q'_{Iv} and the entrained flow along the outer streamline.

We know that $2p_{sg} = \rho v_o^2$, $m_{\beta=g} = 1.0$ and $V_{m\beta=1.0} = .5$; therefore,

$$\frac{M_{II}}{p_{sg}.t} = 4.0\ (M_{\beta=g})(\frac{v_{m\beta=1.0}}{v_o})_{II}(\frac{Q'_{IIv}}{Q'_{Iv}})_{II}(1-\alpha)\frac{\xi}{1-\xi}\ln(\frac{1}{\xi}) \quad (51)$$

The terms $(v_{m\beta=1.0}/v_o)_{II}$ and $(Q'_{IIv}/Q'_{Iv})_{II}$ in the above expression are yet to be determined. The subscript "II" under them indicates flow across section II.

For the flow across section III, l-factor is given by

$$l_3 = \frac{v_{m\beta=1.0}}{V_{m\beta=1.0}} = \frac{v_{m\beta=1.0}}{v_c} \cdot \frac{v_c}{v_o} \frac{v_o}{V_{m\beta=1.0}} \tag{52}$$

where v_c is the magnitude of the uniform velocity across section III if the flow were completely inviscid.

By using the continuity relation, the k-factor can be obtained readily.

$$k_3 = \frac{\frac{m_{\beta=g}}{V_{m\beta=1.0}} \left(\frac{v_{m\beta=1.0}}{v_c}\right)\left(\frac{v_c}{v_o}\right) v_o}{\left(\frac{Q''_{IIIv}}{Q''_{Iv}}\right) Q''_{Iv}} \tag{53}$$

where Q''_{IIIv} is the total flow going across section III. Q''_{Iv} is the portion of the incoming flow through the nozzle due to the part of the jet to the left of the stagnation streamline. In terms of α it is given by

$$Q''_{Iv} = \alpha v_o \frac{\xi t}{1-\xi} \ln\left(\frac{1}{\xi}\right)$$

The momentum flux across section III can then be expressed as

$$M_{III} = \rho \frac{M_{\beta=g} \cdot l_3^2}{k_3} = \rho v_o \frac{M_{\beta=g}}{(m_{\beta=g})(V_{m\beta=1.0})} \left(\frac{v_{m\beta=1.0}}{v_c}\right)\left(\frac{v_c}{v_o}\right)\left(\frac{Q''_{IIIv}}{Q''_{Iv}}\right) Q''_{Iv} \tag{54}$$

but $v_c = \sqrt{\frac{2}{\rho}(p_s - p_c)}$ and $v_o = \sqrt{\frac{2}{\rho}(p_s - p_a)}$; therefore,

$$\frac{v_c}{v_o} = \sqrt{\frac{p_s - p_c}{p_s - p_a}} = \sqrt{1 - \frac{p_{cg}}{p_{sg}}} = \xi \qquad (55)$$

From the wall jet solution we also have $m_{\beta=g} = 1.0$ and $V_{m\beta=1.0} = .5$. Considering the fact that $\rho v_o^2 = 2p_{sg}$ we get

$$\frac{M_{III}}{p_{sg}.t} = 4.0\ (M_{\beta=g})\left(\frac{v_{m\beta=1.0}}{v_c}\right)_{III}\left(\frac{Q''_{IIIv}}{Q''_{Iv}}\right)_{III} \alpha\frac{\xi^2}{1-\xi}\ \ln\left(\frac{1}{\xi}\right) \qquad (56)$$

In the above expression the quantities $(v_{m\beta=1.0}/v_c)_{III}$ and $(Q''_{IIIv}/Q''_{Iv})_{III}$ are still to be determined. The subscript III was added to indicate that the flow takes place across section III.

4.12 Determination of $(Q'_{IIv}/Q'_{Iv})_{III}$ and $(Q''_{IIIv}/Q''_{Iv})_{III}$

Entrainment which contributes to the momentum flux across section II takes place along the outer streamline; therefore, the length of the outer streamline can be taken as the characteristic length in the calculation of $(Q'_{IIv}/Q'_{Iv})_{II}$. As we did in the balanced case we will assume the length of the outer streamline to be the length if the flow were completely inviscid. See Figure 29.
Assuming the shape of the streamline to be circular with points of tangency at M and N we get

$$X_{II} = \frac{2\pi(90° + \theta°)}{360°(1+\sin\theta)}\ (h - \delta)$$

but $\delta = (1 - \alpha)t'$ where t' is the exit jet thickness if the peripheral jet were balanced and is described in Chapter 3 by equation (9). Then

$$\left(\frac{X}{t}\right)_{II} = \frac{2\pi(90° + t)}{360°(1 + \sin\theta)} \left(\frac{h}{t} - (1 - \alpha)\frac{t'}{t}\right) = \tag{57}$$

$$\frac{2\pi(90° + \theta)}{360°(1 + \sin\theta)} \left[\frac{h}{t} - (1-\alpha)\frac{\lambda}{1-\lambda} \ln\left(\frac{1}{\lambda}\right)\right]$$

Now $(Q'_{II\ v}/Q'_{I\ v})_{II}$ can be found directly from the submerged jet theory results as summarized in section 3.22 keeping in mind that entrainment takes place only on one side.

$$\left(\frac{Q_{II'v}}{Q_{I'v}}\right) = 1 + \frac{\sqrt{\pi}}{2} (\sqrt{2} - 1) C_o \left(\frac{X}{t}\right)_{II} ; \quad \left(\frac{X}{t}\right)_{II} < 5.2 \tag{58.a}$$

$$\left(\frac{Q_{II'v}}{Q_{I'v}}\right)_{II} = \frac{1}{2} + \frac{1}{2} \sqrt{2\sqrt{\pi}\ C_o \left(\frac{X}{t}\right)_{II}} ; \quad \left(\frac{X}{t}\right)_{II} > 5.2 \tag{58.b}$$

$(Q''_{III\ v}/Q''_{I\ v})_{III}$ will not be calculated in the same manner but instead will be taken equal to 1.0. This is seen better if the diagram of the two dimensional apparatus of Figure 30 is considered. It is evident from the figure that the mass flow out of the cushion from the left side has to be exactly the same as the flow which enters into the cushion area through the nozzle. Otherwise, there would be continuous increase or decrease of mass in the closed volume of MNOP which is physically impossible. Of course, there is

some entrained flow along the inner streamline zz', but this flow does not go out from the left end of the cushion and stays in the standing weak vortex which is produced in the closed area zz'N. The same argument is not true, however, for the portion of the jet which flows through section II because the mass flow out through section II also includes the entrained flow along the outer streamline.

4.1-3 Determination of $(v_{m\beta=1.0}/v_o)_{II}$ and $(v_{m\beta=1.0}/v_c)_{III}$

Let us consider the split jet which is shown in Figure 28. We will assume that the maximum velocity in the portion of the jet which goes through section II obeys the laws of a submerged jet and the maximum velocity at II is equal to the maximum velocity at X_{II} distance from the nozzle of a submerged jet of thickness t_{II}. This assumption is consistent with the physics of the flow because the thinner t_{II} is then the slower the velocities in section II will be. Similarly, the velocity at section III would be sensitive to the thickness t_{III}.

The thickness t_{II} can be found by equating the mass flow in this region to $(1 - \alpha)m_I$, that is

$$\int_o^{t_{II}} \frac{av_o}{z+a}\,dz = \rho a v_o \ln\left(\frac{t_{II}+a}{a}\right) = (1-\alpha)\rho\, v_o \frac{\lambda t}{1-\lambda} \ln\left(\frac{1}{\lambda}\right)$$

or

$$t_{II} = \frac{\left[\left(\frac{1}{\lambda}\right)^{(1-\alpha)} - 1\right]\lambda t}{(1-\lambda)}$$

and $t_{III} = t - t_{II}$ (60)

Then taking the inner and the outer streamlines of circular shape with points of tangencies at M,N,G,F,as shown in Figure 29, we get

$$\left(\frac{X_{III}}{t_{III}}\right) = \frac{\left[\frac{h}{t}(1-\lambda) - \alpha \ln\left(\frac{1}{\lambda}\right)\right]}{(1-\lambda)-\left[\left(\frac{1}{\lambda}\right)^{(1-\alpha)} - 1\right]\lambda}\left(\frac{2\pi(90°-\theta)}{360°(1-\sin\theta)}\right) \tag{61}$$

$$\left(\frac{X_{II}}{t_{II}}\right) = \frac{\left[\frac{h}{t} - (1-\alpha)\frac{\lambda}{1-\lambda}\ln\left(\frac{1}{\lambda}\right)\right](1-\lambda)}{\left[\left(\frac{1}{\lambda}\right)^{(1-\alpha)} - 1\right]\lambda}\left(\frac{2\pi(90°+\theta)}{360°(1+\sin\theta)}\right) \tag{62}$$

Now the submerged jet theory can be used to obtain the approximate values for $(v_{m\beta=1.0}/v_o)_{II}$ and $(v_{m\beta=1.0}/v_c)_{III}$.

$$\left(\frac{v_{m\beta=1.0}}{v_c}\right)_{III} = 1.0 \quad ; \quad \frac{X_{III}}{t_{III}} < 5.2 \tag{63.a}$$

$$\left(\frac{v_{m\beta=1.0}}{v_c}\right)_{III} = \sqrt{\frac{1}{\sqrt{\pi}\,C_o}\left(\frac{t_{III}}{X_{III}}\right)} \quad ; \quad \frac{X_{III}}{t_{III}} > 5.2 \tag{63.b}$$

Similarly for the flow across section II

$$\left(\frac{v_{m\beta=1.0}}{v_o}\right)_{II} = 1.0 \quad ; \quad \frac{X_{II}}{t_{II}} < 5.2 \tag{64.a}$$

$$\left(\frac{v_{m\beta=1.0}}{v_o}\right)_{II} = \sqrt{\frac{1}{\sqrt{\pi}\,C_o}\left(\frac{t_{II}}{X_{II}}\right)} \quad ; \quad \frac{X_{II}}{t_{II}} > 5.2 \tag{64.b}$$

4.1-4 Wall Jet Reynolds Number

We have seen in chapter 3 that the value $M_{\beta=g}$ in the momentum expressions depend on the wall jet Reynolds number. Here the wall jet Reynolds numbers for the jets which go through sections II and III are $Re_{IIw} = (v_{IIm\beta=g}\ \delta_{IIt})/\nu$ and $Re_{IIIw} = (v_{IIIm\beta=g}\ \delta_{IIIt})/\nu$; however, the data is presented in terms of the jet Reynolds number $Re_j = \frac{v_o t}{\nu}$. Now, the expressions which relate the wall jet Reynolds number to a given Re_j will be derived so that the theoretical results can be expressed in terms of the parameters which were used to plot the data.

$$Re_{IIw} = \frac{v_o \left(\frac{v_{m\beta=g}}{v_o}\right)_{II}\ \eta_{IIt}}{\nu\ k_2} \cong \frac{v_o \left(\frac{v_{m\beta=1.0}}{v_o}\right)_{II}\ \eta_{IIt}}{\nu\ k_2} \qquad (65.a)^*$$

where (η_{IIt}) is the dimensionless wall jet thickness as given in figure 22. But k_2 is given by equation (49); therefore,

$$Re_{IIw} = \frac{(1-\alpha)\ \eta_{IIt}^{\lambda}}{2(1-\lambda)} \ln\left(\frac{1}{\lambda}\right) \left(\frac{Q'_{II}\ v}{Q'_{I}\ v}\right)_{II} Re_j \qquad (65.b)$$

where $(Q'_{II}\ v/Q'_{I}\ v)_{II}$ is defined by equation (58).

Similarly,

$$Re_{IIIw} = \frac{v_o \left(\frac{v_{m\beta=g}}{v_c}\right)_{III} \left(\frac{v_c}{v_o}\right) \eta_{IIIt}}{\nu\ k_3} \cong \frac{v_o \left(\frac{v_{m\beta=1.0}}{v_c}\right)_{III} \left(\frac{v_c}{v_o}\right) \eta_{IIIt}}{\nu\ k_3}$$

---

* The argument which applies to equation (42.a) also applies here.

If k_3 is substituted from equation (53) with $(Q'_{III\ v}/Q'_{I\ v})_{III}$ equal to 1.0. we get

$$Re_{IIIw} = \frac{\alpha\lambda\eta_{IIt}}{2(1-\lambda)} \ln\left(\frac{1}{\lambda}\right) Re_j \tag{66}$$

The wall jet Reynolds number for a given Re_j can be found from these expressions first by guessing a value for η_{IIt} and η_{IIIt} and then iterating the expressions either graphically by using Figure 22 or analytically by using equations which are given in Appendix 2.

Once the wall jet Reynolds numbers are determined the values for $(M_{\beta=g})_{II}$ and $(M_{\beta=g})_{III}$ can be found by using Table I and Figure 22.

The momentum balance applied to the control volume PSTU of Figure 28 then becomes

$$\frac{h}{t}(1-\xi^2) - 2\xi\sin\theta - \frac{M_{II}}{p_{sg}.t} + \frac{M_{III}}{p_{sg}.t} = 0 \tag{67}$$

The computer program in Appendix 4 gives the dimensionless cushion pressures at a given jet Reynolds number for different values of α. The results for $\theta = 30°$ are plotted in the upper half of Figures 34 thru 36 for $Re_j = 2x10^4$ and $Re_j = \infty$. The effect of θ on the results is also depicted in Figure 37. The upper half of this figure shows the results of the viscous theory for overfed jet for $\theta = 0°$, 30°, 45° 69° for h/t ratios of 2 and 4 at

$Re_j = 2 \times 10^4$. The discussions of the results will be deferred until the solution for underfed jet is obtained.

It is clear from the assumptions that the predicted effect of the base plate, i.e. the upper wall of the cushion, is negligible. As a result, the above theory would break down if the thickness of the jet across section III is so big that a boundary layer develops along the upper wall. Considering that when $\eta = 5$ the velocity of the wall jet is practically zero, this breakdown condition can be expressed by stating that the thickness of the wall jet up to the point which corresponds to $\eta = 5.0$ has to be less than the height h, that is $5.0/k_3 < h$ or

$$\frac{5.0}{k_3 t} < \frac{h}{t} .$$

The fourth column of the print out of the computer program of Appendix 4 gives the value of $5.0/k_3.t$. This value was always less than the ratio h/t for the range of α's for which the calculations were carried out.

4.2 Underfed Jet

An underfed jet is shown in Figure 31. In general, by considering the physics of the flow, the following aspects can be pointed out:

a) The flow entering the control volume ABCD is inviscid and irrotational.

b) The maximum velocity v_m can be determined by submerged jet theory and is a function of $p_s - p_a$.

c) The velocity v_{cm} is determined by the magnitude of $p_c - p_a$.

d) In region c, lateral mixing occurs between the low velocity section and the high velocity section of the exit jet.

e) In region d, the velocity profile is the same as the outer portion of a wall jet.

f) In region a, "1/7th profile" prevails.

g) The uniform core, region b, may or may not exist depending on the inner layer thickness.

h) The velocity at section III is uniform.

However, under these approximations, the determination of the profile across section II is quite difficult. At the limiting case $m_c = 0$, we want the solution to approach the results of the balanced jet as described in chapter 3. But with the above description of the flow, the mathematical modeling of the system which satisfies this limiting condition is almost impossible. To simplify the calculations, the model which was described above will be revised by a few assumptions. First, we will assume that the mixing along the streamline L'Y' is negligible when compared with the mixing along the outer boundary of the jet because the former takes place between two jets which flow in the same direction while the later takes place between a jet and a stagnant medium. Next, we will assume that the wall jet profile starts right after

the uniform cushion flow core rather than from the peak of the profile. This assumption does not have any support from a physical point of view; however, it does not introduce a large error into the solution. This is the price paid in turn for simplicity. Now the velocity profile across section II would be similar to the one shown in Figure 32. We will make another simplifying assumption. The boundary layer along the wall is dominated by the effects due to the wall; the inner layer of the wall jet is also governed by the effects of the wall. We will assume that the boundary layer along the wall can be approximated by the missing portion o'c' of the wall jet boundary layer. Then the profile in Figure 32 would be equivalent to the summation of a uniform profile with velocity v_{cm} and m_c mass flow and a wall jet profile with v_m maximum velocity and m_w mass flux where m_w consists of the flow m_I through the nozzle and the entrained flow along the outer stream line. The momentum flux at the exit then would be

$$M_{II} = M_w + M_c \tag{68}$$

where M_w means the momentum flux due to the wall jet and M_c is the momentum flux due to the uniform core.

$$M_w = \rho v_o \frac{M_{\beta=g}}{V_{m\beta=1.0}} \left(\frac{v_{m\beta=1.0}}{v_o}\right) \left(\frac{Q_{wv}}{Q_{Iv}}\right) \frac{\xi t}{1-\xi} \ln \left(\frac{1}{\xi}\right)$$

or

$$\frac{M_w}{P_{sg} \cdot t} = 4.0 \left(M_{\beta=g}\right) \left(\frac{v_{m\beta=1.0}}{v_o}\right) \left(\frac{Q_{wv}}{Q_{Iv}}\right) \frac{\xi}{1-\xi} \ln \left(\frac{1}{\xi}\right) \tag{69}$$

where Q_{wv} is the total volume flux in the wall jet. The values of $(v_{m\beta=1.0}/v_o)$ and (Q_{wv}/Q_{Iv}) have yet to be determined.

The momentum flux at the uniform core is given by

$$M_u = m_c v_c = \alpha\rho v_o \frac{\xi t}{1-\xi} \ln\left(\frac{1}{\xi}\right) v_c = \alpha\rho\, v_o^2 \frac{\xi\, t}{1-\xi} \ln\left(\frac{1}{\xi}\right) \frac{v_c}{v_o}$$

or

$$\frac{M_u}{p_{sg}.t} = 2\alpha \left(\frac{v_c}{v_o}\right) \frac{\xi}{1-\xi} \ln\left(\frac{1}{\xi}\right) \tag{70}$$

Now, the ratio (v_c/v_o) will be found. (v_c/v_o) will be approximated by the value of the same ratio under inviscid flow conditions. Inviscid flow of an underfed jet is shown in Figure 33.

Bernoulli's equation gives

$$\frac{1}{2}\rho\, v_{co}^2 + p_c = \frac{1}{2}\rho v_c^2 + p_a \quad \text{or} \quad v_c^2 - v_{co}^2 = \frac{2}{\rho}(p_c - p_a) \tag{71}$$

Continuity gives $\rho v_{co} h = \rho\, v_c \gamma = \alpha\, m_I$

or

$$v_{co} = \frac{\alpha\, m_I}{\rho h}; \text{ therefore, } \quad \frac{v_{co}}{v_c} = \frac{\alpha\lambda\, t}{h(1-\lambda)} \ln\left(\frac{1}{\lambda}\right) \tag{72}$$

Substitution of v_{co} from equation (72) into (71) gives

$$\frac{v_c}{v_o} = \sqrt{(1-\lambda^2) + \frac{\alpha^2\lambda^2}{\left(\frac{h}{t}\right)^2 (1-\lambda)^2} \left[\ln\left(\frac{1}{\lambda}\right)\right]^2} \tag{73}$$

The momentum flux across section III is

$$M_{III} = m_c v_{co} = \alpha\rho v_o^2 \frac{\xi\, t}{1-\xi} \left[\ln\left(\frac{1}{\xi}\right)\right] \frac{v_{co}}{v_o}$$

Substituting equation (72) for v_{co}/v_o,

$$\frac{M_{III}}{p_{sg}.t} = \frac{2\alpha^2 \lambda\xi}{(\frac{h}{t})(1-\lambda)(1-\xi)} \ln(\frac{1}{\lambda}) \cdot \ln(\frac{1}{\xi}) \qquad (74)$$

The values for $(v_{m\ \beta=1.0}/v_o)$ and (Q_{wv}/Q_{Iv}) can be found by using the submerged jet theory. Taking the characteristic length for the problem as the length of the outer stream line of Figure 33

$$\frac{x}{t} = \frac{2\pi(90°+\theta)}{360°(1+\sin\theta)} (\frac{h}{t} - \frac{t'}{t} - \frac{\gamma}{t}) = \frac{2\ (90°+\theta)}{360°(1+\sin\theta)} [\frac{h}{t} - \frac{t'}{t}(1 + \frac{\gamma}{t'})]$$

but $\rho\ v_c\gamma = m_c = \alpha\rho v_o t'$ or $\alpha \frac{v_o}{v_c} = \frac{\gamma}{t'}$; therefore,

$$\frac{x}{t} = \frac{2\pi(90°+\theta)}{360°(1+\sin\theta)} [\frac{h}{t} - \frac{t'}{t}(1+\alpha \frac{v_o}{v_c})] \qquad (75)$$

where $\frac{t'}{t} = \frac{\lambda}{1-\lambda} \ln(\frac{1}{\lambda})$ and v_o/v_c is given by equation (73).

The values of $(v_{m\beta=1.0}/v_o)$ and (Q_{IIv}/Q_{Iv}) can then be obtained from the submerged jet theory.

$$\frac{v_{m\beta=1.0}}{v_o} = 1.0 \ ; \qquad \frac{x}{t} < 5.2 \qquad (76.a)$$

$$\frac{v_{m\beta=1.0}}{v_o} = \sqrt{\frac{1}{\sqrt{\pi}\ C_o} \frac{t}{x}} \qquad \frac{x}{t} > 5.2 \qquad (76.b)$$

and

$$\frac{Q_{wv}}{Q_{Iv}} = 1 + \frac{\sqrt{\pi}}{2}(\sqrt{2} - 1)\, c_o \frac{x}{t} \qquad \frac{x}{t} < 5.2 \qquad (77.a)$$

$$\frac{Q_{wv}}{Q_{Iv}} = \frac{1}{2} + \frac{1}{2}\sqrt{2\sqrt{\pi}\, c_o \frac{x}{t}} \qquad \frac{x}{t} > 5.2 \qquad (77.b)$$

The only quantity to be determined in the momentum balance expression (69) is $M_{\beta=g}$. The wall jet theory showed that this term changes with β; that is, with the wall jet Reynolds number. As in the case of the overfed jet, jet exit Reynolds number $\frac{v_o t}{\nu}$ can be related to the wall jet Reynolds number and the values for $M_{\beta=g}$ can be found for a specific jet exit Reynolds number.

It can be shown by using a procedure similar to that in section 4.1-4 that Re_w is related to Re_j in the following manner

$$Re_w = \frac{\xi\, \eta_t}{2(1-\xi)} \left(\frac{Q_{wv}}{Q_{Iv}}\right)\left[\ln\left(\frac{1}{\xi}\right)\right] Re_j \qquad (78)$$

The wall jet Reynolds number corresponding to a given Re_j can be found from this expression first by guessing a value for η_t and then iterating the expression either graphically by using Figure 22 or analytically by using the equations which are given in Appendix 2.

The momentum balance applied to the control volume ABCD gives

$$\frac{h}{t}(1-\xi^2) - 2\xi \sin\theta - \frac{M_{II}}{p_{sg}.t} + \frac{M_{III}}{p_{sg}.t} = 0 \qquad (79)$$

where the second and the third terms on the right hand side are given by equations (68) and (74).

The computer program which is given in Appendix 4 calculates the dimensionless cushion pressures for underfed jets by utilizing the viscous theory which is summarized above. The results for a nozzle angle of $\theta = 30°$ which correspond to the $Re_j = 2 \times 10^4$ and $Re_j = \infty$ are plotted on the lower half of the Figures 34 thru 36. Figure 37, on the other hand, shows the effect of varying θ on the results. The lower half of this figure shows the predicted behavior of an underfed jet operating at h/t ratios of 2 and 4 and $Re_j = 2 \times 10^4$ with nozzle angles of $\theta = o°$, 30°, 45°, and 60°.

5. ANALYTICAL PROCEDURE

In this section the procedure, which must be followed to get the results of the viscous theory without getting into the details of the problem, will be outlined. Solutions for the viscous peripheral jet performance can be obtained following the steps described below. This procedure involves the use of the computer programs presented in the appendices. The results of the Glauert's wall jet solution are already entered into the computer programs of Appendix 3 and 4. Therefore, the results obtained in Appendix 2 are not needed directly for the calculations. For the case of infinite Reynolds number ($\beta = 1.0$) we used the results of the exact solutions. Then the results of the exact solution for $\beta = 1.0$ and the results from the computer program of Appendix 2 for the other values of β's were combined together and analytical expressions which give the change of certain parameters with β were found as given in Appendix 2.

The range of the Reynolds number which may be encountered in a full sized vehicle is given in Table III. We assumed that the vehicle would be 10 ft. wide and would weigh from 250 lbs. to 1000 lbs. per feet along its length. As one can see, it changes between 1.5×10^3 and 10^4.

TABLE III

Range of Reynolds Numbers of Interest

Maximum Values T = 60° F	Minimum Values T = 60° F
t_c = 3.0 in h/t=3.0 p_{cg} = 100lb/ft^2 Re_j = 8.3x10^3	t = 1.0 h/t=3.0 p_{cg} = 25lb/ft^2 Re_j = 1.4 x 10^3

Keeping in mind the above comments, the steps for obtaining a numerical answer from the viscous theory can be outlined as follows:

For the balanced jet, the computer program No. 3 of Appendix 3 for overfed and underfed jets and programs No. 1 and No.2 of Appendix 4 will be used respectively. The following comments apply to all of them. The use of each program is also explained more extensively in the appendices.

a) Specify the values of THETA (θ in degress), SIN ($\sin\theta$) U (h/t), RG (Re_j) and S(λ). To find the value for S, i.e. λ, which corresponds to a given h/t use the curves of Figure 20. Specify the limits of the DO statements by following the instructions given before the programs.

b) The solution occurs when SUN, the first column of the printout, goes through zero. The value of PR on the line which SUN goes through zero gives the value of p_{cg}/p_{sg} as the answer to the problem.

The computer programs which are given in Appendices 3 and 4 give solutions only when the wall jet Reynolds number is between 33 and 4.1×10^4 which covers the range of interest. However, the solutions which correspond to other Reynolds numbers can also be obtained by using the results of the viscous theory. Among these, the solution which corresponds to infinite Reynolds number is of special interest; therefore, it was given in Figures 25 and 36.

6. CONCLUSIONS

The theoretical results for a balanced jet are shown in Figure 26. As one can see, the theory predicts the data within 3-4 percent, but still one can see that the difference between the cases for $Re_j = 2x10^3$ and $Re_j = \infty$ are more pronounced in data than in theory. This effect is probably due to the possible differences between the actual shape of the velocity profile along the wall and the theoretical profile or is due to nozzle losses. It is obvious that in the actual case the velocities do not go to zero asymptotically at large distances from the wall. It was observed clearly during the water table experiments that standing vortices exist on both sides of the jet. Although Hsu(6) showed that the effect of these standing vortices compared with the effect of the mixing is negligible, there is some error introduced into the solution because the effects of the vortices are neglected. At large distances from the wall, the velocity has "-x" component rather than being zero due to the standing vortices. Another possible error may be introduced to the solution because of the assumption that the wall jet is fully developed. It is possible that the profile may not be fully developed jet although quite close to it. As one can see from Figures 8 and 9, the maximum velocity peaks of the data curves are not as pointed as the theoretical profiles. But even under these assumptions the theoretical results are quite good. They clearly give much better

results than the inviscid theories which give 5% to 40% errors. The errors are now reduced to 3-4 percent by the viscous theory.

The real merit of the viscous theory comes in the unbalanced case because now it makes the prediction of the dynamic behavior of the fluid suspension systems possible. Until now, the pressure-flow characteristics of the unbalanced peripheral jet could not be calculated adequately to describe the suspension behavior. Inviscid theories applied to the unbalanced jet gave discontinuities in slope about the point which the differential equations which describe the dynamics of the suspension were linearized. Therefore, this character of the inviscid theories made them of limited value from the point of view of dynamics.

The viscous theory on the other hand does not have this drawback. Although the upper and the lower halves of the curves shown in Figures 34 through 37 are calculated independently, when they are plotted they give continuous slopes at the point of junction which is the point corresponding to the balanced flow. Moreover, near this point the slopes of the theoretical curves are almost the same as the slopes of the data curves. Since the intersection points of these curves with the horizontal axis is not pertinent to the dynamics but is just an indication of error in predicting the static cushion pressure, the theoretical results can be used satisfactorily in the dynamic equations given by Richardson and Ribich (1).

The reason why the upper halves of the curves in Figure 34 deviate from data for the values of α greater than .2 can be due to two reasons. First, it may be due to the defects in the model of the experimentation. Viscous theory assumes that the length of the cushion area in the x-direction is large compared to the nozzle height h which is also true in a real vehicle while the 2-D Suspension Apparatus has a cushion area length of about 7 inches. This means that the data taken may very well be inadequate to represent the actual phenomenon due to 2-dimensional effects. Secondly, the assumed flow pattern in the cushion area for overfed jet may not hold true at large values of α. However, in any case, the behavior at very large α's is not of great interest in practice.

Here we should note one characteristic of the viscous theory which is also true for the Barratt theory. When the results for balanced jet is plotted in the form p_{cg}/p_{sg} vs. $\bar{h}$ where $\bar{h} = (h/t)/(1+\sin\theta)$, they fall approximately on the same curve as shown in Figure 39. By this characteristic of the theory, the results for different nozzle angles can be obtained from the results obtained for one nozzle angle without spending too much effort.

The effect of Reynolds number on the slopes of the curves of α vs. p_{cg}/p_{sg} for unbalanced jets is negligible as can be seen from Figure 36. However, the slopes are effected by changing nozzle angle θ as shown in Figure 37. The values of the slopes are given in the graphs of Figures 40 and 41.

The sensitivities a_c and a_s which are used in predicting the dynamic behavior of the system* are calculated for a case when p_a = 1 atm, T = 60°F, t = 0.1", $Re_j = 2 \times 10^4$ and θ = 30° by using the values given in Figure 40 in the below given expressions:

$$a_c = \frac{p_c}{p_{sg}} \frac{\partial \alpha}{\partial (p_{cg}/p_{sg})} \qquad a_s = - \frac{p_s \, p_{cg}}{(p_{sg})^2} \frac{\partial \alpha}{\partial (p_{cg}/p_{sg})} \tag{80}$$

The results are shown in Figures 42 and 43 respectively along with the data and the results of the Barratt theory. The viscous theory predicts the sensitivities for this example within a maximum error of 8% while the maximum error for Barratt theory is over 100% in many cases. Another aspect of the viscous theory solution is that it follows the trends of the data for changing h/t ratios closely as can be seen clearly in Figure 43. Barratt theory on the other hand predicts that the sensitivity a_s increases as h/t goes from 2 to 6 while the data do not follow this. These are good indications that the viscous theory is adequate in predicting the dynamics of the system. Although, the sensitivities a_c and a_s are calculated only for θ = 30° here, the excellent agreement between the data and the viscous theory for this case makes us to believe strongly that the theory would give satisfactory results for the other nozzle angles. However, we will not be able to test the theory for other angles, because there is no data available for the other values of θ.

---

* See reference (1).

REFERENCES

1. Ribich, W. A. and Richardson, H. H., Dynamic Analysis of Heave Motion for a Transport Vehicle Fluid Suspension, Engineering Projects Laboratory Report No. DSR-76110-3, Massachusetts Institute of Technology, Cambridge, Mass., January 1967.

2. Strand, T., Exact Inviscid Incompressible Flow Theory of Static Peripheral Jets in Proximity to the Ground, Convair, San Diego, California, ERR-50-002, November 1959.

3. Jones, R.S., Some Design Problems of Hovercraft, Institute of the Aerospace Sciences, IAS Paper No. 61-45, January 1961.

4. Burgess A. J., A Two-Dimensional Static Stability Theory for an Air Cushion Vehicle with a Central Stability Jet, University of Southampton, A.A.S.U. Report No. 256, May 1964.

5. Chaplin, H. R., Theory of the Annular Nozzle in Proximity to the Ground, DTMB Aero Report No. 923, 1957.

6. Ribich, W. A. and Richardson, H. H., A Two-Dimensional Fluid Suspension Test Apparatus for Investigation of Pressure Ratio, Mach Number and Reynolds Number Effects, Engineering Projects Laboratory Report No. DSR-76110-2, Massachusetts Institute of Technology, Cambridge, Mass., November 1966.

7. Richardson, H. H., Ribich, W. A., Ercan, Y., Pressure-Flow-Displacement Characteristics of a Peripheral Jet Fluid Suspension, Engineering Projects Laboratory Report No. DSR-76110-7, Massachusetts Institute of Technology, Cambridge, Mass., 1967.

8. Ben-Chie Yen, Patterns of Flow Under a Two-Dimensional GEM, Iowa Institute of Hydraulic Research, State University of Iowa, Iowa City, January 1962.

9. Hsu, C. C. Viscous Effects on Balanced Jets in Ground Proximity, Hydronautics Incorporated Technical Report No. 241-1.

10. Albertson, M. B., Dai, Y. B., Jensen R. A. and Rouse, H., Diffusion of Submerged Jets, ASCE Transactions Paper No. 2409, 19.

11. Glauert, M. B., The Wall Jet, Journal of Fluid Mechanics, 1956.

12. Sabersky, R. H., and Acosta, A. J., Fluid Flow, The Macmillan Co., New York, 1966

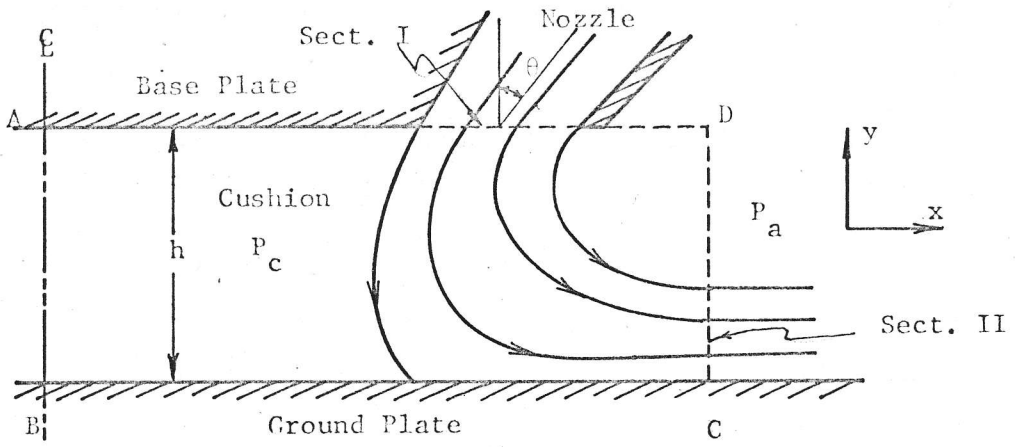

Figure I

Peripheral Jet Fluid Suspension

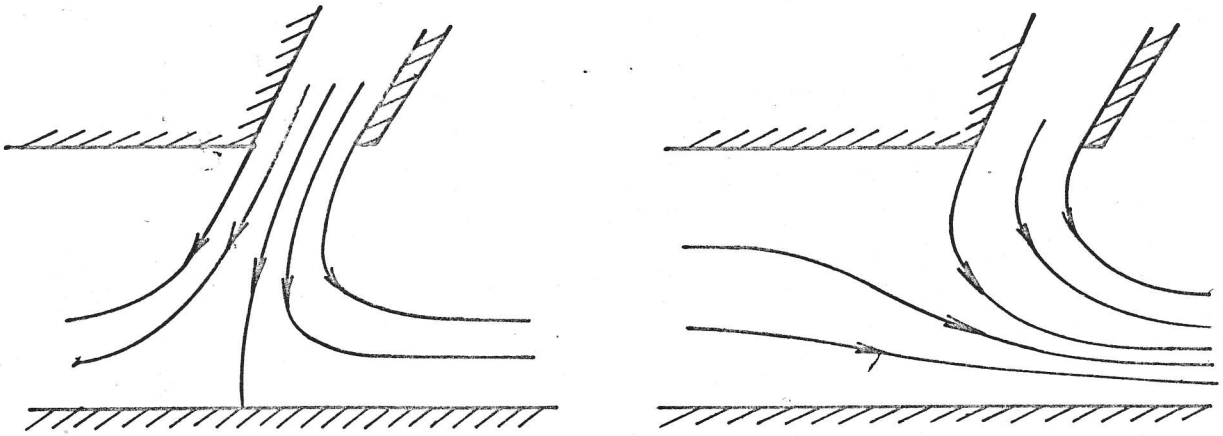

(a) Overfed Cushion

(b) Underfed Cushion

Figure 2

Unbalanced Peripheral Jet

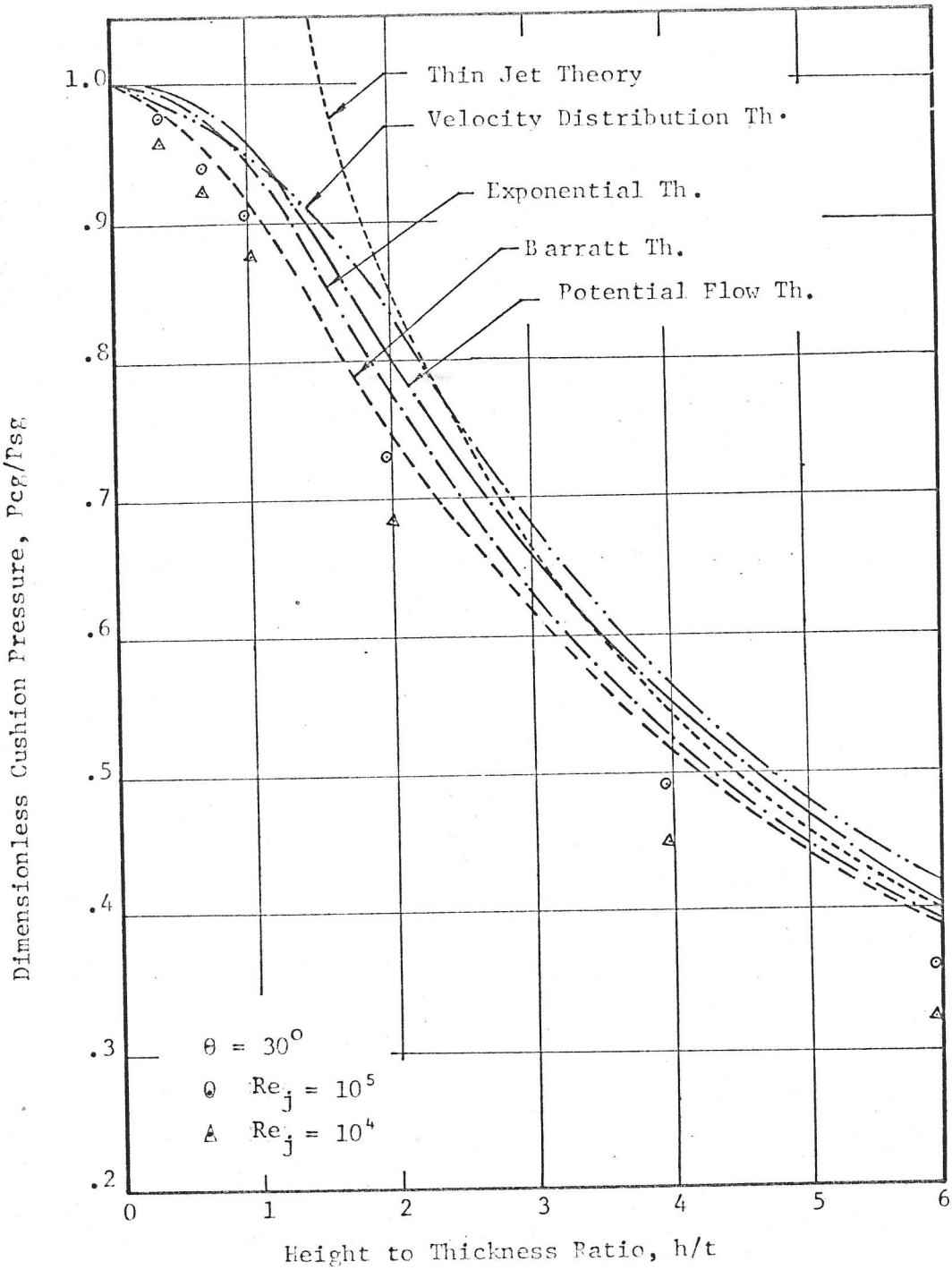

Fig. 3 Comparison of Inviscid Theories for Balanced Peripheral Jet

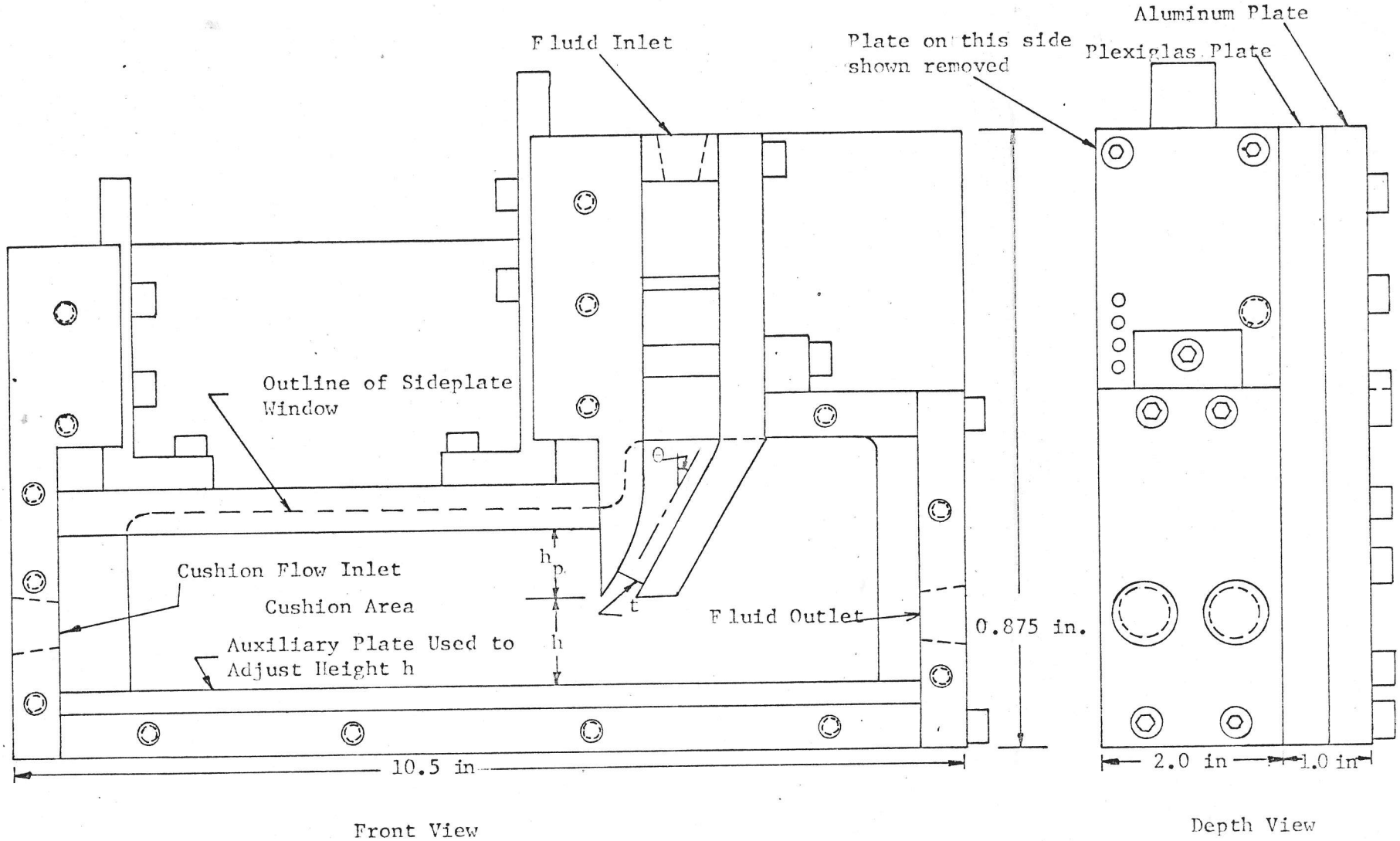

Fig. 4 2-D Fluid Suspension Test Apparatus of M.I.T.

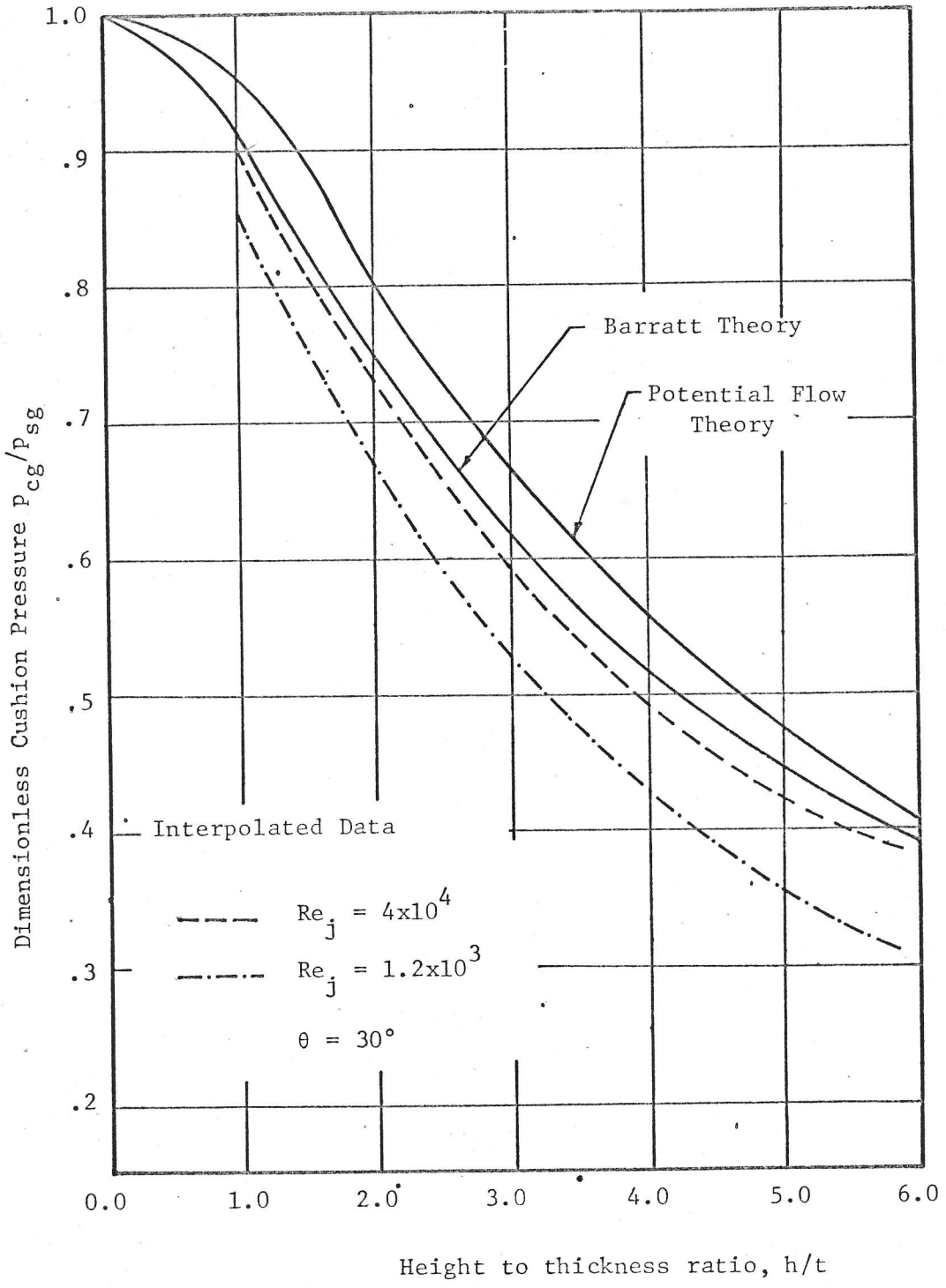

Fig. 5 Interpolated Data for $Re_j = 2.0x10^3$ and $Re_j = 4.1x10^4$

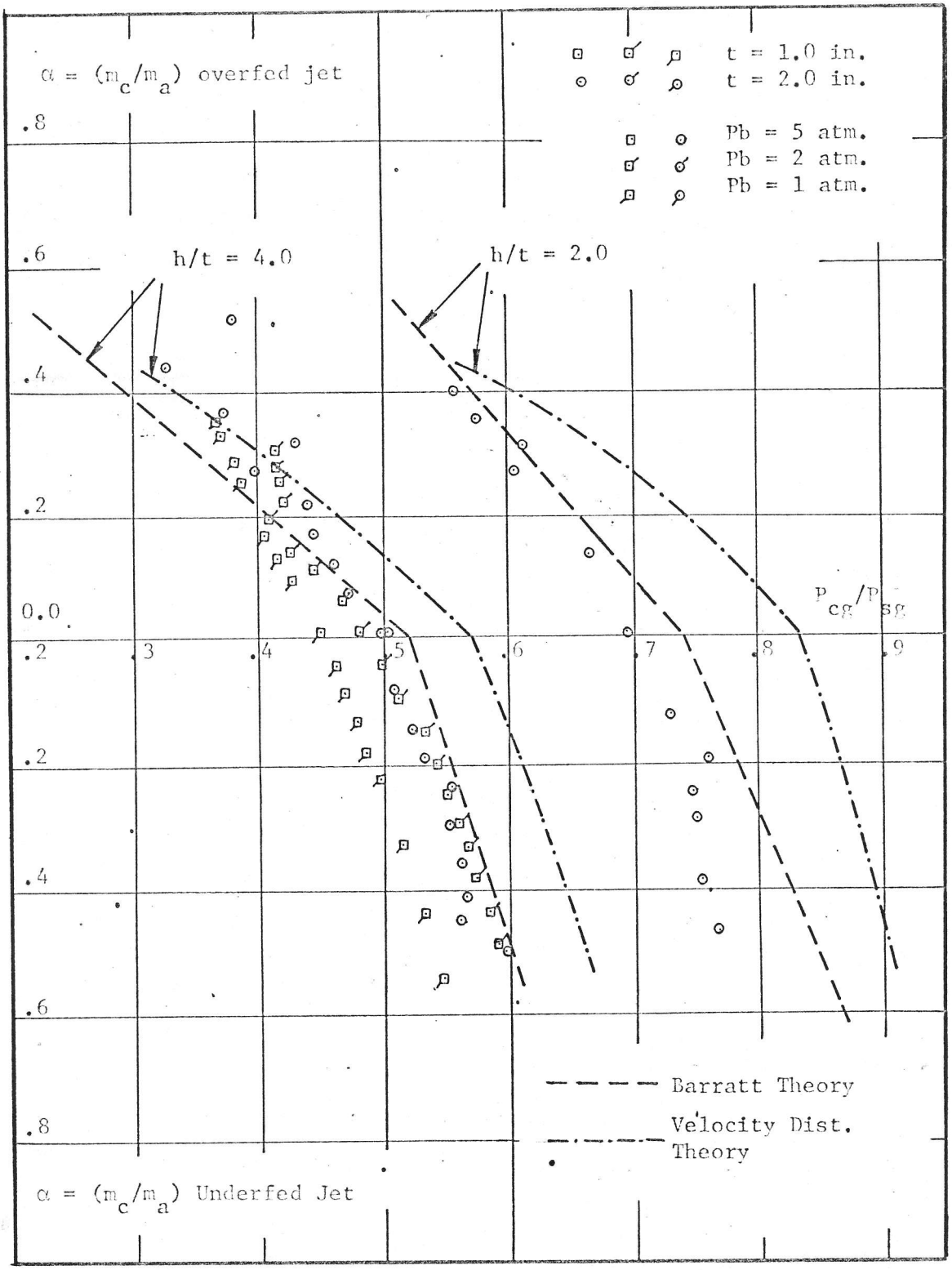

Fig. 6 Data and Inviscid Theories for Unbalanced Jet $\theta = 30^{\circ}$

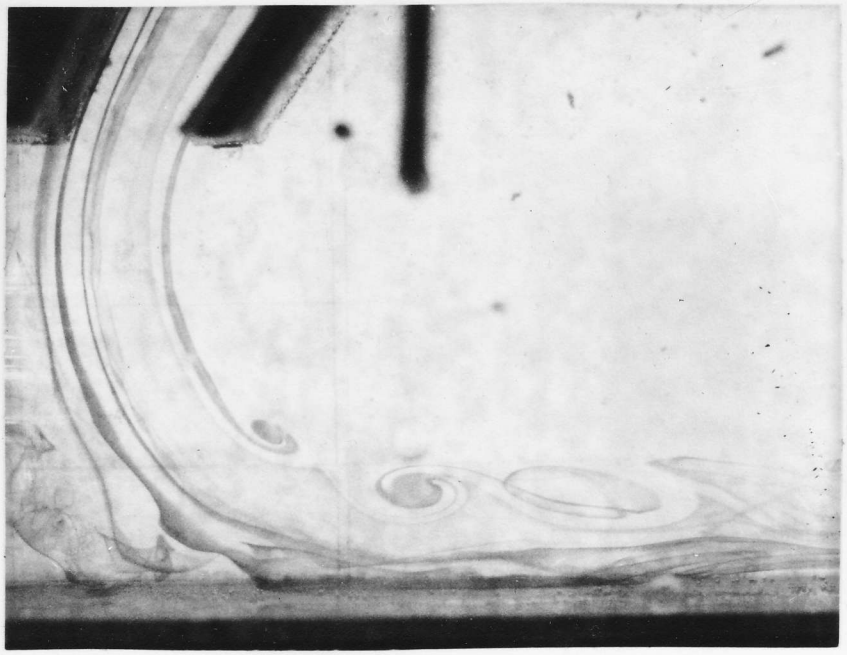

a) Re_j = 1200

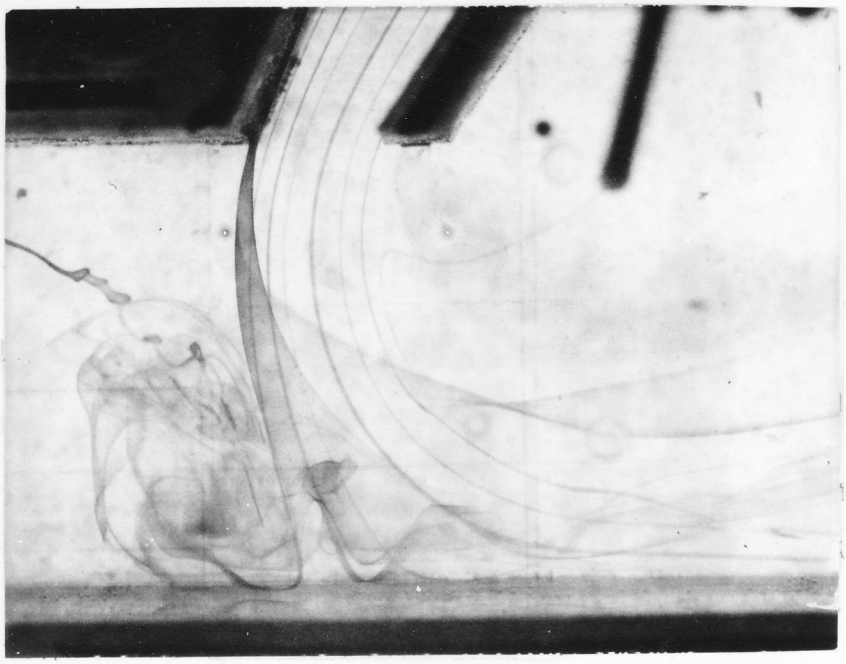

b) Re_j = 500

Fig. 7 Flow Visualization Pictures from Water Table

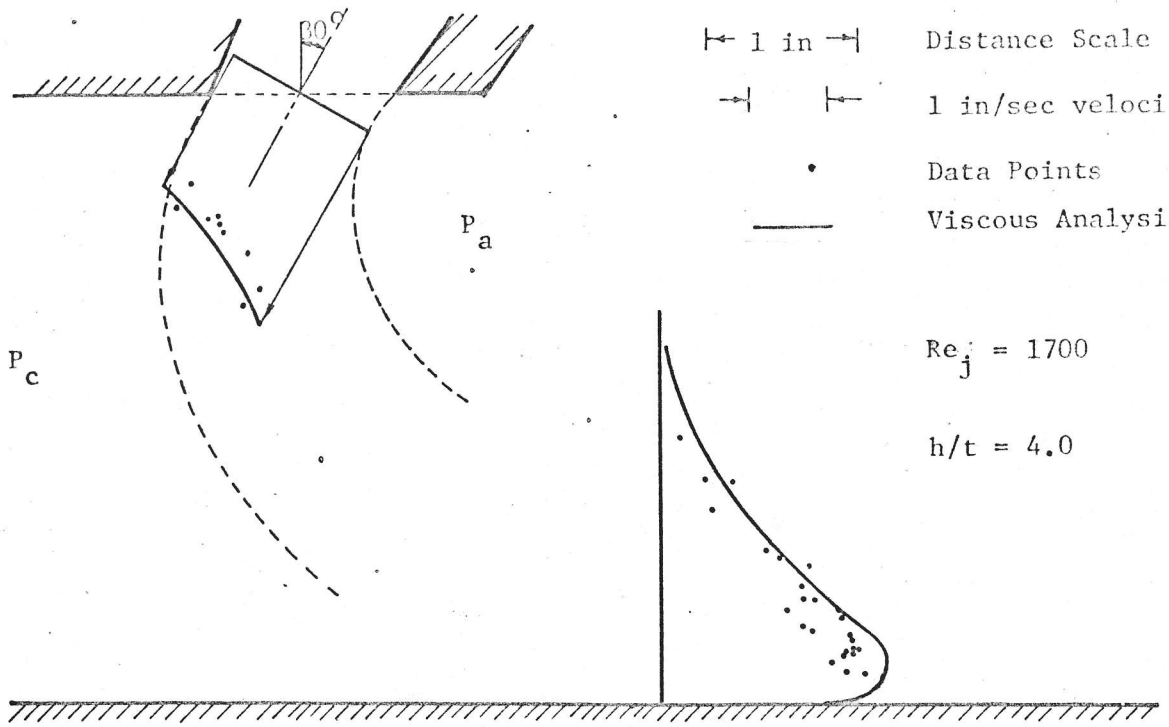

(a)

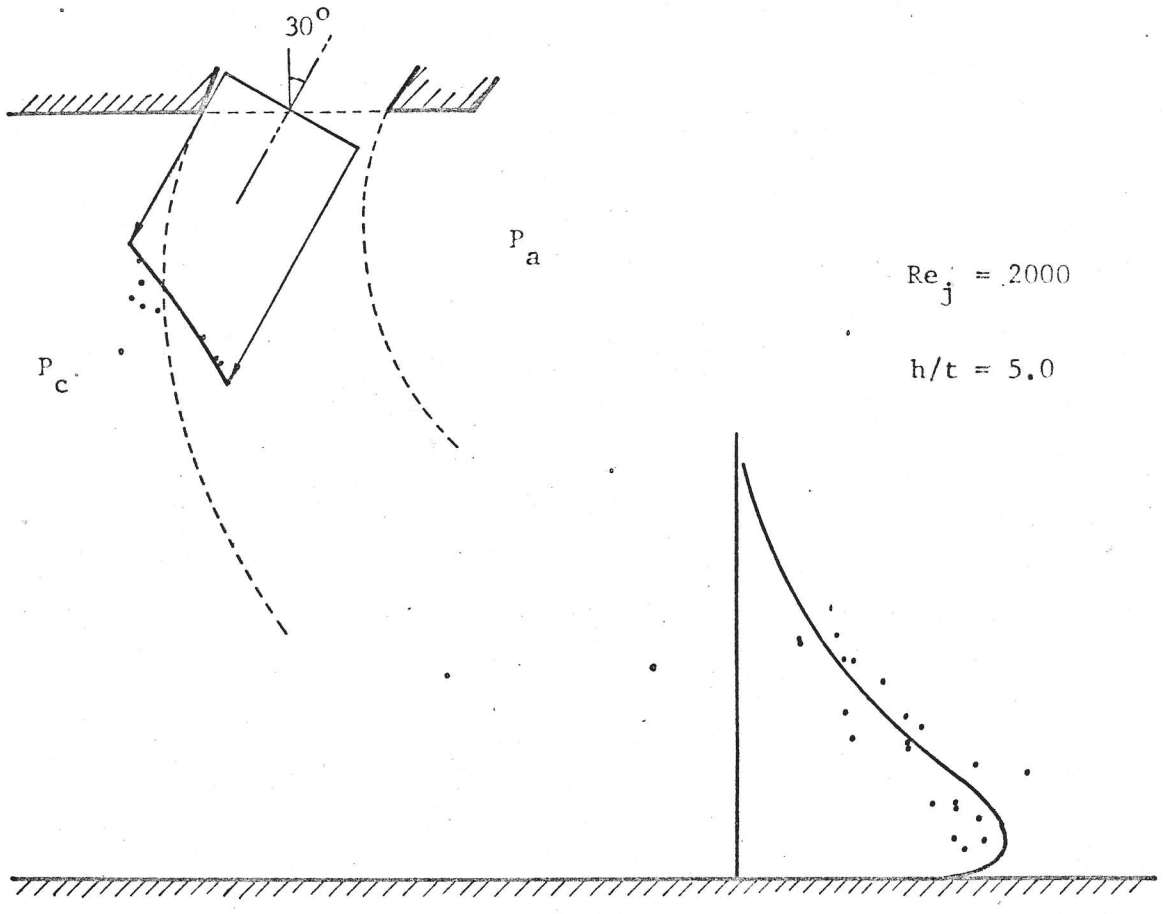

(b)

Figure 8 Velocity Profiles from Water Table

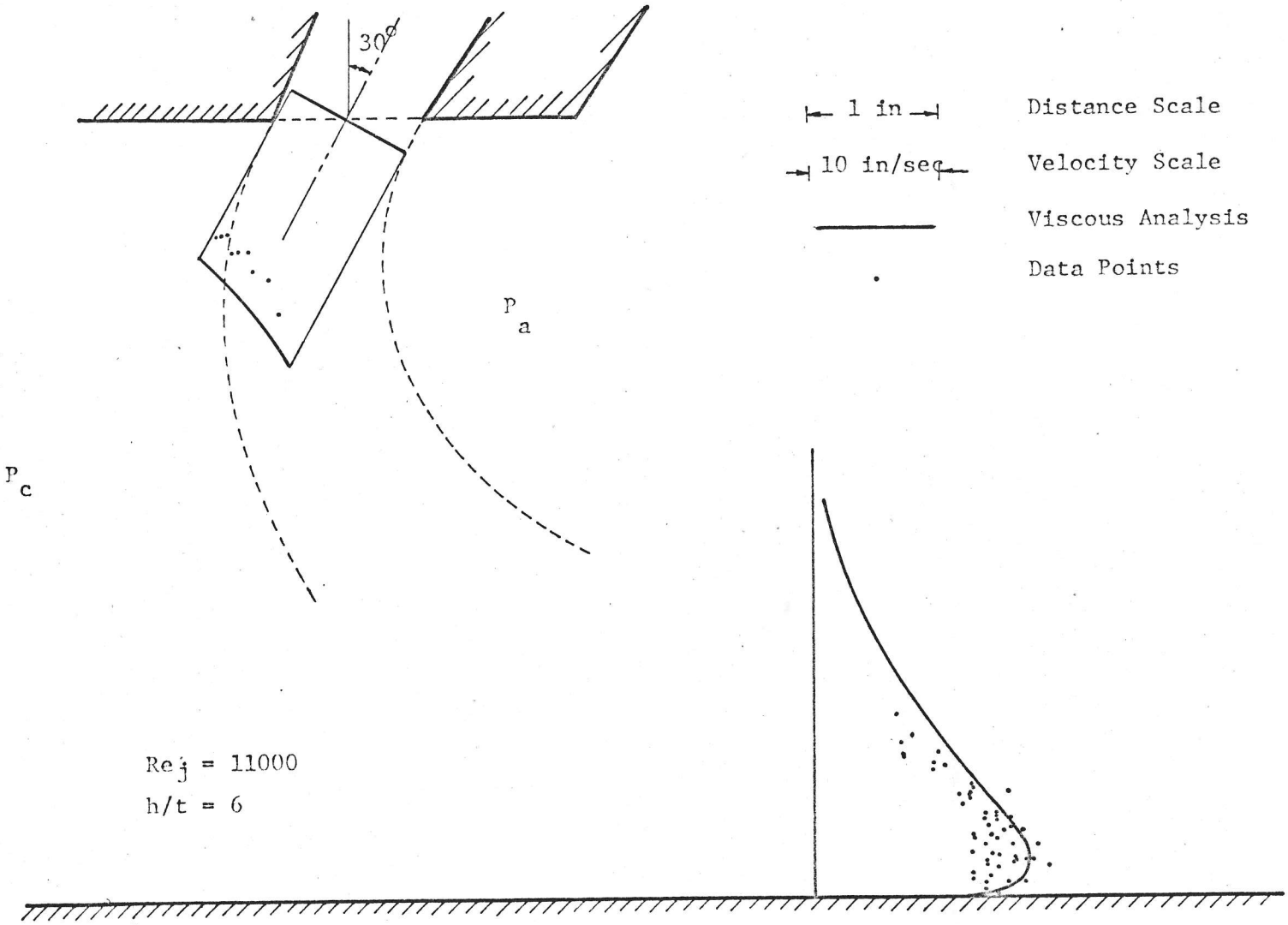

Figure 9 Velocity Profiles from Water Table

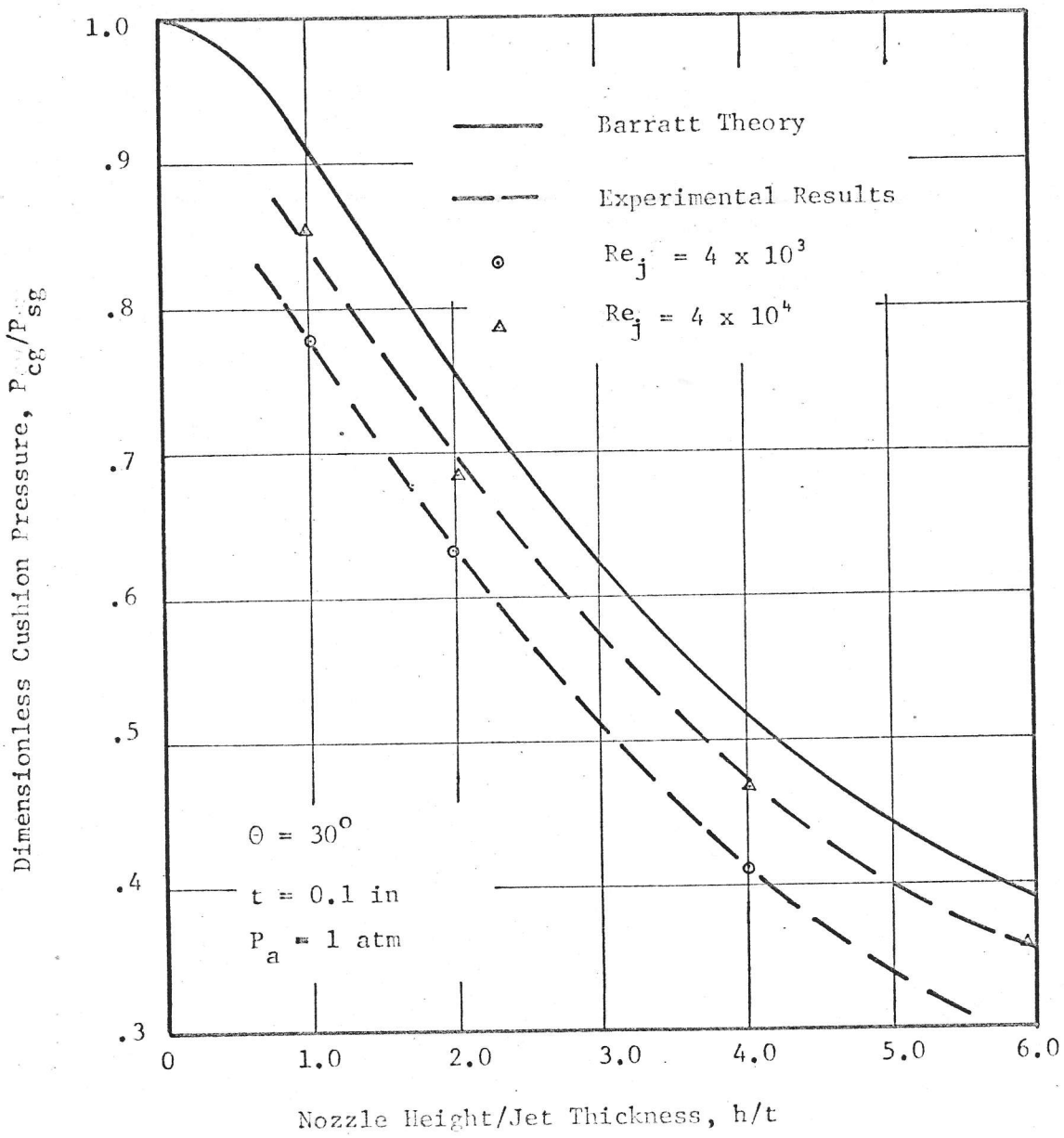
1.0
.9
.8
.7
.6
.5
.4
.3
0
1.0
2.0
3.0
4.0
5.0
6.0
Barratt Theory
Experimental Results
$Re_j = 4 \times 10^3$
$Re_j = 4 \times 10^4$
$\Theta = 30^o$
t = 0.1 in
P_a = 1 atm
Dimensionless Cushion Pressure, P_{cg}/P_{sg}
Nozzle Height/Jet Thickness, h/t

Fig. 10

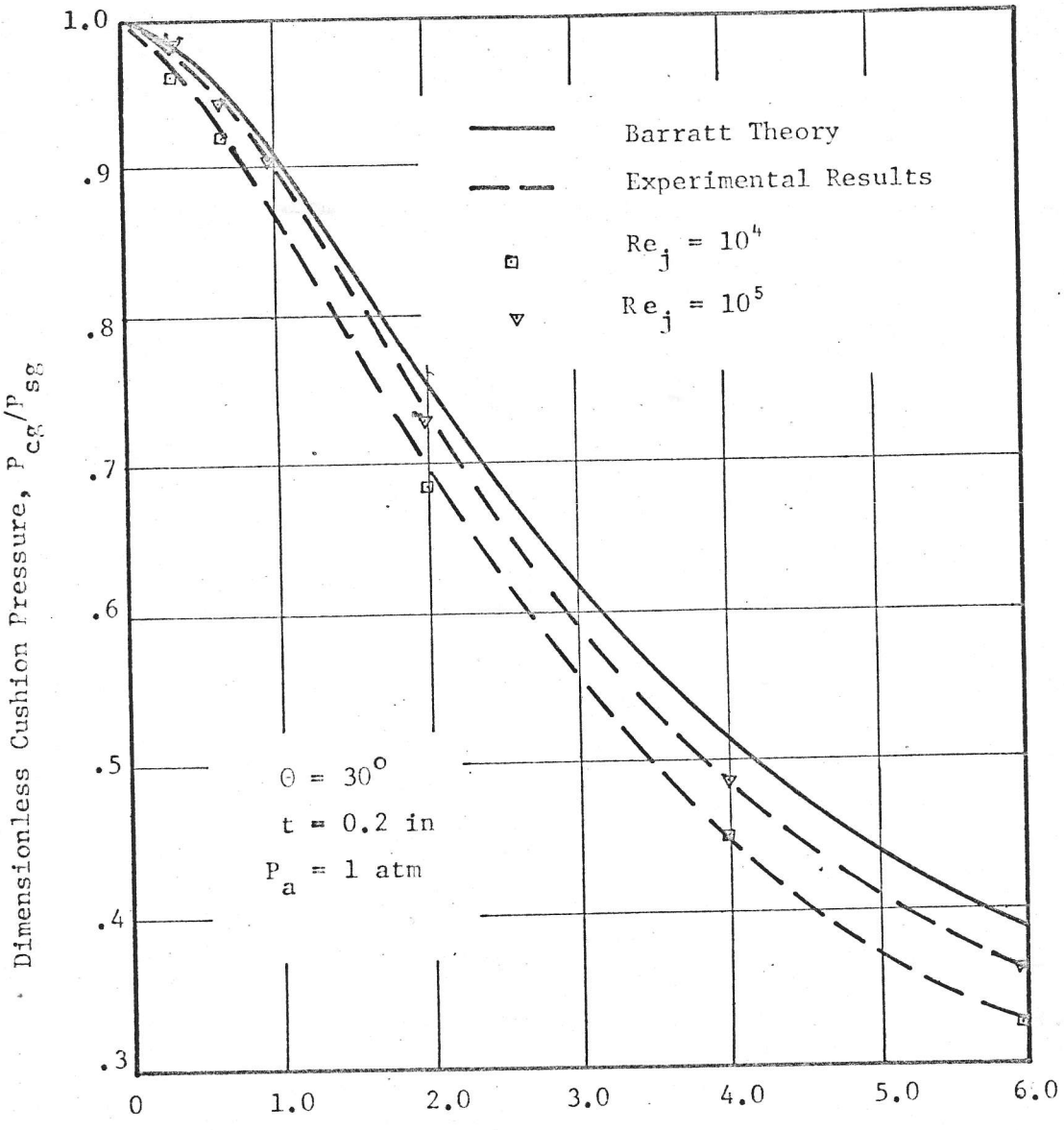
1.0
.9
.8
.7
.6
.5
.4
.3
0
1.0
2.0
3.0
4.0
5.0
6.0
Barratt Theory
Experimental Results
Re_j = 10^4
Re_j = 10^5
θ = 30°
t = 0.2 in
P_a = 1 atm
Dimensionless Cushion Pressure, P_cg/P_sg
Nozzle Height/Jet Thickness, h/t

Fig. 11

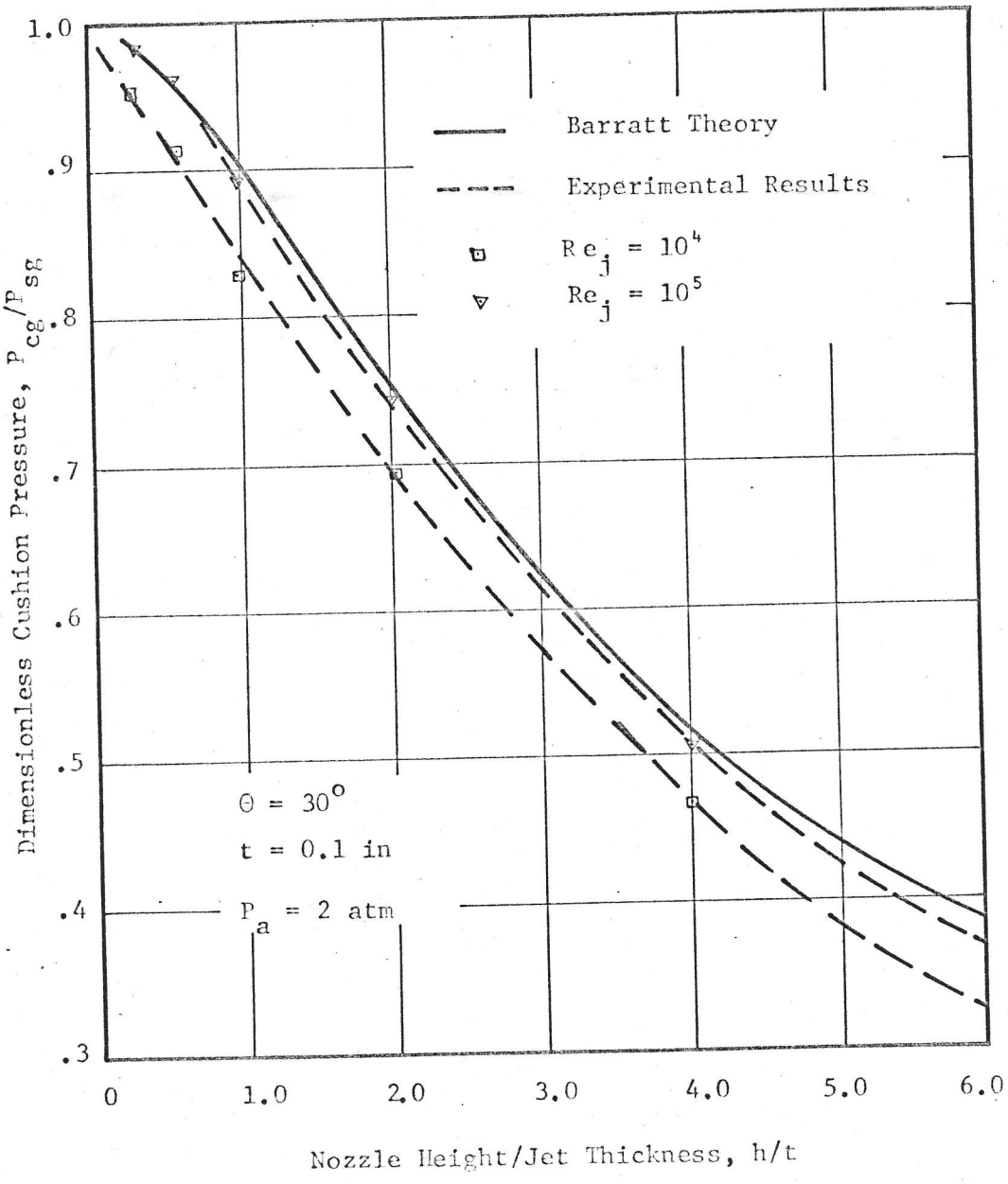
1.0
.9
.8
.7
.6
.5
.4
.3
0
1.0
2.0
3.0
4.0
5.0
6.0
Barratt Theory
Experimental Results
$Re_j = 10^4$
$Re_j = 10^5$
$\Theta = 30^o$
t = 0.1 in
P_a = 2 atm
Dimensionless Cushion Pressure, P_{cg}/P_{sg}
Nozzle Height/Jet Thickness, h/t

Fig. 12

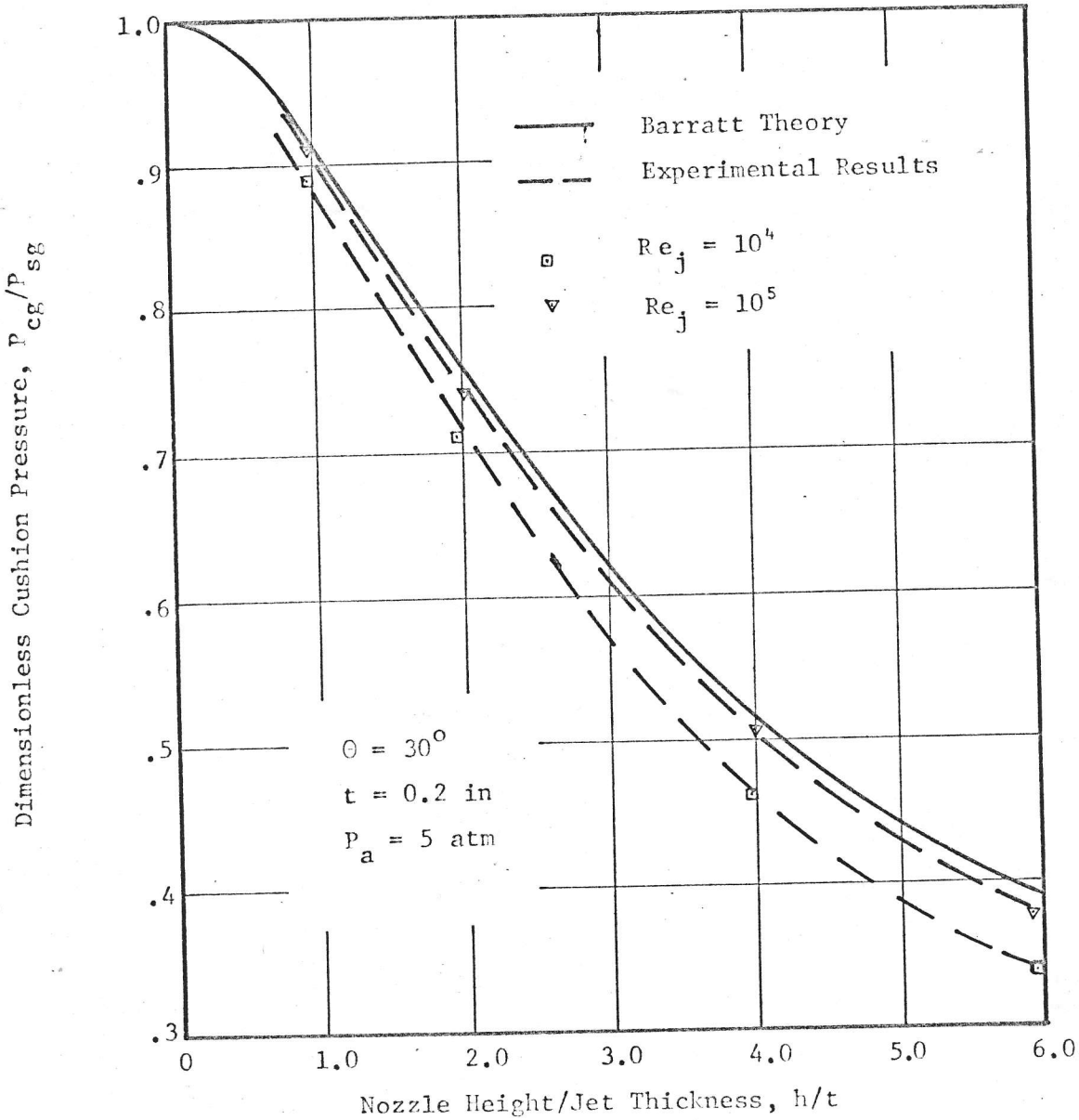
Dimensionless Cushion Pressure, P_{cg}/P_{sg}
1.0
.9
.8
.7
.6
.5
.4
.3
0
1.0
2.0
3.0
4.0
5.0
6.0
Barratt Theory
Experimental Results
$Re_j = 10^4$
$Re_j = 10^5$
$\theta = 30^o$
t = 0.2 in
P_a = 5 atm
Nozzle Height/Jet Thickness, h/t

Fig. 13

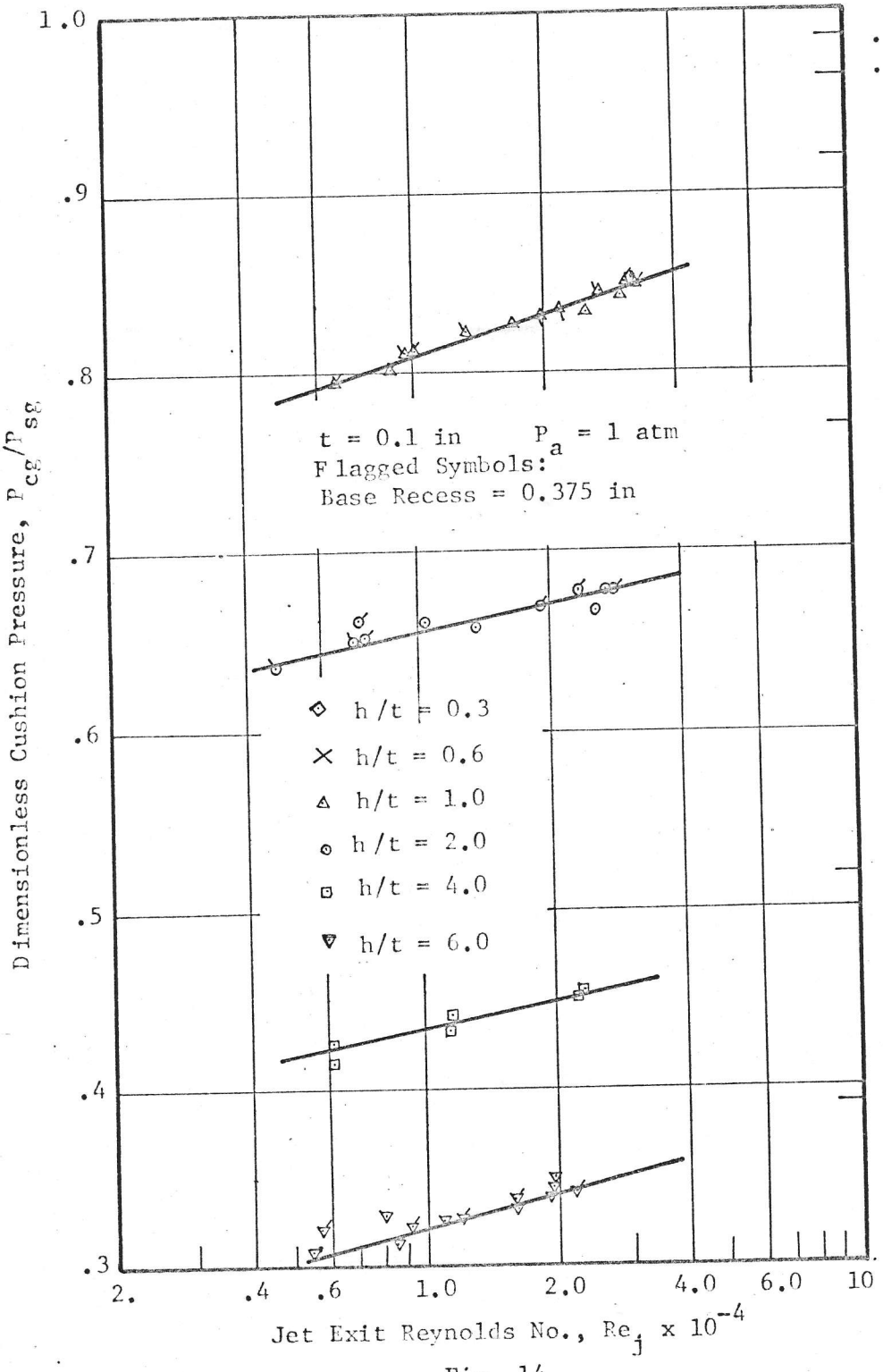
1.0
.9
.8
.7
.6
.5
.4
.3
2.
.4
.6
1.0
2.0
4.0
6.0
10
Dimensionless Cushion Pressure, P_{cg}/P_{sg}
Jet Exit Reynolds No., $Re_j \times 10^{-4}$
t = 0.1 in
P_a = 1 atm
Flagged Symbols:
Base Recess = 0.375 in
h/t = 0.3
h/t = 0.6
h/t = 1.0
h/t = 2.0
h/t = 4.0
h/t = 6.0
.3
.6
1
2
4
6
Theoretical Values From Barratt Theory
(Number Indicates h/t Ratio)

Fig. 14

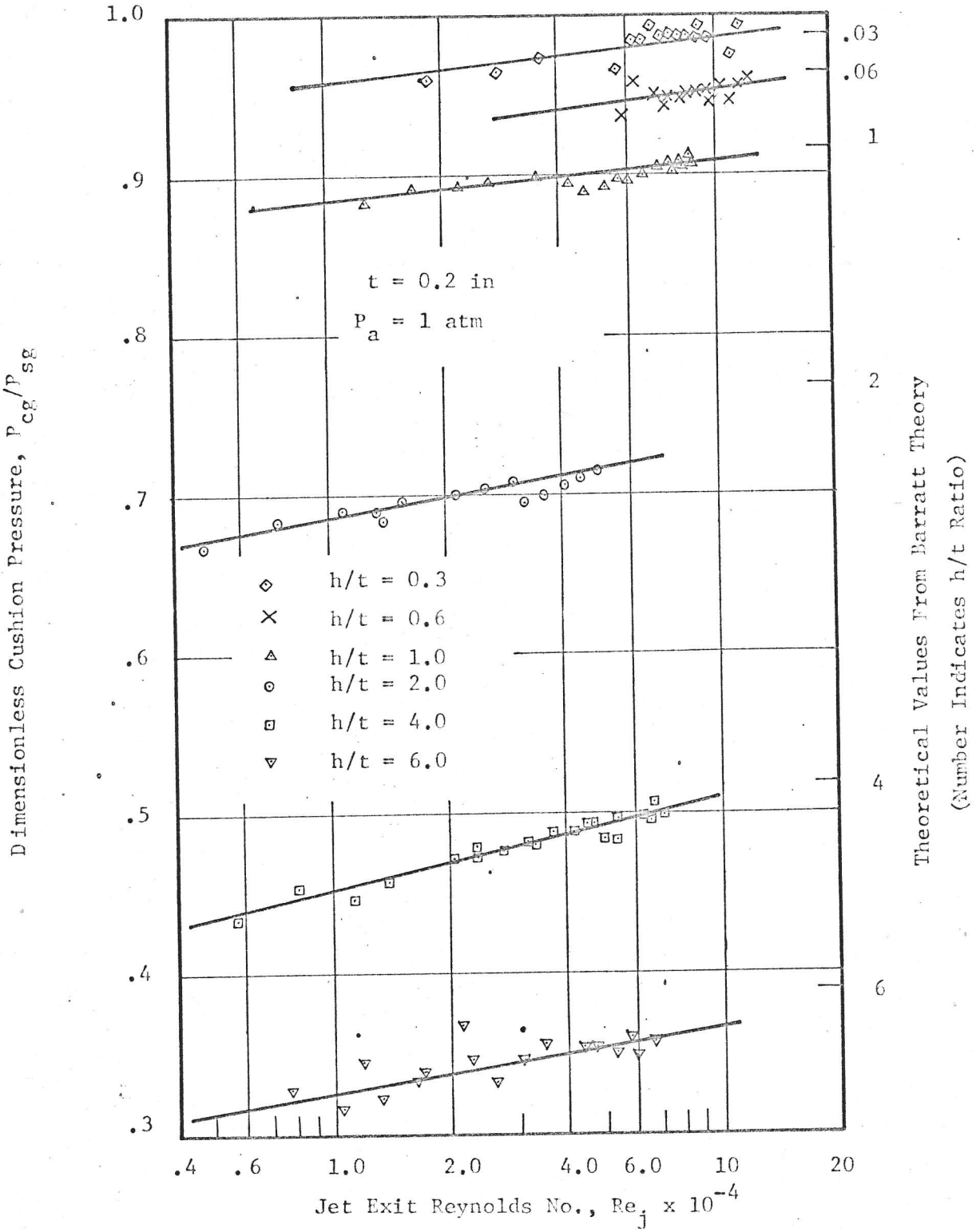
1.0
.9
.8
.7
.6
.5
.4
.3
.4
.6
1.0
2.0
4.0
6.0
10
20
Jet Exit Reynolds No., Re_j x 10^-4
Dimensionless Cushion Pressure, P_cg/P_sg
t = 0.2 in
P_a = 1 atm
h/t = 0.3
h/t = 0.6
h/t = 1.0
h/t = 2.0
h/t = 4.0
h/t = 6.0
.03
.06
1
2
4
6
Theoretical Values From Barratt Theory
(Number Indicates h/t Ratio)

Fig. 15

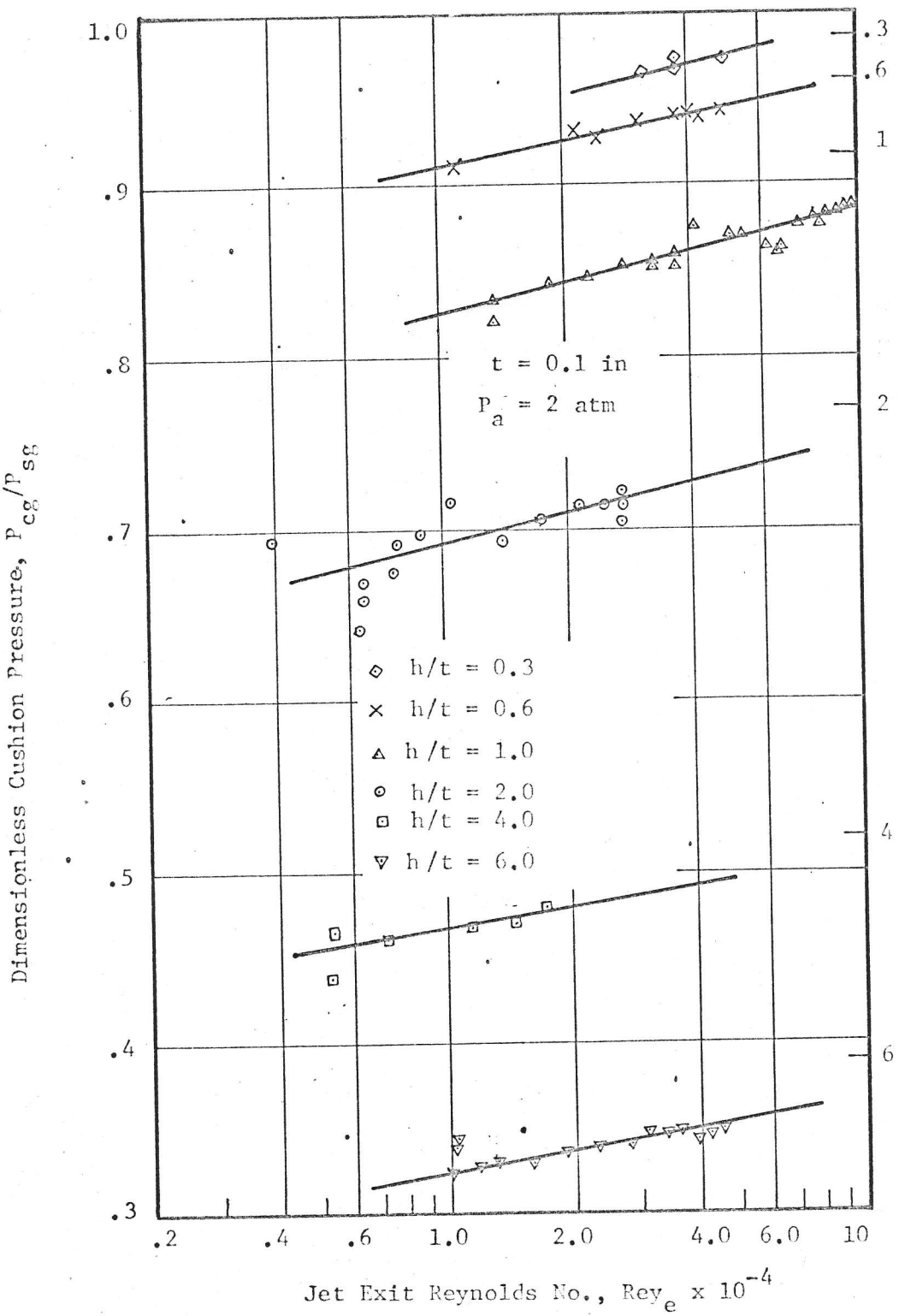
Dimensionless Cushion Pressure, P_{cg}/P_{sg}
1.0
.9
.8
.7
.6
.5
.4
.3
.2
.4
.6
1.0
2.0
4.0
6.0
10
Jet Exit Reynolds No., $Rey_e \times 10^{-4}$
t = 0.1 in
P_a = 2 atm
h/t = 0.3
h/t = 0.6
h/t = 1.0
h/t = 2.0
h/t = 4.0
h/t = 6.0
.3
.6
1
2
4
6
Theoretical Values From Barratt Theory
(Number Indicates h/t Ratio)

Fig. 16

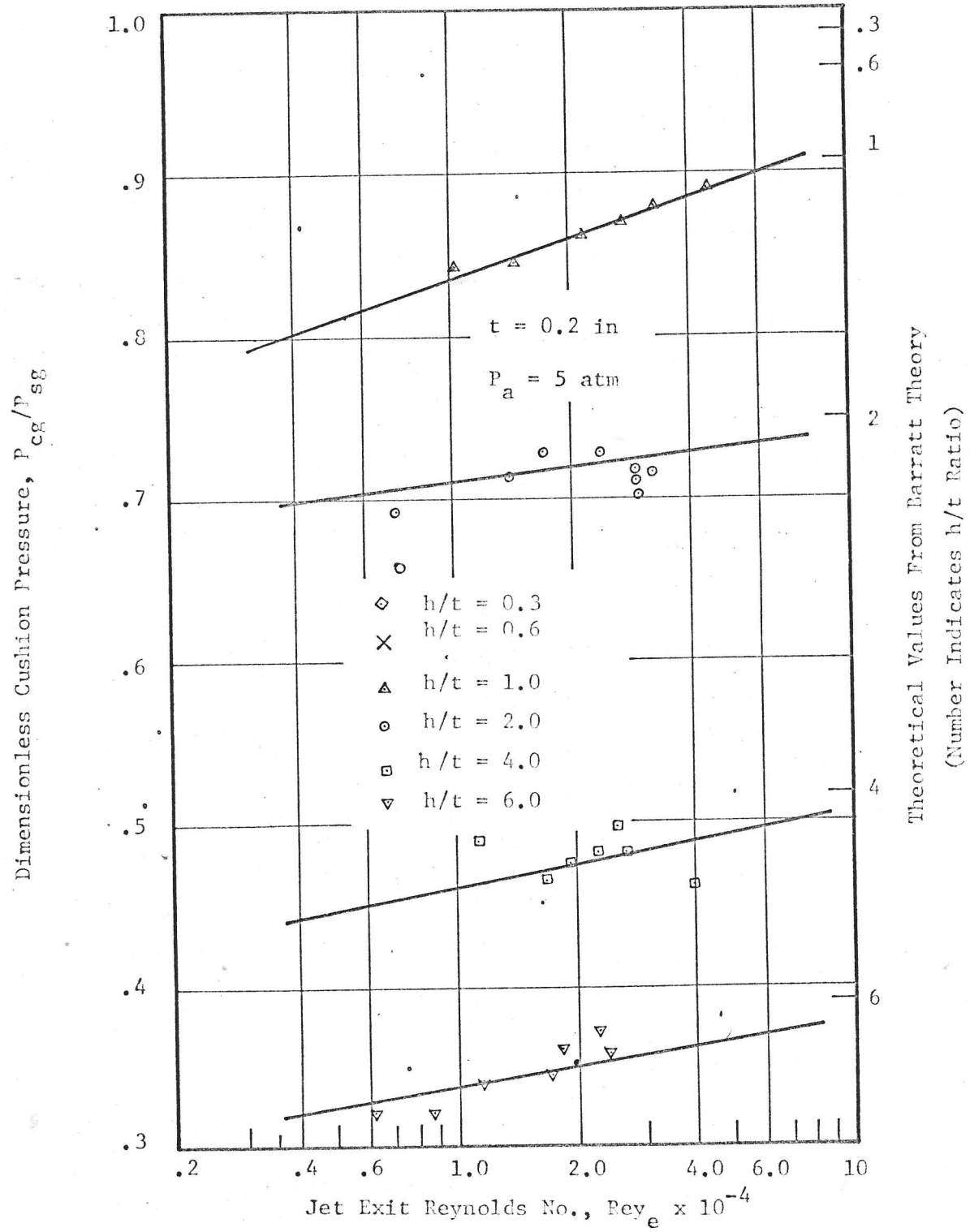
Dimensionless Cushion Pressure, P_{cg}/P_{sg}
1.0
.9
.8
.7
.6
.5
.4
.3
.2
.4
.6
1.0
2.0
4.0
6.0
10
Jet Exit Reynolds No., $Rey_e \times 10^{-4}$
t = 0.2 in
P_a = 5 atm
h/t = 0.3
h/t = 0.6
h/t = 1.0
h/t = 2.0
h/t = 4.0
h/t = 6.0
.3
.6
1
2
4
6
Theoretical Values From Barratt Theory
(Number Indicates h/t Ratio)

Fig. 17

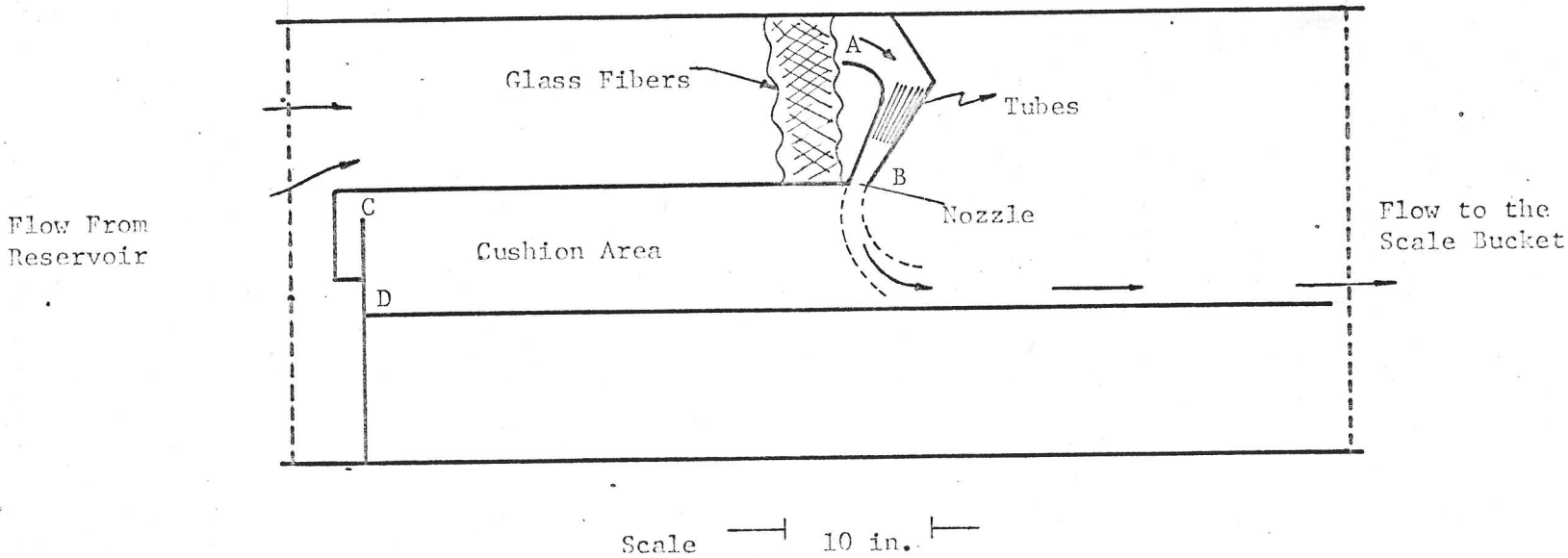

Fig. 18 Top View of the Water Table

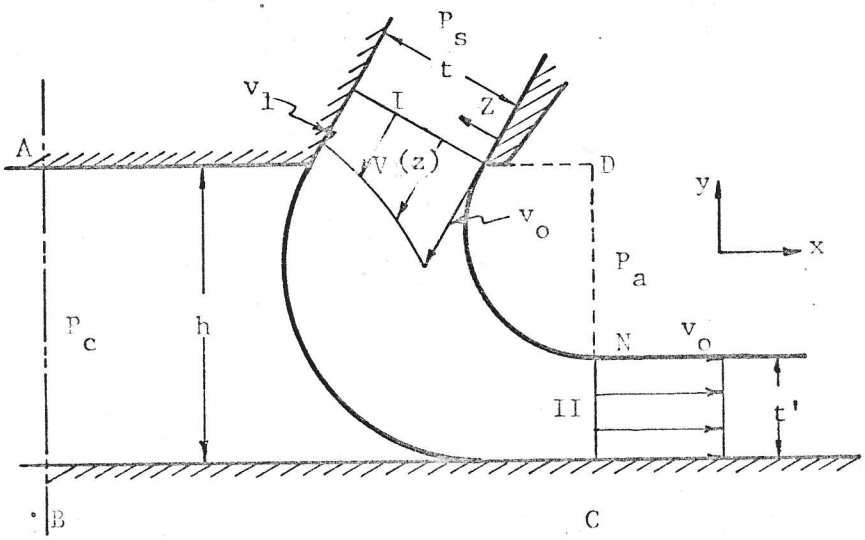

Fig. 19 Inviscid Peripheral Jet Model

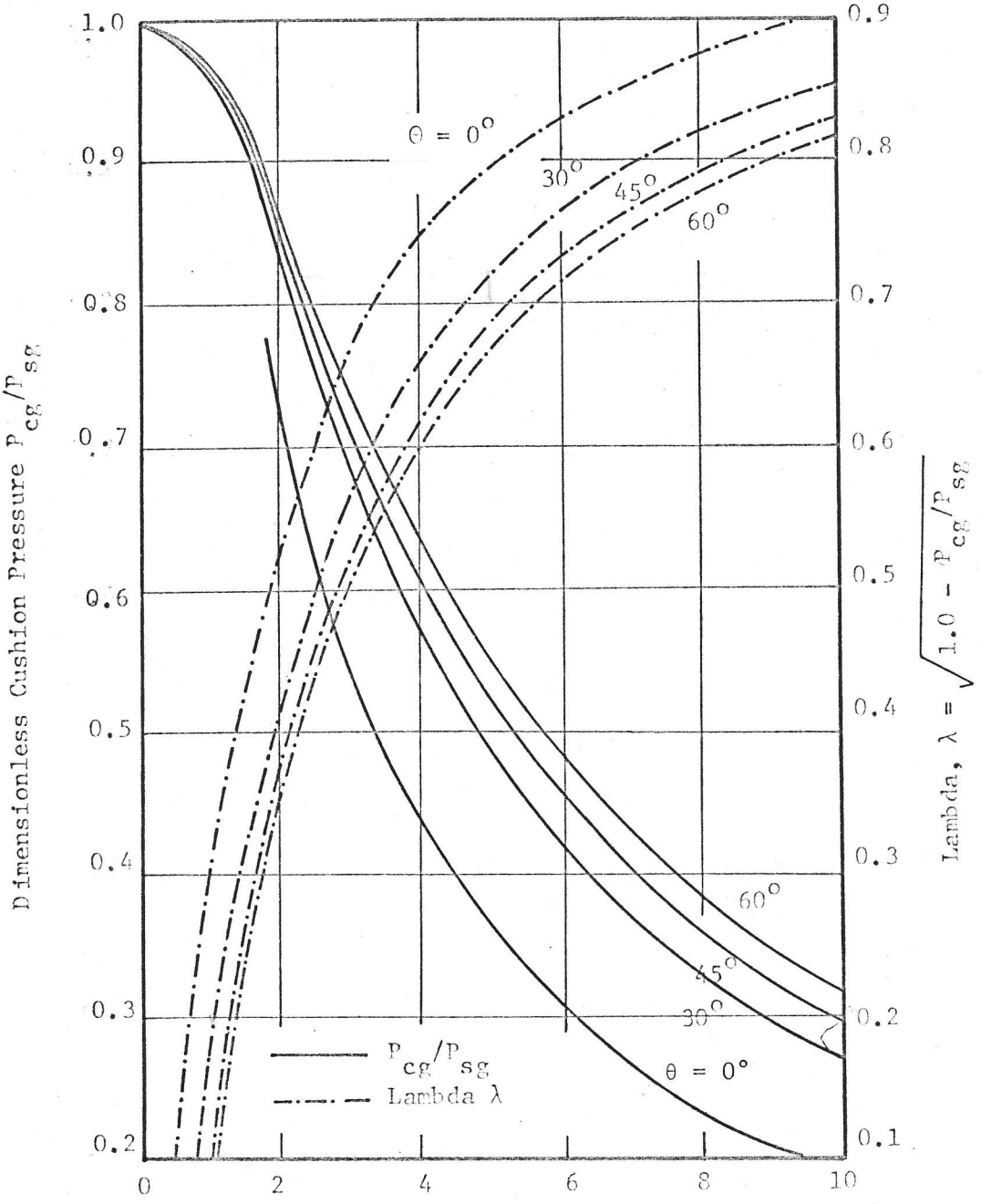

Fig. 20 Velocity Distribution Theory for Inviscid Jet

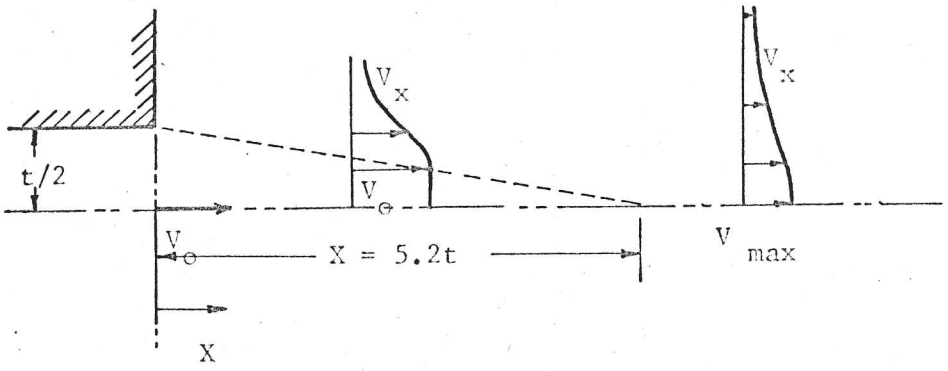

Fig. 21 Submerged Jet

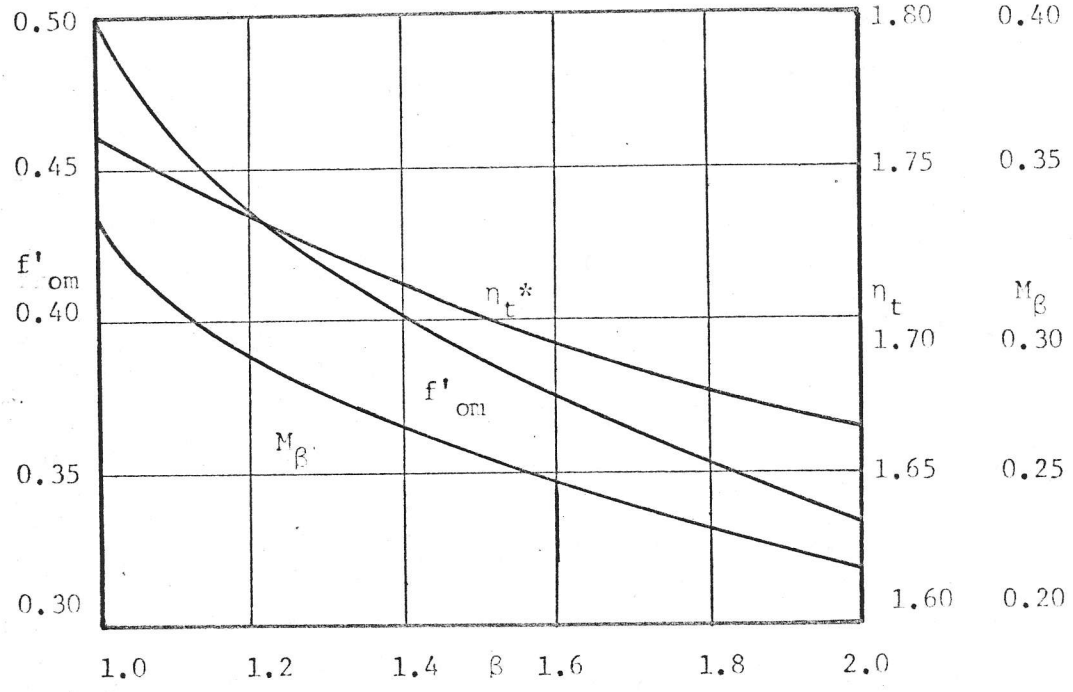

Fig. 22 Results from Turbulent Wall Jet

* From Glauert Solution

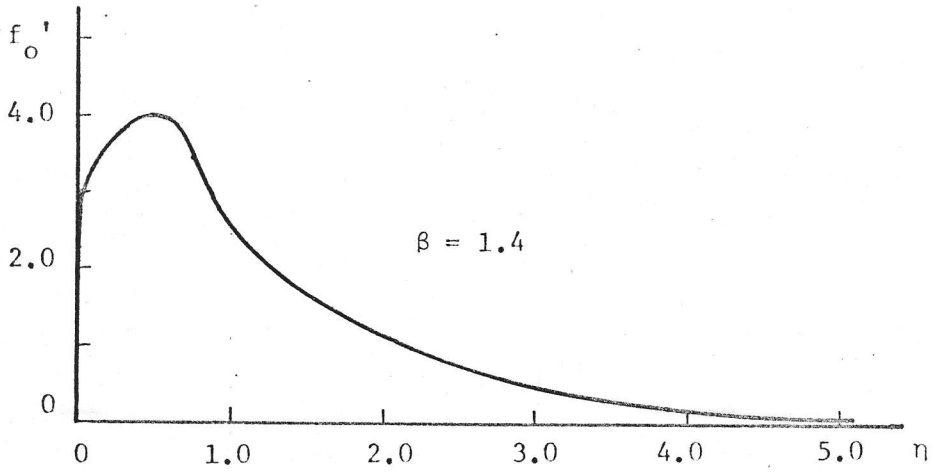

Fig. 23 Dimensionless Velocity Profile For Wall Jet

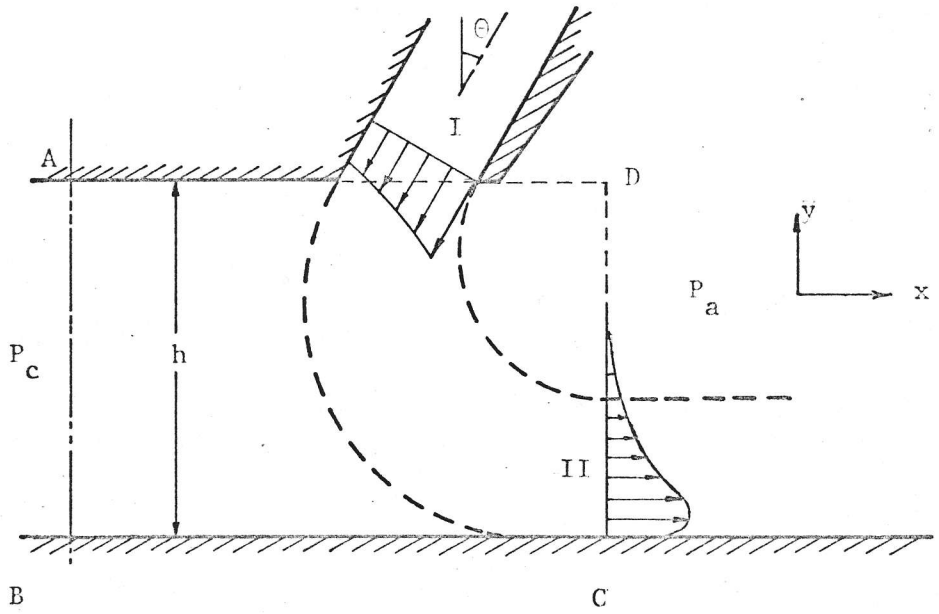

Fig. 24 Viscous Peripheral Jet Model

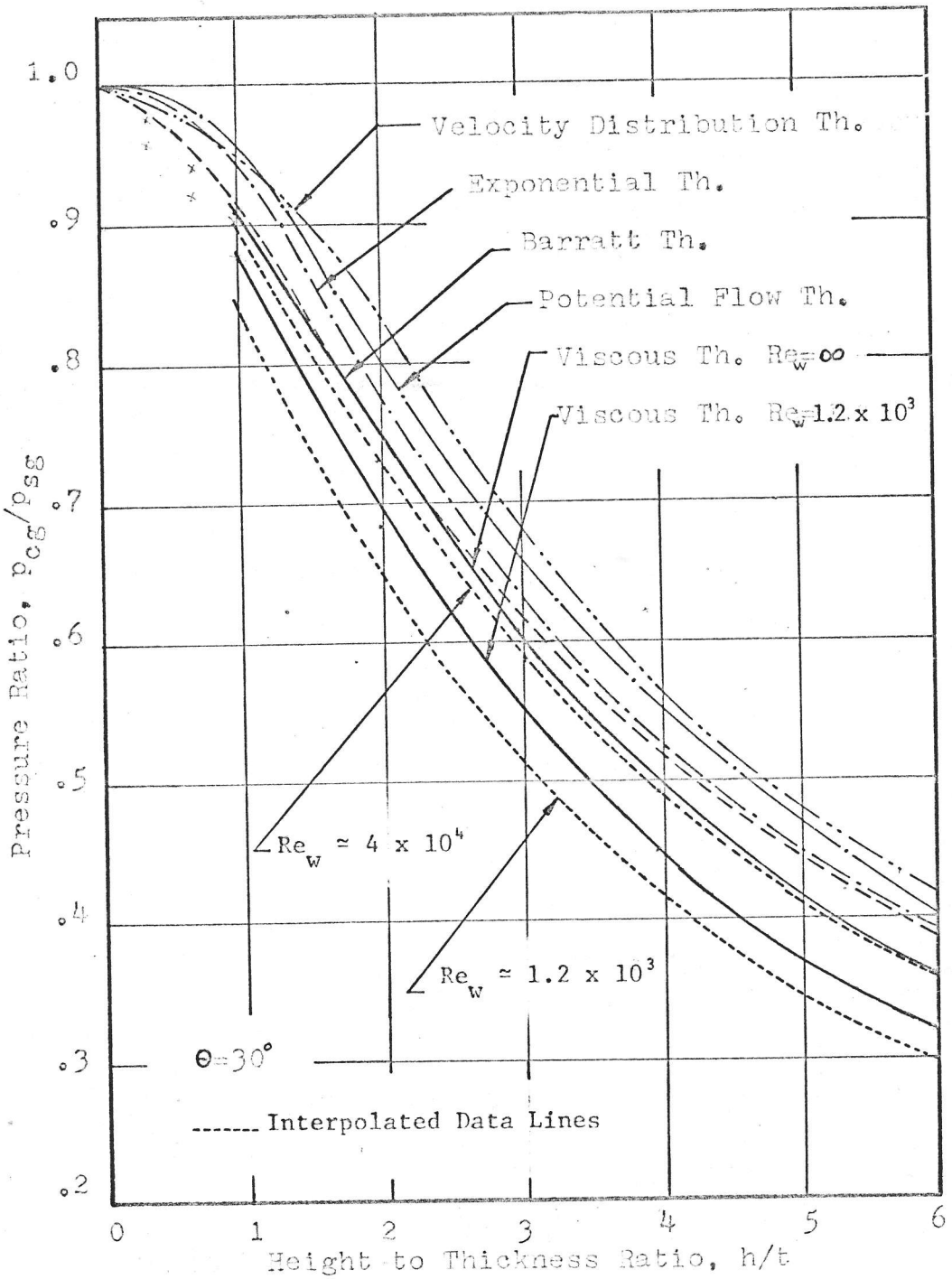

Fig.25 Comparison of Theories for Peripheral Jet

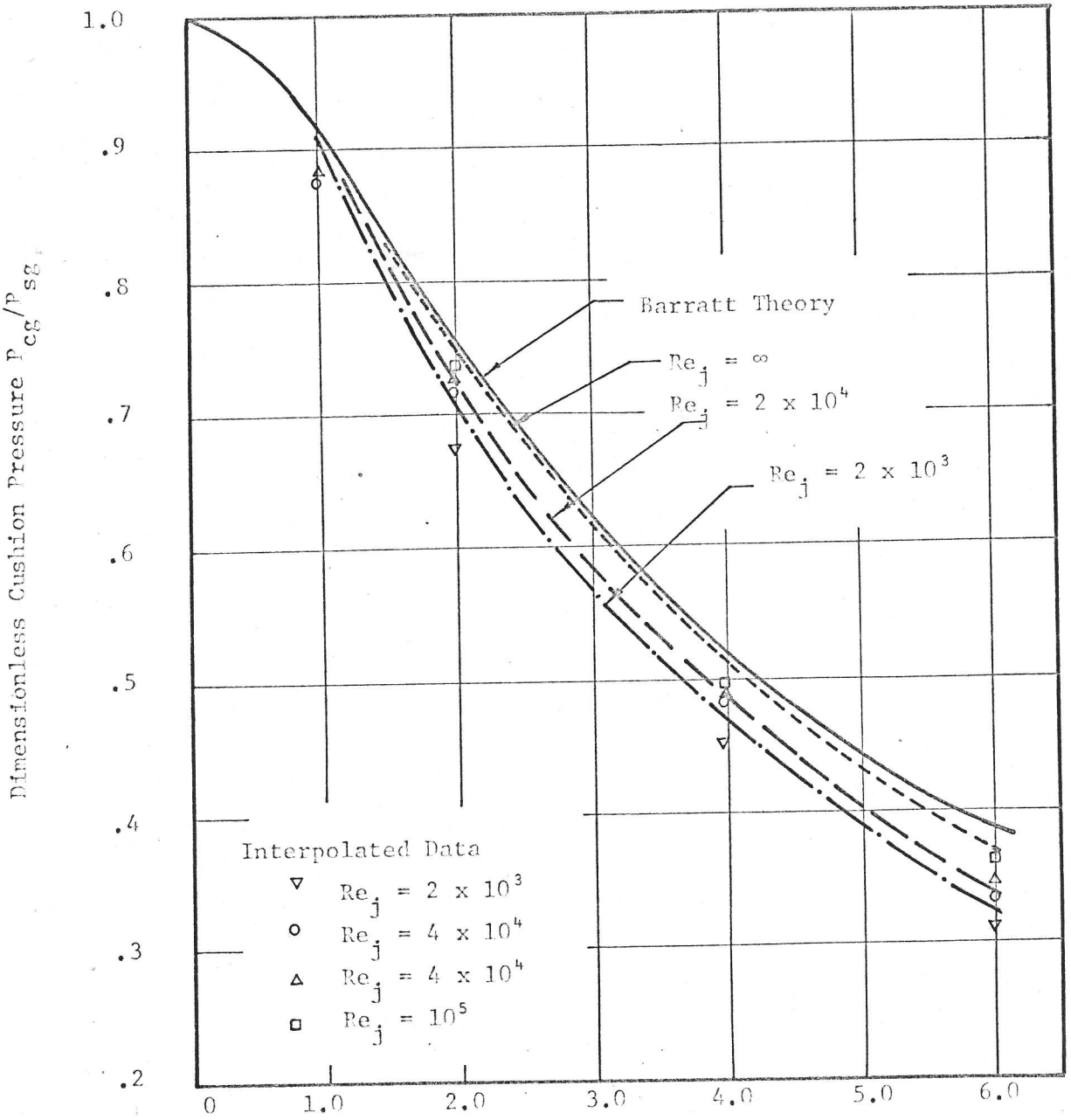

Fig. 26 Viscous Theory Results for a Given Re_j

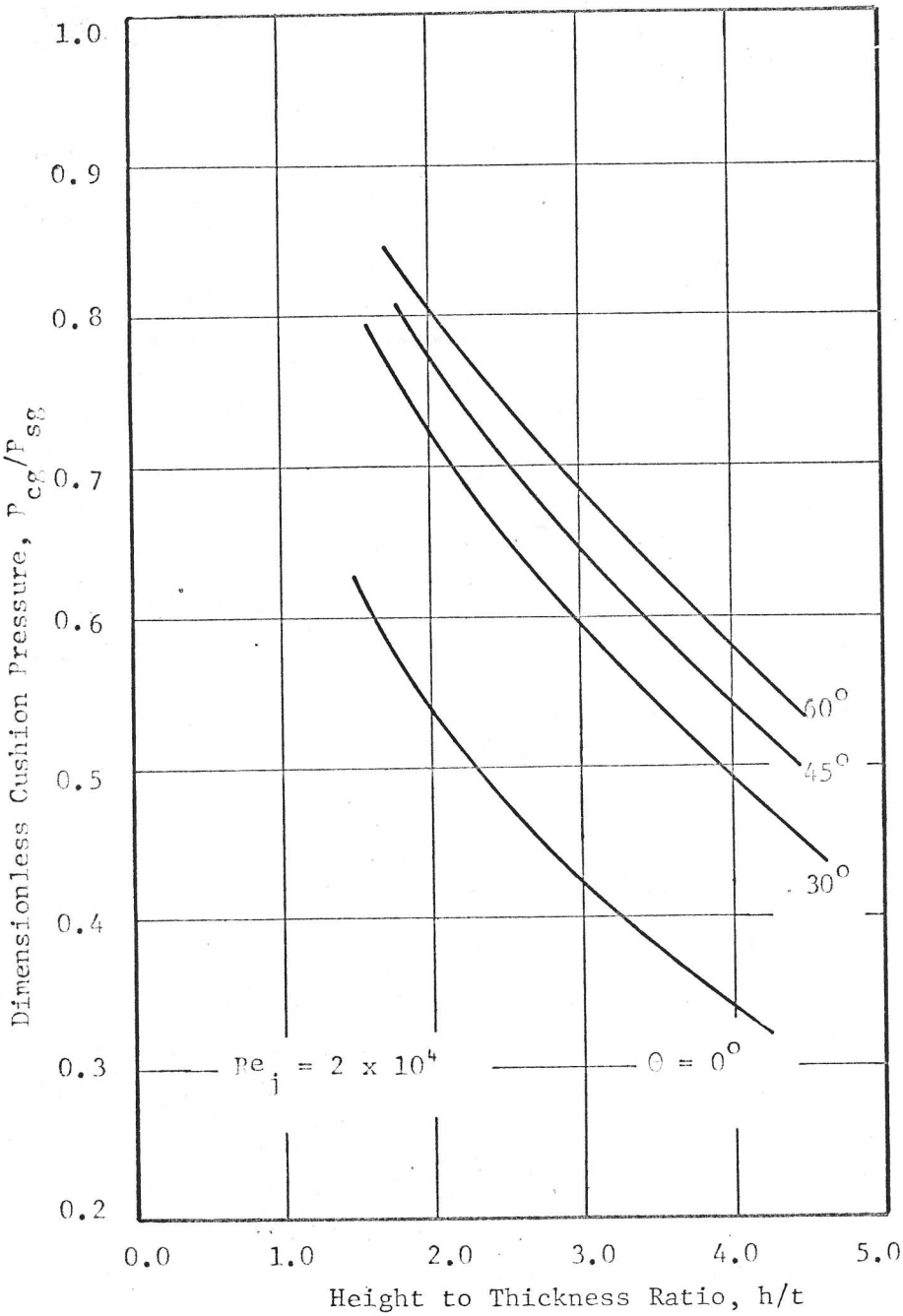

Fig.27 Effect of θ on Viscous Theory, $Re_j = 2 \times 10^4$

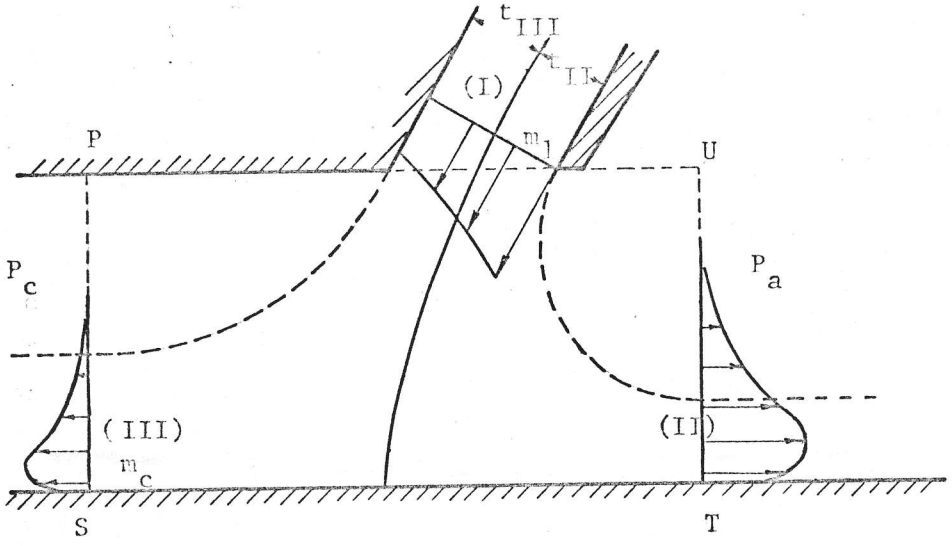

Fig. 28 Overfed Jet

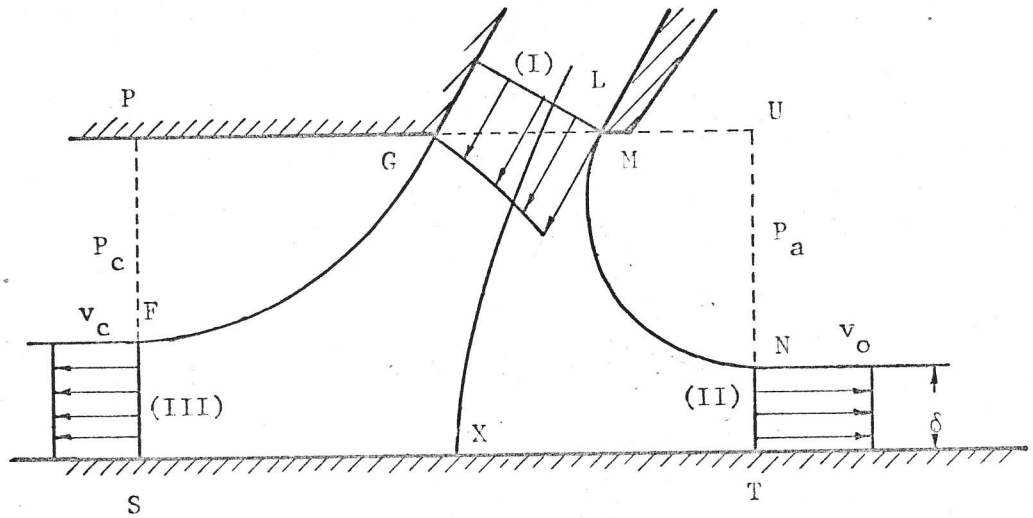

Fig. 29 Inviscid Overfed Jet

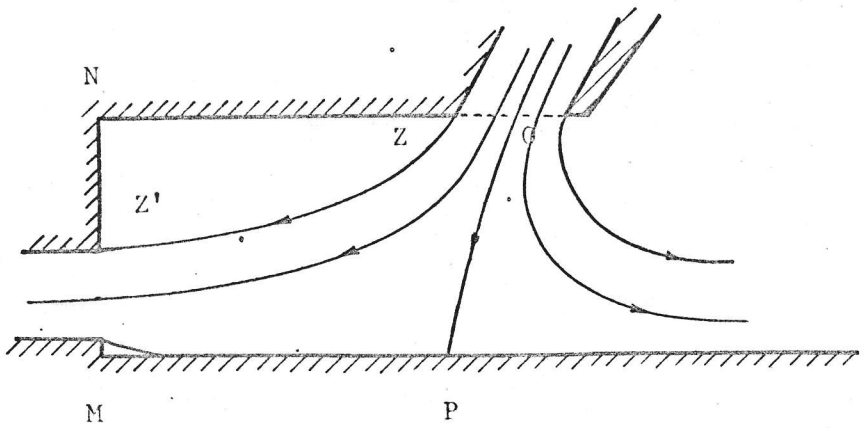

Fig. 30 Flow Pattern in 2-D Test Apparatus

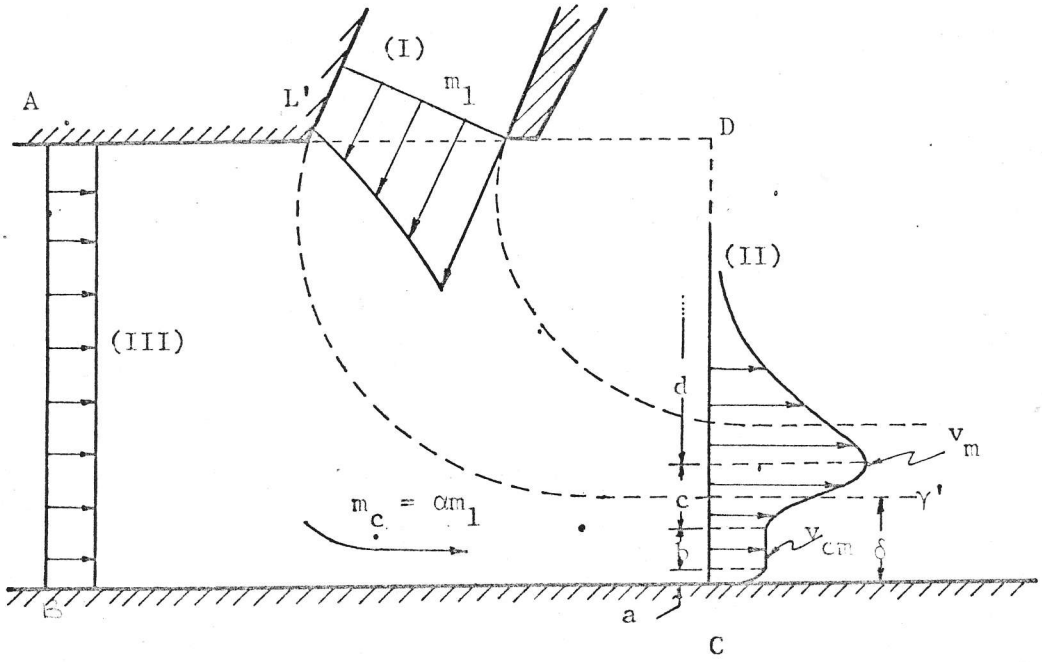

Fig. 31 Underfed Jet

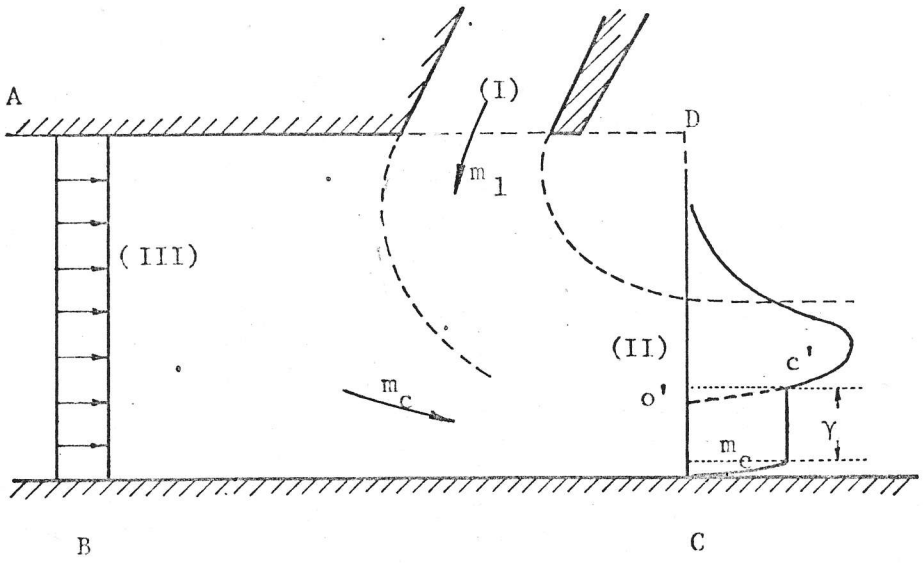

Fig. 32 Modified Underfed Jet

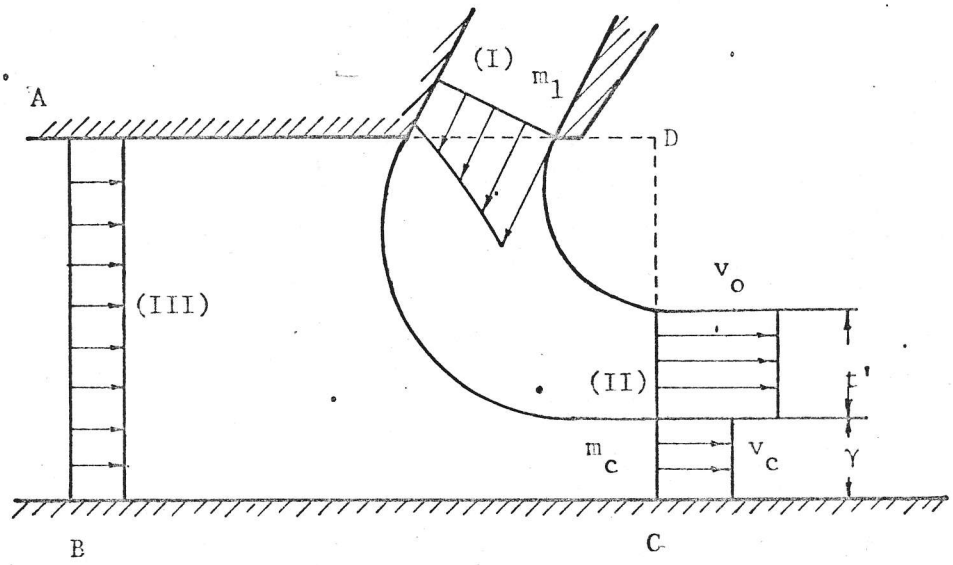

Fig. 33 Inviscid Underfed Jet

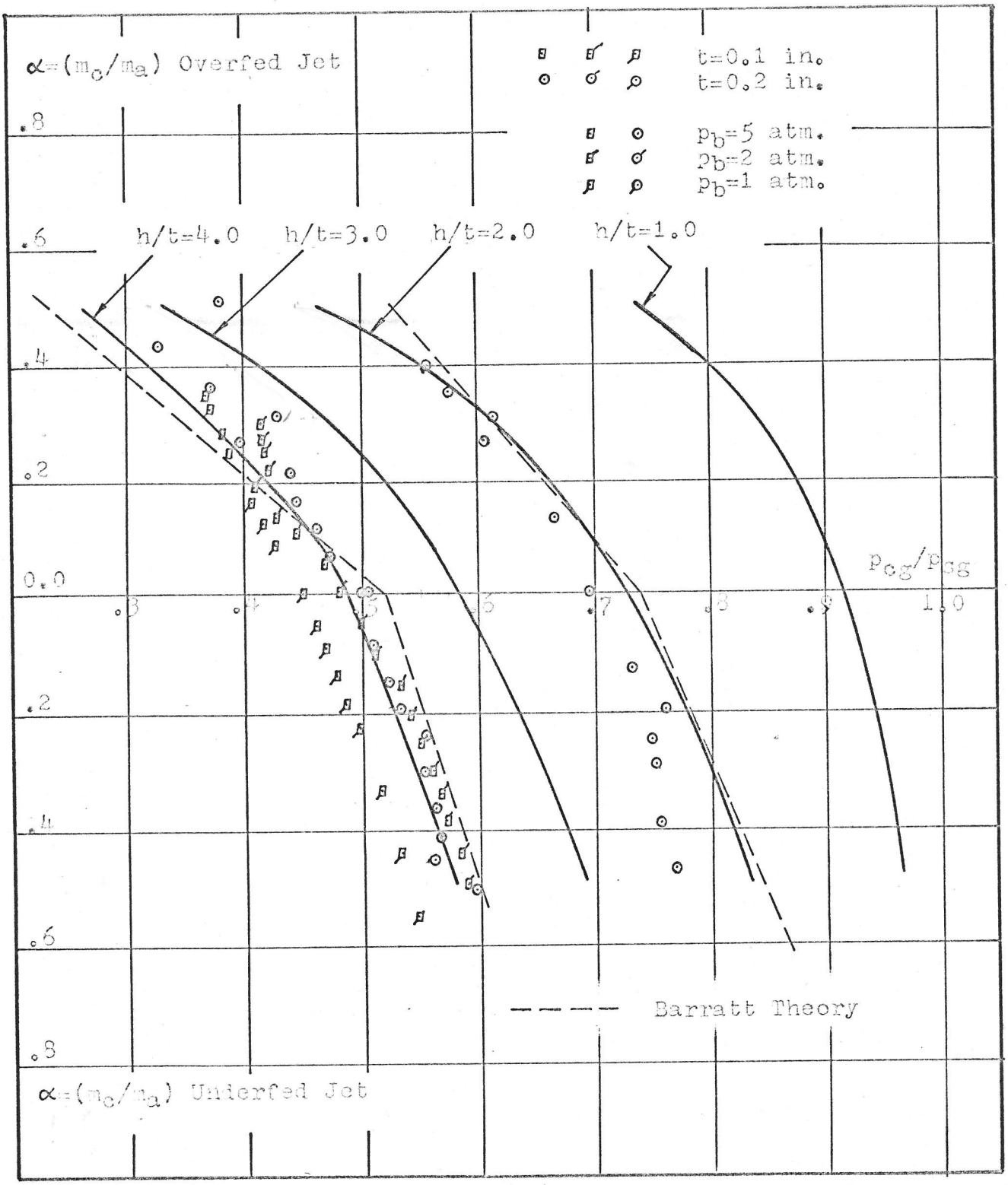

Fig. 34 Unbalanced Jet--Viscous Theory

$Re_j \approx 2 \times 10^4$

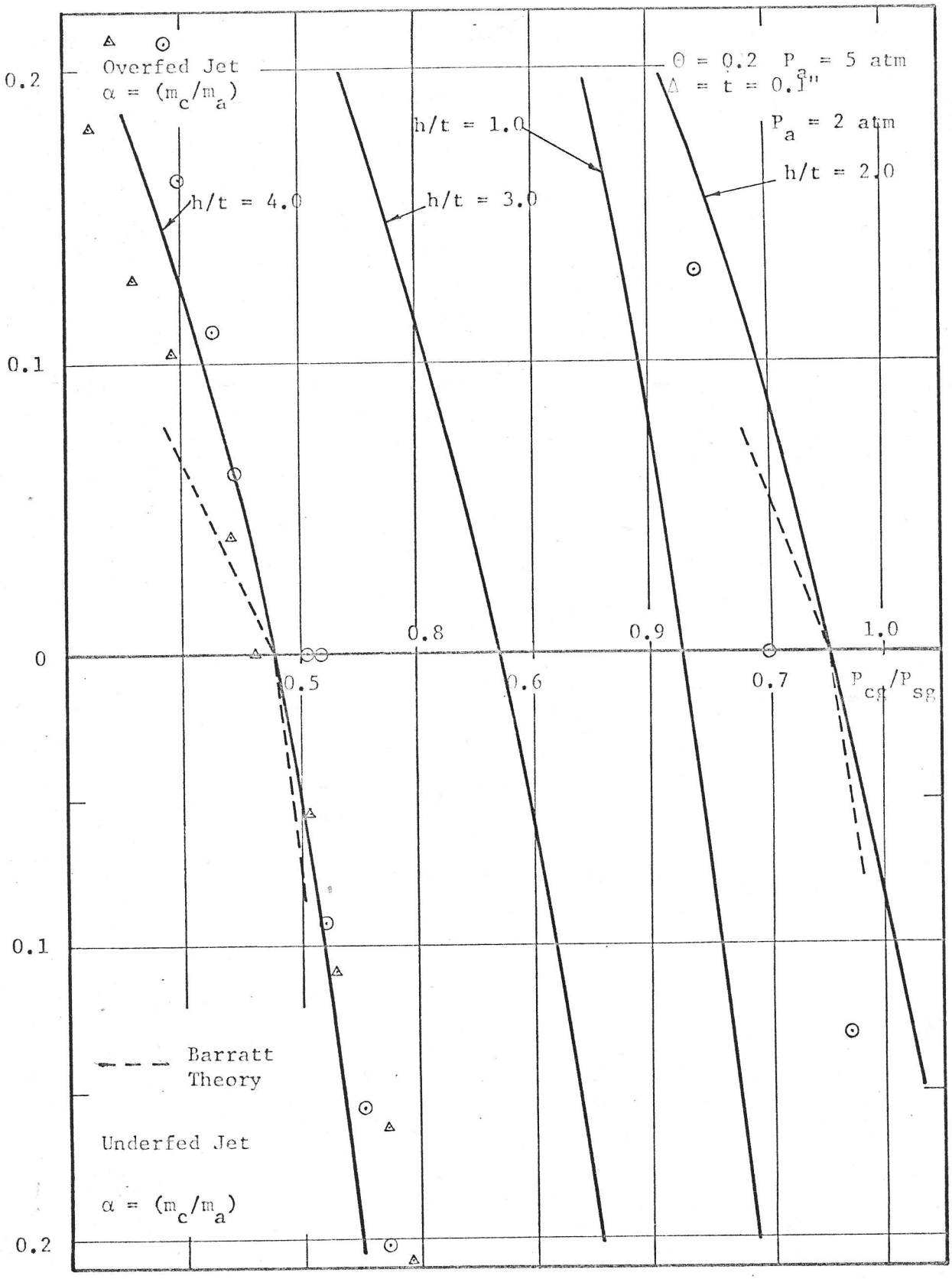

Fig. 35 Unbalanced Jet - Viscous Theory Re_j 2 x 10^4

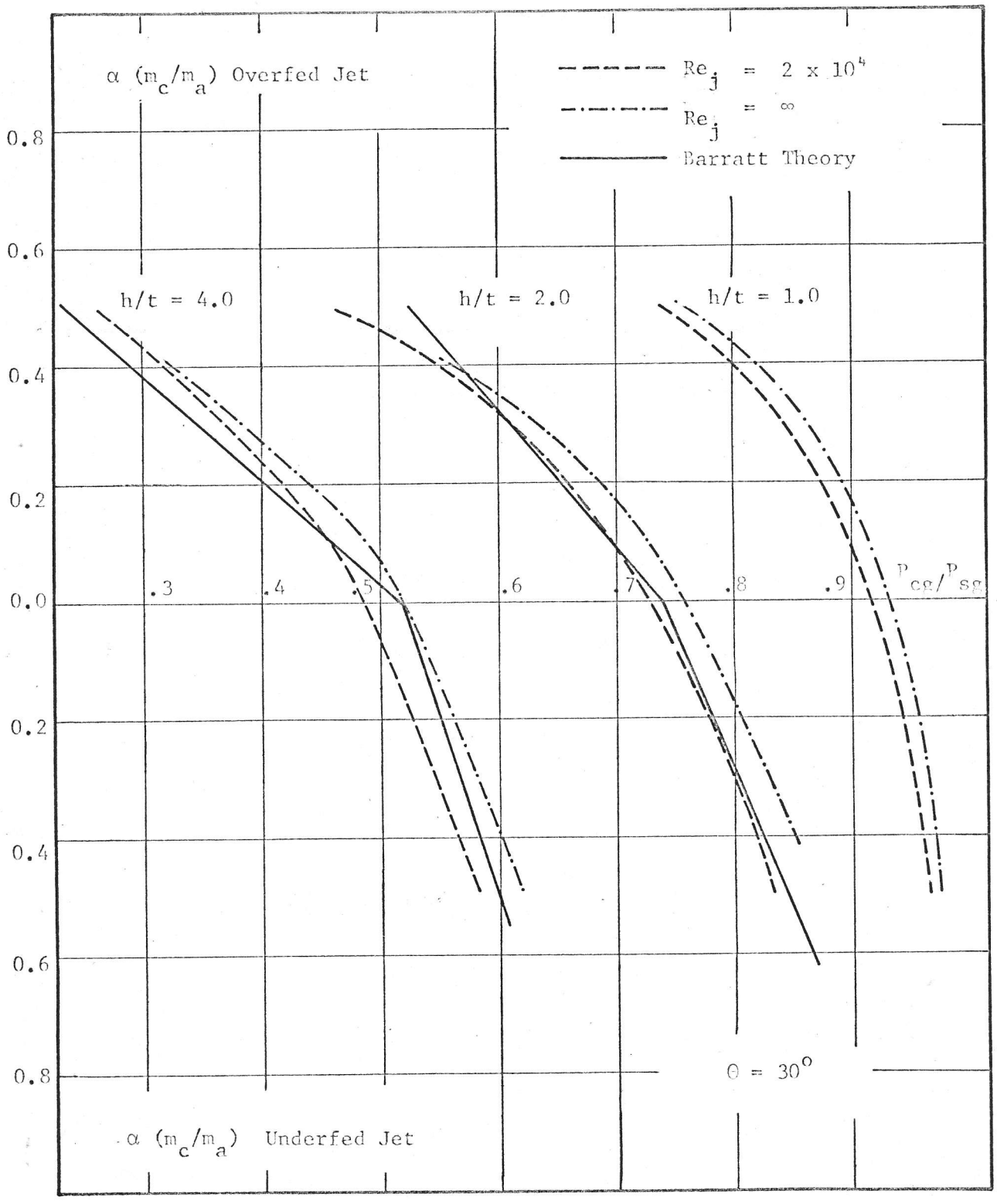

Fig. 36 Effect of Re_j on the Unbalanced Jet Viscous Theory Results

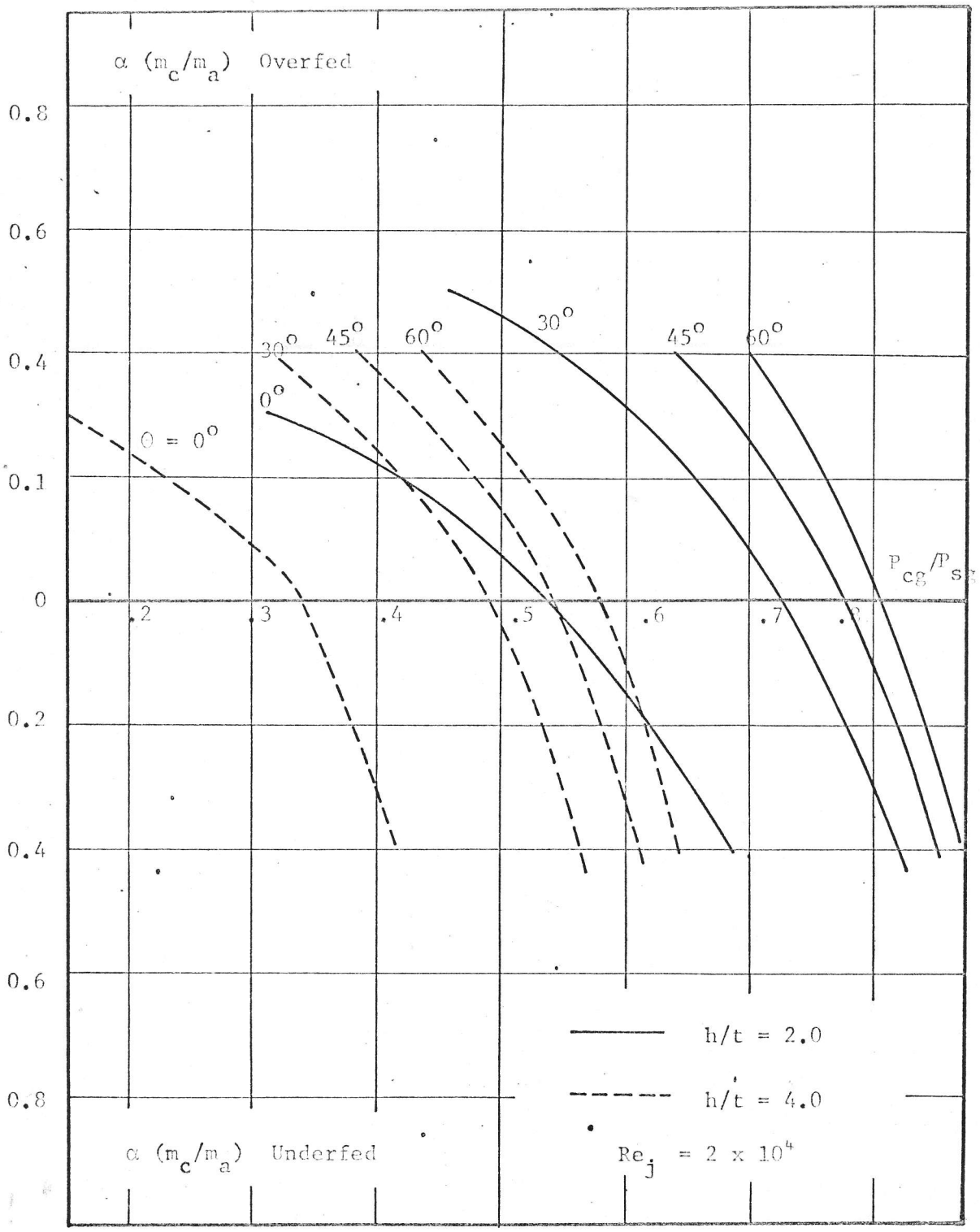

Fig.37 Effect of Nozzle Angle on the Unbalanced Jet Viscous Theory Results

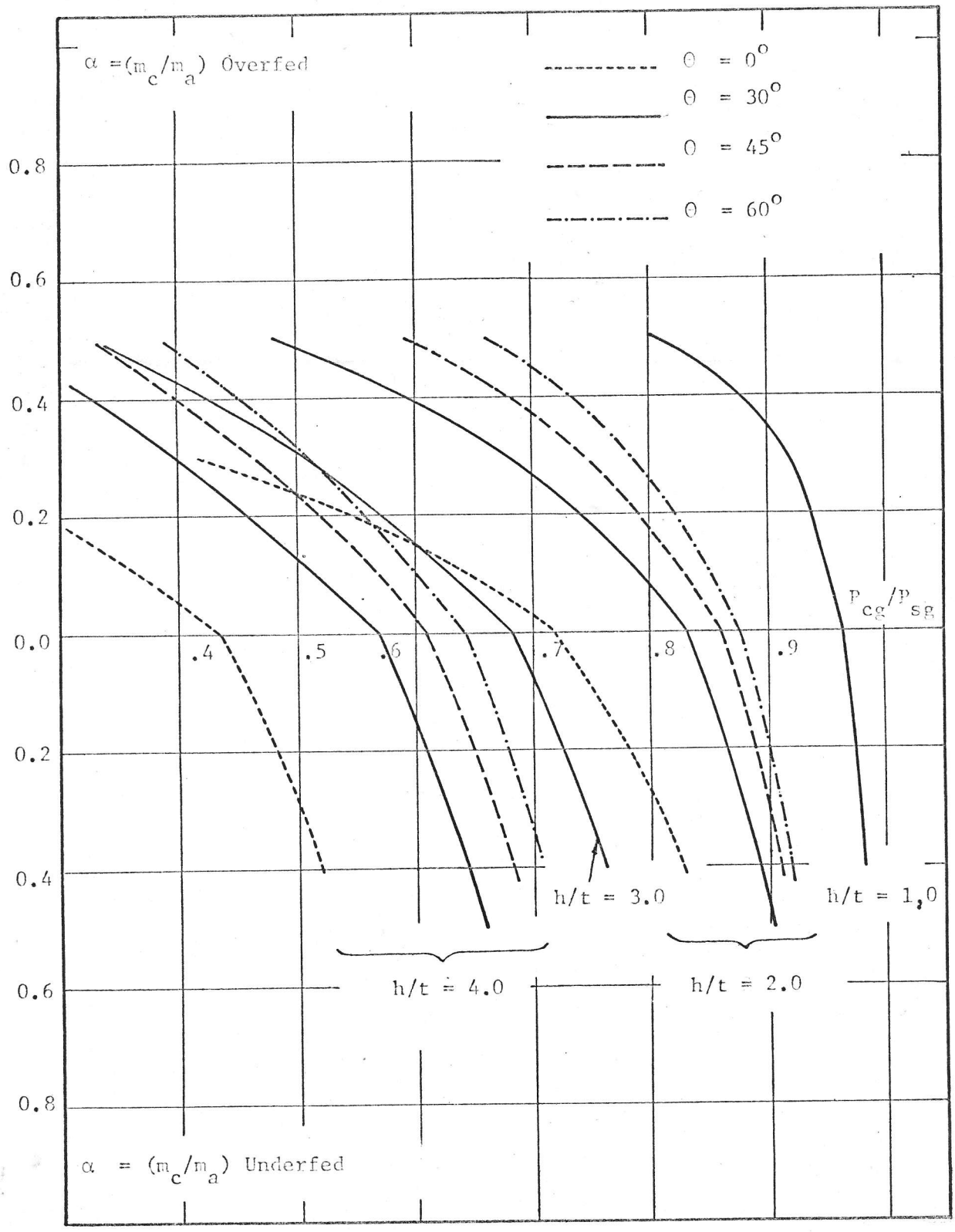

Fig. 38 Velocity Distribution Theory for Unbalanced Peripheral Jet

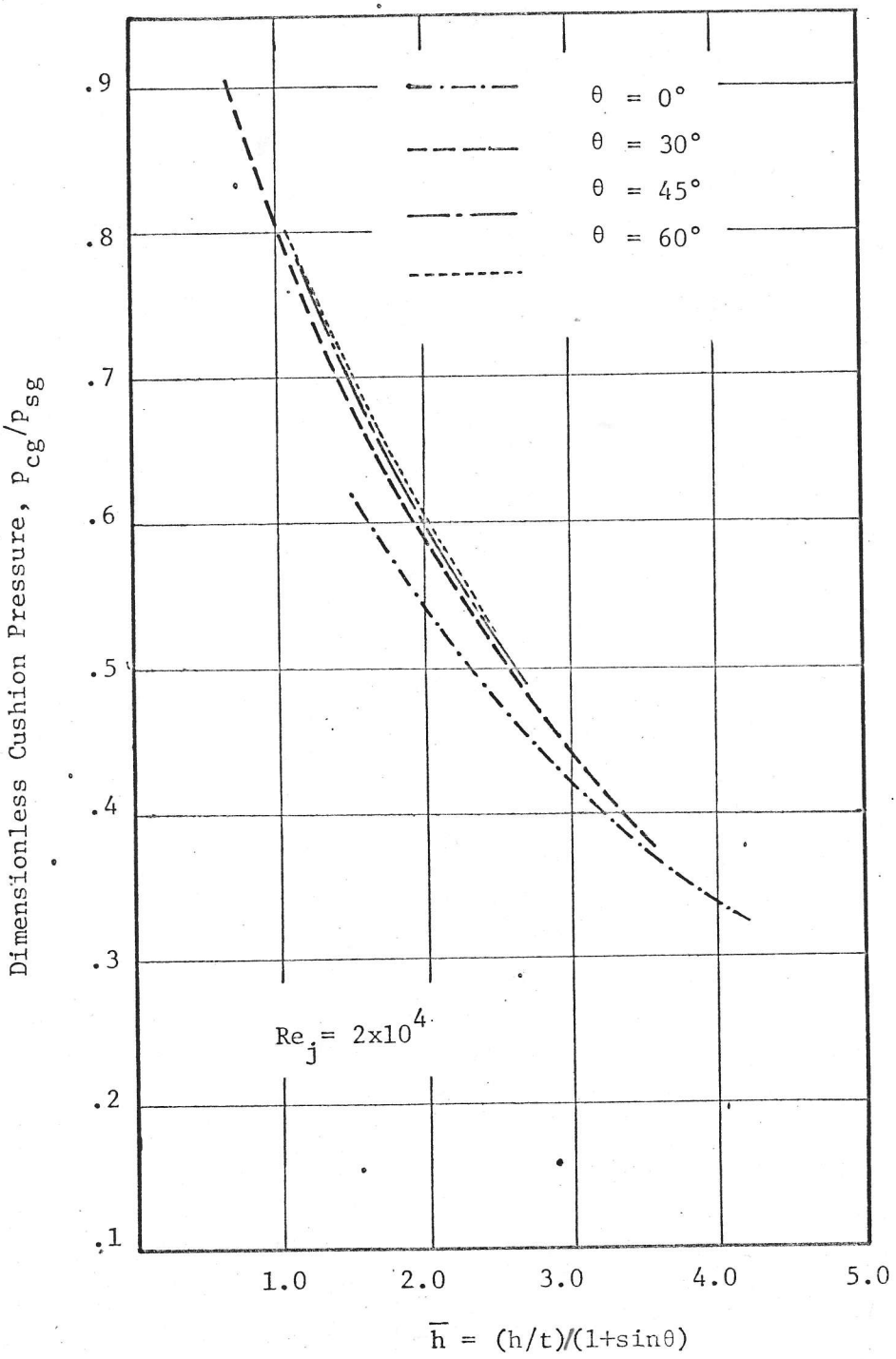

Fig. 39 Viscous Theory for Balanced Jet, p_{cg}/p_{sg} vs $\bar{h}$

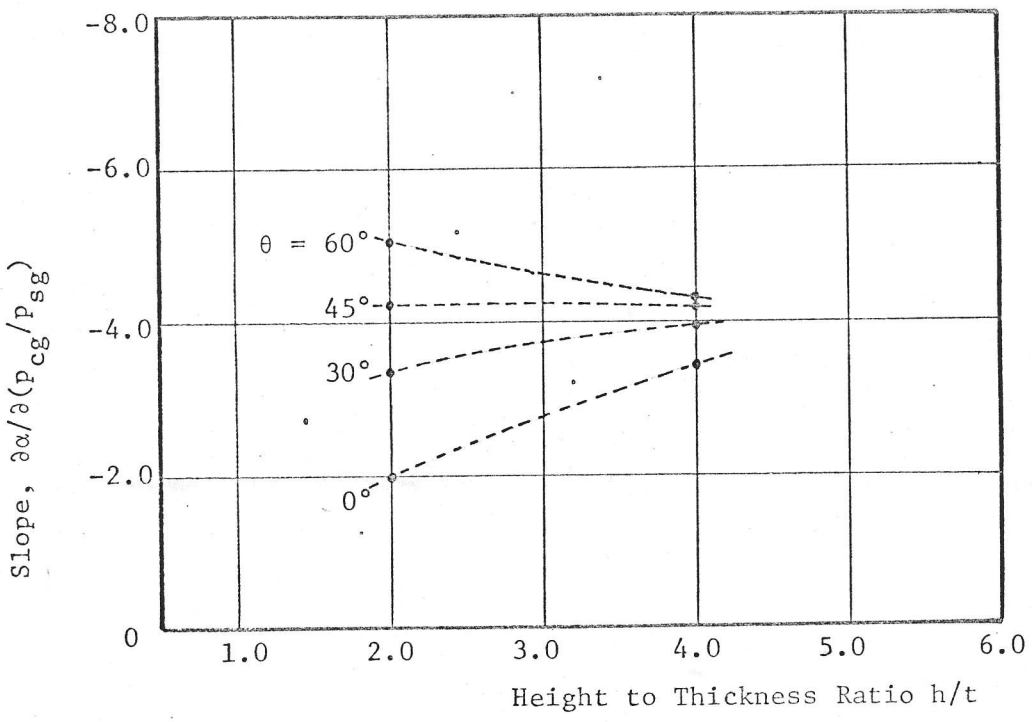

Fig. 40 The Slope $\partial\alpha/\partial\ (p_{cg}/p_{sg})$ from Viscous Theory $Re_j = 2x10^4$

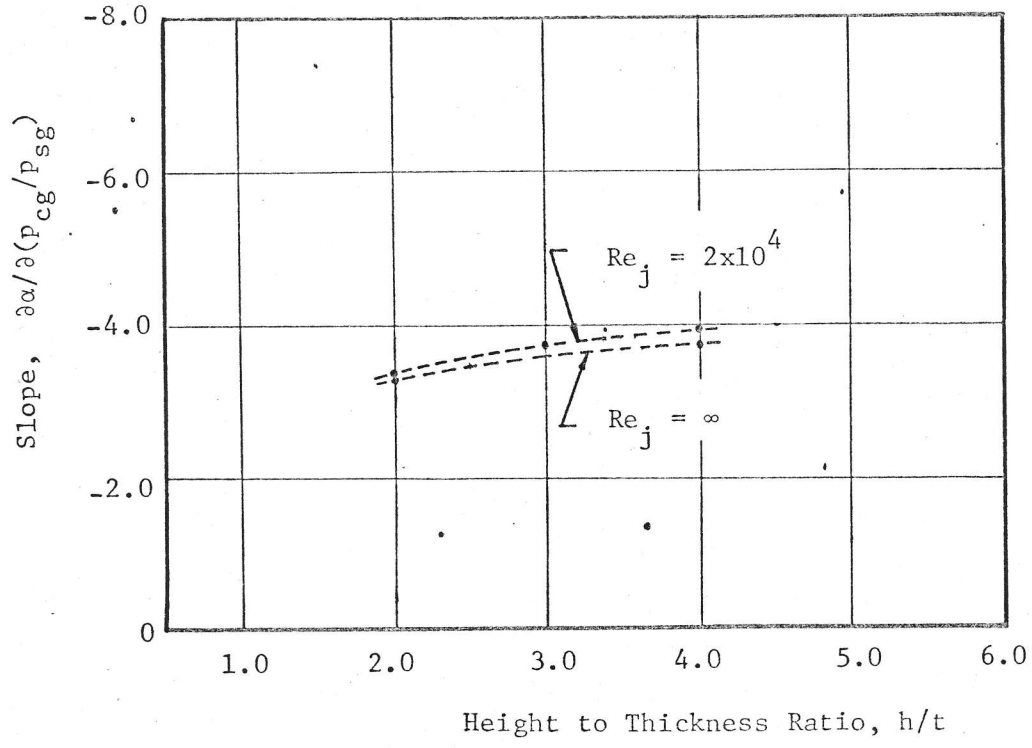

Fig. 41 The Slope $\partial\alpha/\partial\ (p_{cg}/p_{sg})$ from Viscous Theory

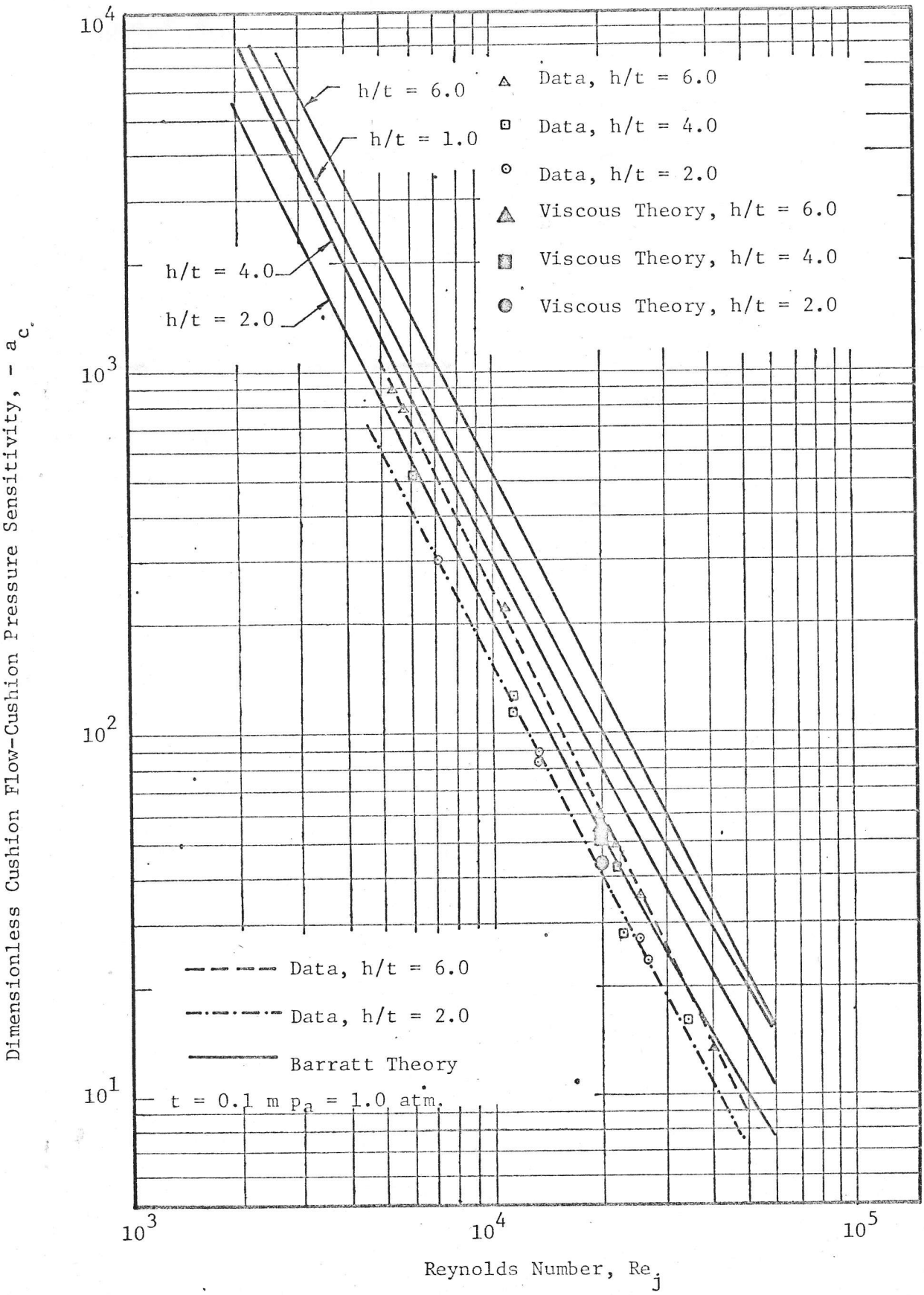

Fig. 42 Dimensionless Cushion Flow-Cushion Pressure Sensitivity a_c vs. Reynolds Number Re_j, $\theta = 30°$

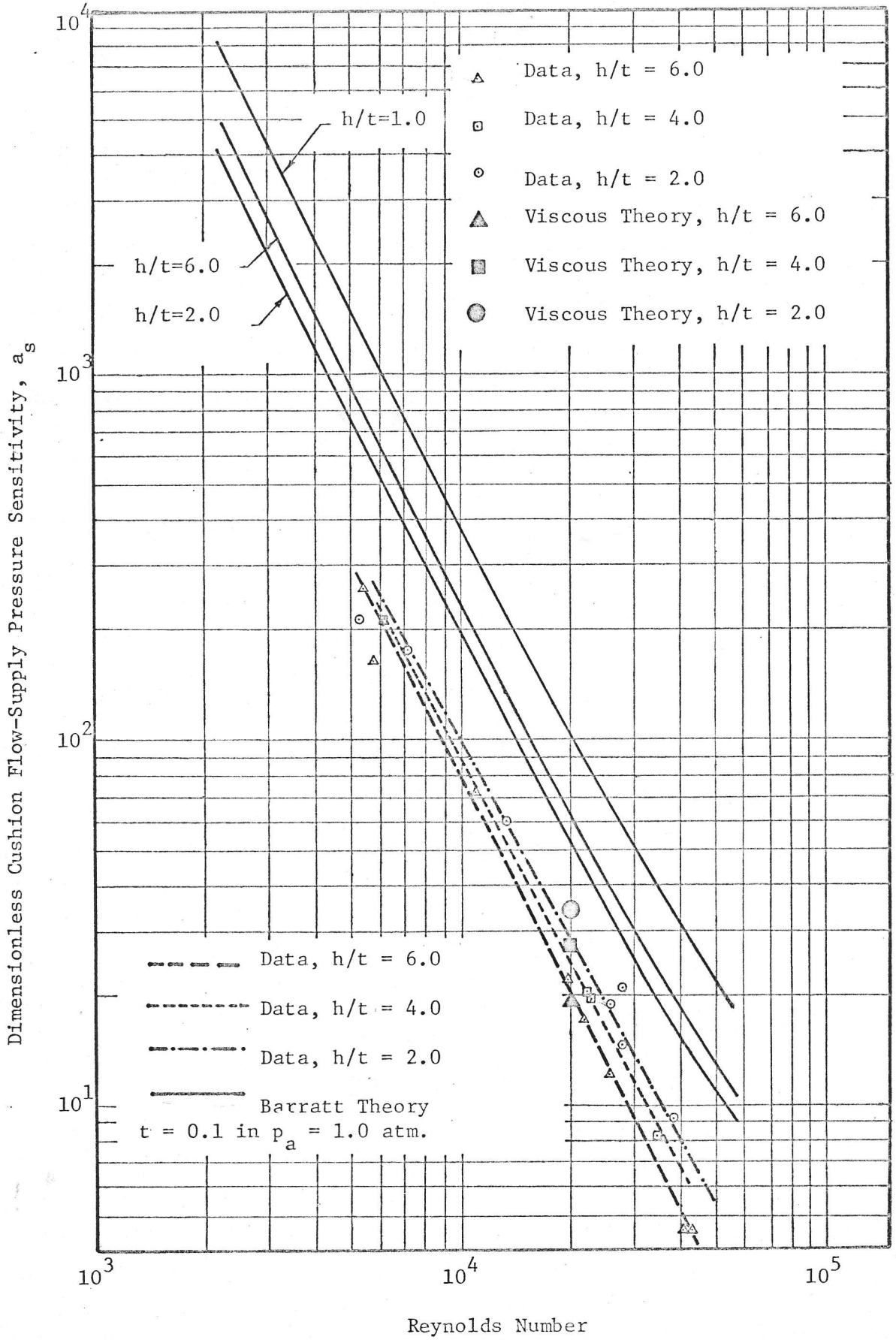

Fig. 43 Dimensionless Cushion Flow-Supply Pressure Sensivity a_s vs. Reynolds Number, $\theta = 30°$

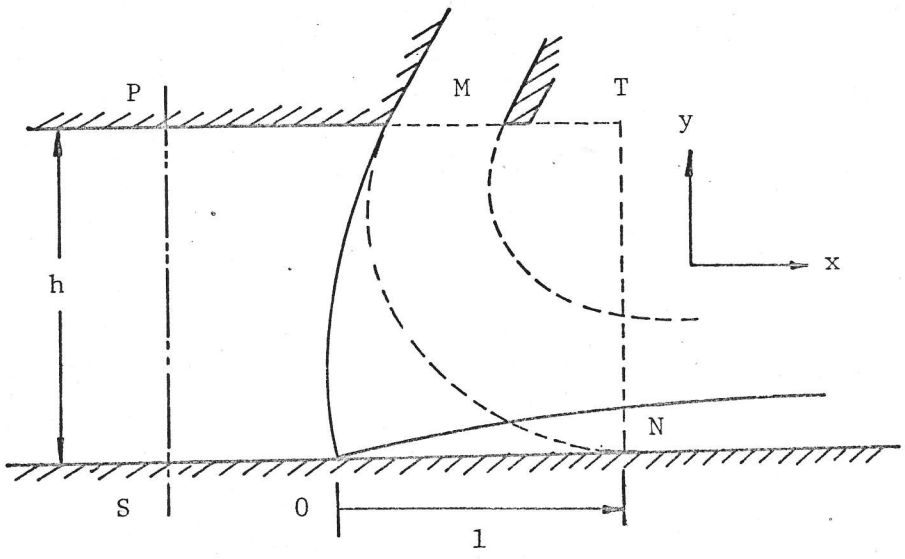

Fig. 44 Model for Calculating the Shear Force at the Walls

APPENDIX 1

THE EFFECT OF THE SHEAR FORCE AT THE WALLS

Assume that the boundary layer starts developing from point 0 where the stagnation streamline hits the ground plate as shown in Figure 44. Calling 1 the distance between point o and the point N where the jet becomes parallel to the ground, the average drag coefficient is given by*

$$C_D = .118 \left(\frac{\alpha}{Re_1}\right)^{1/5}$$

where

$$\alpha = \int_0^1 \left(1 - \frac{v}{V_o}\right) \frac{v}{V_o} \, d\left(\frac{y}{\delta}\right)$$

Assuming 1/7 profile within the boundary layer $\alpha = .0972$ and the total drag force becomes

$$D = \frac{C_o \, l\rho \, V_o^2}{2} = .118 \left(\frac{\alpha}{Re_1}\right)^{1/5} \frac{l\rho \, V_o^2}{2} \qquad (81)$$

Let us assume the following example:

$Re_t = 4x10^4$, T = 70° F, t=0.1 in and θ = 30°, then at 70° F , ν = .57 $ft^2/hr.$ and ρ = .075 lb m/ft^3.

---

*See reference (2).

$$V_o = \frac{4x10^4 \text{ x } .57 \text{ x } 12}{3600 \text{ x } .1} = 760 \text{ ft/sec} \qquad p_{sg} = \frac{\rho V_o^2}{2} = 675 \text{ lbf/ft}^2$$

Assume that 1 is half the length of the innermost streamline which is circular in shape and has point of tangencies at M and N. Then

$$x = \frac{4\pi h}{9} \qquad \text{or} \qquad 1 \simeq \frac{x}{2} = \frac{2\pi}{9} h$$

If the values are substituted into equation (81), the drag force on the control surface PSNT can be found. Table IV shows the result for this specific example.

TABLE IV

H/t	D, lbf	P lbf
1	$.38x10^{-1}$	5.15
2	$.65x10^{-1}$	8.6
3	$.90x10^{-1}$	10.6
4	$1.14x10^{-1}$	11.8
5	$1.37x10^{-1}$	12.3
6	$1.57x10^{-1}$	13.2

The value of the pressure term which enters the momentum equation applied to the control volume is given by

$$P = h\, p_{cg} = h \frac{p_{cg}}{p_{sg}}\, p_{sg}$$

For this specific example $p_{sg} = 675$ lbf/ft^2. Taking the values of p_{cg}/p_{sg} from the Barratt theory results P can be calculated. The values of P is given in Table IV.

It is apparent that P >> D; therefore, the shear force term in the momentum equation can be neglected when compared with the pressure term.

APPENDIX 2

SOLUTION FOR THE WALL JET

a) Computer Program for Large η's

Language: IBM 1130 Fortran IV

Procedure:

a) Specify the limits of the first DO statement. This sets the values of β = IQX/10.0

b) Specify the value of D. This determines the largest value of η

Outputs

D - Dimensionless distance from wall, η

SOLNO - Dimensionless mass flow, f

SOLN1 - Dimensionless velocity, f'

SOLN2 - Derivative of dimensionless velocity, f"

DMOM - Dimensionless memonetum, $\int_{\eta}^{\infty} f'^2 \, d\eta$

ERR1 - Maximum error in velocity

ERR2 - Maximum error in momentum

```
// JOB
// FOR
*IOCS (CARD,TYPEWRITER,KEYBOARD,1132 PRINTER)
C       YUCEL ERCAN 1967
C       WALL JET SOLUTION FOR THE OUTER LAYER
C       OF THE JET
        DO 110 IQX=10,20
        QX=IQX
        ALPHA=QX/10.0
        D=1.0
        A1=-1.0
        A2=(A1**2.0)*(1.0+ALPHA)/4.0
        A3=(A1**3.0)*(1.0+ALPHA)*(5.0+4.0*ALPHA)/72.0
        A4=(4.0*(A2**2.0)*(1.0+ALPHA)+A1*A3*(10.0+6.0*
       1ALPHA))/48.0
        A5=(A1*A4*(17.0+8.0*ALPHA)+A2*A3*(13.0+12.0*
       1ALPHA))/100.0
        A6=(A1*A5*(26.0+10.0*ALPHA)+A2*A4*(20.0+16.0*
       1ALPHA)+9.0*(A3**2.0)*(1.0+ALPHA))/180.0
        A7=(A1*A6*(37.0+12.0*ALPHA)+A2*A5*(29.0+20.0*
       1ALPHA)+A3*A4*(25.0+24.0*ALPHA))/294.0
        A8=(A1*A7*(50.0+14.0*ALPHA)+A2*A6*(40.0+24.0*
       1ALPHA)+A3*A5*(34.0+30.0*ALPHA)+16.0*(A4**2.0)*
       2(1.0+ALPHA))/448.0
        A9=(A1*A8*(65.0+16.0*ALPHA)+A2*A7*(53.0+28.0*
       1ALPHA)+A3*A6*(45.0+36.0*ALPHA)+A4*A5*(39.0+
       240.0*ALPHA))/648.0
        A10=(A1*A9*(82.0+18.0*ALPHA)+A2*A8*(68.0+32.0*
       1ALPHA)+A3*A7*(58.0+42.0*ALPHA)+A4*A6*(50.0+48.0
       2*ALPHA)+25.0*(A5**2.0)*(1.0+ALPHA))/900.0
        A11=(A1*A10*(101.0+20.0*ALPHA)+A2*A9*(85.0+36.0*
       1ALPHA)+A3*A8*(73.0+48.0*ALPHA)+A4*A7*(65.0+56.0*
       2ALPHA)+A5*A6*(61.0+60.0*ALPHA))/1210.0
        A12=(A1*A11*(122.0+22.0*ALPHA)+A2*A10*(104.0+40.0
       1*ALPHA)+A3*A9*(90.0+54.0*ALPHA)+A4*A8*(78.0+64.0*
       2ALPHA)+A5*A7*(74.0+70.0*ALPHA)+36.0*(A6**2.0)*
       3(1.0+ALPHA))/1584.0
        A13=(A1*A12*(145.0+24.0*ALPHA)+A2*A11*(125.0+44.0
       1*ALPHA)+A3*A10*(109.0+60.0*ALPHA)+A4*A9*(97.0+
       272.0*ALPHA)+A5*A8*(89.0+80.0*ALPHA)+A6*A7*(85.0
       3+84.0*ALPHA))/2028.0
        A14=(A1*A13*(170.0+26.0*ALPHA)+A2*A12*(148.0+48.0
       1*ALPHA)+A3*A11*(130.0+66.0*ALPHA)+A4*A10*(116.0
       2+80.0*ALPHA)+A5*A9*(106.0+90.0*ALPHA)+A6*A8*(100.0
       3+96.0*ALPHA)+49.0*(A7**2.0)*(1.0+ALPHA))/2548.0
        A15=(A1*A14*(197.0+28.0*ALPHA)+A2*A13*(173.0+52.0
       1*ALPHA)+A3*A12*(153.0+72.0*ALPHA)+A4*A11*(137.0
       2+88.0*ALPHA)+A5*A10*(125.0+100.0*ALPHA)+A6*A9*(117.0
       3+108.0*ALPHA)+A7*A8*(113.0+112.0*ALPHA))/3150.0
```

```
      A16=(A1*A15*(226.0+30.0*ALPHA)+A2*A14*(200.0+
     156.0*ALPHA)+A3*A13*(178.0+78.0*ALPHA)+A4*A12*
     2(160.0+96.0*ALPHA)+A5*A11*(146.0+110.0*ALPHA)+
     3A6*A10*(136.0+120.0*ALPHA)+A7*A9*(130.0+126.0*
     4ALPHA)+64.0*(A8**2.0)*(1.0+ALPHA))/3840.0
      A17=(A1*A16*(257.0+32.0*ALPHA)+A2*A15*(229.0+60.0
     1*ALPHA)+A3*A14*(205.0+84.0*ALPHA)+A4*A13*(185.0
     2+104.0*ALPHA)+A5*A12*(169.0+120.0*ALPHA)+A6*A11*(157.0
     3+132.0*ALPHA)+A7*A10*(149.0+140.0*ALPHA)+A8*A9*(145.0
     4+144.0*ALPHA))/4624.0
      A18=(A1*A17*(290.0+34.0*ALPHA)+A2*A16*(260.0+64.0*ALPHA
     1)+A3*A15*(234.0+90.0*ALPHA)+A4*A14*(212.0+112.0*ALPHA)
     2+A5*A13*(194.0+130.0*ALPHA)+A6*A12*(180.0+144.0*ALPHA)
     3+A7*A11*(170.0+154.0*ALPHA)+A8*A10*(164.0+160.0*ALPHA)
     4+81.0*(A9**2.0)*(1.0+ALPHA))/5508.0
      A19=(A1*A18*(325.0+36.0*ALPHA)+A2*A17*(293.0+68.0*ALPHA
     1)+A3*A16*(265.0+96.0*ALPHA)+A4*A15*(241.0+120.0*ALPHA)
     2+A5*A14*(221.0+140.0*ALPHA)+A6*A13*(205.0+156.0*ALPHA)
     3+A7*A12*(193.0+168.0*ALPHA)+A8*A11*(185.0+176.0*ALPHA)
     4+A9*A10*(181.0+180.0*ALPHA))/6498.0
C     A'S ARE THE COEFFICIENTS OF THE DIMENSIONLESS
C     MASS FLOW
      B2=A1**2.0
      B3=4.0*A1*A2
      B4=6.0*A1*A3+4.0*(A2**2.0)
      B5=8.0*A1*A4+12.0*A2*A3
      B6=10.0*A1*A5+16.0*A2*A4+9.0*(A3**2.0)
      B7=12.0*A1*A6+20.0*A2*A5+24.0*A4*A3
      B8=14.0*A1*A7+24.0*A2*A6+30.0*A3*A5+16.0*(A4**2.0)
      B9=16.0*A1*A8+28.0*A2*A7+36.0*A3*A6+40.0*A4*A5
      B10=18.0*A1*A9+32.0*A2*A8+42.0*A3*A7+48.0*A4*A6+
     125.0*(A5**2.0)
      B11=20.0*A1*A10+36.0*A2*A9+48.0*A3*A8+56.0*A4*A7
     1+60.0*A5*A6
      B12=22.0*A1*A11+40.0*A2*A10+54.0*A3*A9+64.0*A4*A8+
     170.0*A5*A7+36.0*(A6**2.0)
      B13=24.0*A1*A12+44.0*A2*A11+60.0*A3*A10+72.0*A4*A9
     1+80.0*A5*A8+84.0*A6*A7
      B14=26.0*A1*A13+48.0*A2*A12+66.0*A3*A11+80.0*A4*A10
     1+90.0*A5*A9+96.0*A6*A8+49.0*(A7**2.0)
      B15=28.0*A1*A14+52.0*A2*A13+72.0*A3*A12+88.0*A4*A11
     1+100.0*A5*A10+108.0*A6*A9+112.0*A7*A8
      B16=30.0*A1*A15+56.0*A2*A14+78.0*A3*A13+96.0*A4*A12
     1+110.0*A5*A11+120.0*A6*A10+126.0*A7*A9+64.0*(A8**2.0)
      B17=32.0*A1*A16+60.0*A2*A15+84.0*A3*A14+104.0*A4*A13
     1+120.0*A5*A12+132.0*A6*A11+140.0*A7*A10+144.0*A8*A9
      B18=34.0*A1*A17+64.0*A2*A16+90.0*A3*A15+112.0*A4*A14
     1+130.0*A5*A13+144.0*A6*A12+154.0*A7*A11+160.0*A8*A10
     2+162.0*(A9**2.0)
      B19=36.0*A1*A18+68.0*A2*A17+96.0*A3*A16+120.0*A4*A15
```

```
     1+140.0*A5*A14+156.0*A6*A13+168.0*A7*A12+176.0*A8*A11
     2+180.0*A9*A10
C      B'S ARE THE COEFFICIENTS OF THE "SQUARED VELOCITY"
C      SERIES
   12 C1=EXP(-1.0*D)
      C2=EXP(-2.0*D)
      C3=EXP(-3.0*D)
      C4=EXP(-4.0*D)
      C5=EXP(-5.0*D)
      C6=EXP(-6.0*D)
      C7=EXP(-7.0*D)
      C8=EXP(-8.0*D)
      C9=EXP(-9.0*D)
      C10=EXP(-10.0*D)
      C11=EXP(-11.0*D)
      C12=EXP(-12.0*D)
      C13=EXP(-13.0*D)
      C14=EXP(-14.0*D)
      C15=EXP(-15.0*D)
      C16=EXP(-16.0*D)
      C17=EXP(-17.0*D)
      C18=EXP(-18.0*D)
      C19=EXP(-19.0*D)
C      SOLNO IS THE DIMENSIONLESS MASS FLOW
      SOLNO=1.0+A1*C1+A2*C2+A3*C3+A4*C4+A5*C5+A6*C6+A7*C7+
     1A8*C8+A9*C9+A10*C10+A11*C11+A12*C12+A13*C13+A14*C14+
     2A15*C15+A16*C16+A17*C17+A18*C18+A19*C19
C      SOLN1 IS THE DIMENSIONLESS VELOCITY
      SOLN1=-A1*C1-2.0*A2*C2-3.0*A3*C3-4.0*A4*C4-5.0*A5*C5
     1-6.0*A6*C6-7.0*A7*C7-8.0*A8*C8-9.0*A9*C9-10.0*A10*C10
     2-11.0*A11*C11-12.0*A12*C12-13.0*A13*C13-14.0*A14*C14
     3-15.0*A15*C15-16.0*A16*C16-17.0*A17*C17-18.0*A18*C18
     4-19.0*A19*C19
C      SOLN2 IS THE DERIVATIVE OF THE DIMENSIONLESS VELOCITY
      SOLN2=A1*C1+4.0*A2*C2+9.0*A3*C3+16.0*A4*C4+25.0*A5*C5
     1+36.0*A6*C6+49.0*A7*C7+64.0*A8*C8+81.0*A9*C9+100.0*A10
     2*C10+121.0*A11*C11+144.0*A12*C12+169.0*A13*C13+196.0*
     3A14*C14+225.0*A15*C15+256.0*A16*C16+289.0*A17*C17
     4+324.0*A18*C18+361.0*A19*C19
      DMOM=B2*C2/2.0+B3*C3/3.0+B4*C4/4.0+B5*C5/5.0+B6*C6/6.0+
     1B7*C7/7.0+B8*C8/8.0+B9*C9/9.0+B10*C10/10.0+B11*C11/11.0
     2+B12*C12/12.0+B13*C13/13.0+B14*C14/14.0+B15*C15/15.0+
     3B16*C16/16.0+B17*C17/17.0+B18*C18/18.0+B19*C19/19.0
      ERR1=-19.0*A19*C19
      ERR2=B19*C19/19.0
      WRITE(3,16) D,SOLNO,SOLN1,SOLN2,DMOM,ERR1,ERR2
   16 FORMAT (7F10.6)
      D=D-0.01
      IF (D)110,11,11
   11 CONTINUE
      IF (SOLN2-1.0) 12,12,110
  110 CONTINUE
      CALL EXIT
      END
// XEQ
```

b) Computer Program for the Complete Wall Jet Solution

Language: IBM 1130 Fortran IV

Procedure:

a) Given a wall jet Reynolds number, find the corresponding β from Table I and enter ALPHA = β

b) Find the corresponding values of the initial values Y(1), Y(2), Y(3) and DMOMI from Table V.

c) Substitute the initial values into the program and run it through an 1130 IBM computer.

Outputs

The first set of results includes five quantities

DMASS(I) - Dimensionless mass flow between a point on the outer layer and the wall, f_o.

VEL(I) - Dimensionless velocity at a point on the outer layer, f'_o.

DMOM - Total dimensionless momentum flux due to the outer layer

D(I) - Dimensionless distance from the wall, η

DMMX - Dimensionless mass flux between the wall and the point of maximum velocity

VELMX - Maximum dimensionless velocity, f'_{om}.

The second set of results include five quantities

DMX - Dimensionless distance between the point of maximum velocity and the wall, η_m

E(I) - Dimensionless distance between the wall and and a point on the inner layer.

SOLO(I) - Dimensionless mass flow between the wall and the above mentioned point

SOLI(I) - Dimensionless velocity at the above mentioned point on the inner layer.

EMOM - Dimensionless momentum flux due to inner layer

TMOM - Total dimensionless momentum due to the entire wall jet

TMASS - Total dimensionless mass flux due to the entire wall jet.

TABLE I

β	Re_w	β	Re_w
1.0	∞	1.4	1200
1.1	1.4×10^6	1.6	380
1.2	4.1×10^4	1.8	150
1.3	5200	2.0	33

Values of β and Re_w Corresponding to each other

TABLE V

β	Y(1)	Y(2)	Y(3)	DMOMI	β	Y(1)	Y(2)	Y(3)	DMOMI
1.0	.534604	.357097	-.190903	.091495	1.6	.566155	.309202	-.129528	.076180
1.1	.540135	.348490	-.179365	.088680	1.7	.571054	.302034	-.121008	.073962
1.2	.545552	.340145	-.168381	.085976	1.8	.575857	.295080	-.112957	.071828
1.3	.550860	.332052	-.157926	.083380	1.9	.580568	.288334	-.105389	.069774
1.4	.556061	.324204	-.147977	.080885	2.0	.585188	.281794	-.098330	.067796
1.5	.561159	.311590	-.138516	.078486					

The Initial Values for the Computer Program for the Solution of the Wall Jet

```
// JOB T          ERCAN
// FOR
      FUNCTION F1 (X,Y1,Y2,Y3,Y4,Y5,Y6)
      F1=Y2
      RETURN
      END
// DUP
*STORE       WS  UA  F1
// FOR
      FUNCTION F2 (X,Y1,Y2,Y3,Y4,Y5,Y6)
      F2=Y3
      RETURN
      END
// DUP
*STORE       WS  UA  F2
// FOR
      FUNCTION F3 (X,Y1,Y2,Y3,Y4,Y5,Y6)
      ALPHA=1.4
      F3=-Y1*Y3-ALPHA*(Y2**2.0)
      RETURN
      END
// DUP
*STORE       WS  UA  F3
// FOR
      FUNCTION F4 (X,Y1,Y2,Y3,Y4,Y5,Y6)
      F4=0.0
      RETURN
      END
// DUP
*STORE       WS  UA  F4
// FOR
      FUNCTION F5 (X,Y1,Y2,Y3,Y4,Y5,Y6)
      F5=0.0
      RETURN
      END
// DUP
*STORE       WS  UA  F5
// FOR
      FUNCTION F6 (X,Y1,Y2,Y3,Y4,Y5,Y6)
      F6=0.0
      RETURN
      END
// DUP
*STORE       WS  UA  F6
// FOR
*LIST ALL
*IOCS(CARD,TYPEWRITER,KEYBOARD,1132 PRINTER)
```

```
C       YUCEL ERCAN AUGUST 1967
C       COMPLETE SOLUTION FOR THE WALL JET; Y'S ARE
C       THE INITIAL VALUES OBTAINED FROM THE SERIES
C       SOLUTION AT DIMENSIONLESS DISTANCE 0.5 FROM
C       THE WALL; DMOMI IS THE MOMENTUM FLUX AT THE SAME
C       POINT FROM THE SAME PROGRAM
        EXTERNAL F1,F2,F3,F4,F5,F6
        DIMENSION YI(6),VAL(6,100),PES(100),VEL(100),DMAS(100),
       1Z(100),SES(100),D(100),XSI(54),ETHA(54),SOLN0(54),
       2SOLN1(54),SOL1(54),SOL0(54),E(54)
        DMOMI=0.080885
        YI(1)=0.556061
        YI(2)=0.324204
        YI(3)=-0.147977
        YI(4)=0.0
        YI(5)=0.0
        YI(6)=0.0
        XI=0.5
        H=-0.01
        CALL RK3(F1,F2,F3,F4,F5,F6,H,XI,YI,1,100,VAL)
        DO 71 I=1,100
        QP=I
   71   D(I)=0.50+H*QP
        DO 31 I=1,100
   31   PES(I)=VAL(2,I)
        DO 21 I=1,100
   21   SES(I)=VAL(1,I)
        DO 4 J=2,100
        IF (PES(1)-PES(J)) 2,4,4
    2   TEMP=SES(1)
        PES(1)=PES(J)
        PES(J)=TEMP
        TEMP=SES(1)
        SES(1)=SES(J)
        SES(J)=TEMP
    4   CONTINUE
        VELMX=PES(1)
        DMMX=SES(1)
        DO 13 I=1,100
   13   VEL(I)=VAL(2,I)
        DO 15 I=1,100
   15   DMAS(I)=VAL(1,I)
        DO 33 I=1,100
   33   Z(I)=(VEL(I))**2.0
        CALL QUADR(Z,100,0.01,S,IER)
        DMOM=S+DMOMI
        DO 11 I=1,100
   11   WRITE (3,99) DMAS(I),VEL(I),DMOM,D(I),DMMX,VELMX
```

```
   99 FORMAT(6F10.6)
      H=0.005
C     INNER LAYER OF THE TURBULENT WALL JET
C     PARABOLIC RULE IS USED TO CALCULATE THE INTEGRAL
      I=2
    8 A=I
      G1=(A-1.0)/100.0
      G2=(A/100.0)-0.005
      G3=A/100.0
      F0FG1=1.0/((1.0-G1**(9.0/7.0))**(1.0/7.0))
      F0FG2=1.0/((1.0-G2**(9.0/7.0))**(1.0/7.0))
      F0FG3=1.0/((1.0-G3**(9.0/7.0))**(1.0/7.0))
      XSI(1)=(H/3.0)*(1.0+4.0*(1.0/((1.0-0.005**(9.0/7.0))
     1**(1.0/7.0)))+1.0/((1.0-0.01**(9.0/7.0))**(1.0/7.0)))
      XSI(I)=XSI(I-1)+(H/3.0)*(F0FG1+4.0*F0FG2+F0FG3)
      ETHA(I)=XSI(I)/((7.0/8.0)*((56.0/9.0)**(1.0/7.0)))
      SOLN0(I)=G3**(8.0/7.0)
      SOLN1(I)=((56.0/9.0)*((SOLN0(I))**(7.0/8.0)-(SOLN0(I))
     1**2.0))**(1.0/7.0)
      IF (I-2) 3,3,5
    3 I=I+1
      GO TO 8
    5 CONTINUE
      IF ((SOLN1(I-1))-(SOLN1(I))) 7,103,103
    7 I=I+1
      GO TO 8
  103 VMAX=SOLN1(I-1)
      EMX=ETHA(I-1)
      DMAMX=SOLN0(I-1)
      P=VELMX/VMAX
      DO 9 I=2,54
    9 SOL1(I)=P*SOLN1(I)
      Q=(VMAX*DMMX)/(DMAMX*VELMX)
      DMX=Q*EMX
      DO 29 I=2,54
   29 E(I)=Q*ETHA(I)
      DO 39 I=2,39
   39 SOL0(I)=(SOLN0(I))*Q*P
      DO 95 I=2,53
   95 Z(I)=(SOL1(I))**2.0
      Z(1)=0.0
      CALL QUADR(Z,53,H,S,IER)
      EMOM=S*Q
      TMOM=EMOM+DMOM
      TMASS=1.0
      DO 77 I=2,54
   77 WRITE (3,10) DMX,E(I),SOL0(I),SOL1(I),EMOM,TMOM,TMASS
   10 FORMAT (7F10.6)
      CALL EXIT
      END
// XEQ
```

c) Approximate Analytical Presentation of Results

Some of the results of the wall jet calculations which are used in the viscous analysis will be subjected to iteration. Therefore, here we give these in analytical form.

$$M_\beta = 0.333-0.183\ \ln\beta$$

$$\eta_t = 1.762 - 0.1325\ \ln\beta$$

Table I also can be represented in analytical form:

$$\beta = 1.71 - 0.0486\ \ln (Re_w) \qquad 5.2\times10^3 < Re_w < 4.1\times10^4$$

$$\beta = 1.892 - 0.0695\ \ln (Re_w) \qquad 1.2\times10^3 < Re_w < 5.2\times10^3$$

$$\beta = 1.981 - 0.082\ \ln (Re_w) \qquad 380 < Re_w < 1.2\times10^3$$

$$\beta = 2.106 - 0.102\ \ln (Re_w) \qquad 150 < Re_w < 380$$

$$\beta = 2.26 - 0.132\ \ln (Re_w) \qquad 33 < Re_w < 150$$

APPENDIX 3

COMPUTER PROGRAMS FOR VISCOUS THEORY

a) Inviscid Velocity Distribution Theory for Balanced and Unbalanced Peripheral Jet

Language: IBM 1130 Fortran IV

Procedure:

a) Specify U(h/t) and SIN(sinθ)

b) Specify the limits of the first DO statement. This sets the values of $\alpha = (J-1)/10.0$

c) Specify the limits of the second DO statement. These limits represent the limits of the range of dimensionless cushion pressure in which a solution is searched. $p_{cg}/p_{sg} = I/100.0$

Outputs

PR - Dimensionless cushion pressure p_{cg}/p_{sg}

A - Fractional cushion flow, α

OVR - Overfed jet parameter

UND - Underfed jet parameter

Solution - overfed and underfed cases take place when OVR and UND - ough zero respectively. The values of PR and A on the lin- -ich OVR and UND is zero give the solution.

```
// JOB T
// FOR
*IOCS (CARD,TYPEWRITER,KEYBOARD,1132 PRINTER)
C       INVISCID VELOCITY DISTRIBUTION THEORY FOR
C       BALANCED AND UNBALANCED JET
        DO 12 J=1,5,2
        AT=J-1
        U=4.0
        SIN=0.7071
        DO 10 I=61,71
        V=I
        PR=V/100.0
        P=SQRT(1.0-PR)
        R=1.0/P
        C=2.0*P/PR
        D=C*SIN
        E=(C*(ALOG(R)))/(1.0-P)
        F=(1.0-A)*E
        T1=D+F
        T2=E*P*A
        OVR=U-T1+T2
        VCVO=SQRT(PR+(((A*P*(ALOG(R)))/(U*(1.0-P)))**2.0))
        VCOVO=(A*P*(ALOG(R)))/(U*(1.0-P))
        UND=U-D-E*A*VCVO-E+VCOVO*A*E
        WRITE (3,8) PR,OVR,UND,A
     8  FORMAT (4F10.6)
    10  CONTINUE
    12  DUMMY=1.0
        CALL EXIT
        END
// XEQ
```

b) Viscous Theory for a Given Re_w

Language: IBM 1130 Fortran IV

Procedure:

a) Specify U(h/t), THETA (θ), SIN ($\sin\theta$), REW (Re_w), and S(λ). Figure 20 can be used to determine the values of λ.

b) Specify the limits of the DO statement. This determines the range of dimensionless pressure in which the solution is searched.

Outputs

PR - Dimensionless cushion pressure

SUN - A parameter

Solution occurs when SUN goes through zero. The value of PR on the line on which SUN goes through zero is the solution.

```
// JOB T
// FOR
*IOCS (CARD,TYPEWRITER,KEYBOARD,1132 PRINTER)
C       VISCOUS THEORY FOR BALANCED JET
C       GIVEN WALL JET REYNOLDS NUMBER
        REW=10000.0
        U=2.0
        S=0.412
        THETA=30.0
        SIN=0.5
        IF (41000.0-REW) 7,8,8
    8   DUMMY=1.0
        IF (5200.0-REW) 9,9,10
    9   AG=1.71-0.0486*(ALOG(REW))
        GO TO 20
   10   DUMMY=1.0
        IF (1200.0-REW) 11,11,12
   11   AG=1.892-0.0695*(ALOG(REW))
        GO TO 20
   12   DUMMY=1.0
        IF (380.0-REW) 13,13,14
   13   AG=1.981-0.082*(ALOG(REW))
        GO TO 20
   14   DUMMY=1.0
        IF (150.0-REW) 15,15,16
   15   AG=2.106-0.102*(ALOG(REW))
        GO TO 20
   16   DUMMY=1.0
        IF (33.0-REW) 17,17,7
   17   AG=2.26-0.132*(ALOG(REW))
   20   CONTINUE
        SM=0.3333-0.183*(ALOG(AG))
        SU=1.0/S
        T=(S/(1.0-S))*(ALOG(SU))
        X=(2.0*3.14159*(90.0+THETA))/(360.*(1.0+SIN))*(U-T)
        SOR=1.0/((SQRT(3.14159))*0.109)
        IF (X-5.2) 1,1,2
    1   V=1.0
        Q=1.0+0.04001234*X
        GO TO 5
    2   V=SQRT(SOR/X)
        Q=0.5+0.5*(SQRT((2.0/SOR)*X))
    5   DUMMY=1.0
        DO 7 I=1,99
        C=I
        PR=C/100.0
        P=SQRT(1.0-PR)
        R=1.0/P
```

```
      B=U*PR
      SUN=B-2.0*P*SIN-4.0*SM*V*Q*(P/(1.0-P))*(ALOG(R))
      WRITE (3,4) SUN,PR
    4 FORMAT (2F10.6)
    7 CONTINUE
      CALL EXIT
      END
// XEQ
```

c) Computer Program for the Viscous Balanced Jet Theory for a Given Re_j

Language: IBM 1130 Fortran IV

Procedure:

There are six statements which have to be specified. RG stands for Re_j; U stands for h/t. Enter the desired values of these terms into the program. S stands for λ. It can be found from the results of the inviscid velocity theory. The values of λ are given in Figure 20 as a function of h/t for various θ's. The limits of the first DO statement should also be entered into the program. These limits define the region of p_{cg}/p_{sg} in which a solution will be searched by the program. The limits of I = 1,99 will always give the solution. The other two terms are THETA the value of the nozzle angle in degrees and SIN, the sine of the nozzle angle.

Outputs

The program has three outputs:

SUN - A parameter

PR - Dimensionless cushion pressure, p_{cg}/p_{sg}

P - $\xi = \sqrt{1 - P_{cg}/p_{sg}}$

The solution occurs when SUN goes through zero and the corresponding PR on the same line of the computer printout gives the value of the dimensionless cushion pressure.

```
// JOB T
// FOR
*IOCS (CARD, TYPEWRITER, KEYBOARD, 1132 PRINTER, DISK)
C       VISCOUS THEORY FOR BALANCED PERIPHERAL JET
C       YUCEL ERCAN
        U=1.0
        S=0.223
        RG=1200.0
        THETA=30.0
        SIN=0.5
        DGL1=1.70
        DO 110 I=75,95
        V=I
        PR=V/100.0
        P=SQRT(1.0-PR)
        R=1.0/P
        SU=1.0/S
        B=U*PR
        Z1=(2.0*3.14159*(90.0+THETA))/(360.0*(1.0+SIN))
        PO=(S/(1.0-S))*(ALOG(SU))
        X1T1=Z1*(U-PO)
        SOR=1.0/((SQRT(3.14159))*0.109)
        IF (X1T1-5.2) 2,2,300
    2   V1=1.0
        Q2=1.0+0.0400123*X1T1
        GO TO 4
  300   V1=SQRT(SOR/X1T1)
        Q2=0.5+0.5*(SQRT((2.0/SOR)*X1T1))
    4   DUMMY=1.0
        K=1
    7   CONTINUE
        RT1=0.5*Q2*DGL1*P*((ALOG(R))/(1.0-P))*RG
        IF (41000.0-RT1) 38,8,8
    8   DUMMY=1.0
        IF (5200.0-RT1) 9,9,10
    9   AG1=1.71-0.0486*(ALOG(RT1))
        GO TO 20
   10   DUMMY=1.0
        IF (1200.0-RT1) 11,11,12
   11   AG1=1.892-0.0695*(ALOG(RT1))
        GO TO 20
   12   DUMMY=1.0
        IF (380.0-RT1) 13,13,14
   13   AG1=1.981-0.082*(ALOG(RT1))
        GO TO 20
   14   DUMMY=1.0
        IF (150.0-RT1) 15,15,16
   15   AG1=2.106-0.102*(ALOG(RT1))
        GO TO 20
```

```
   16 DUMMY=1.0
      IF (33.0-RT1) 17,17,38
   17 AG1=2.26-0.132*(ALOG(RT1))
   20 CONTINUE
      DGL1=1.762-0.1325*(ALOG(AG1))
      K=K+1
      IF (K-1) 7,7,21
   21 DUMMY=1.0
      SM1=0.3333-0.183*(ALOG(AG1))
      SUN=B-2.0*P*SIN-4.0*SM1*V1*Q2*(P/(1.0-P))*(ALOG(R))
      WRITE (3,99) SUN,PR,P
   99 FORMAT (3F10.6)
  110 CONTINUE
   38 DUMMY=1.0
      CALL EXIT
      END
// XEQ
```

APPENDIX 4

Computer Programs for the Viscous Analysis of Overfed and Underfed Jets

Language: IBM 1130 Fortran IV

Procedure: The terms U,S,R,G, THETA and SIN should be specified in a way similar for the program of Appendix II. The region in which the solution is being searched for can be set by setting the limits of the second DO statement (DO 110 I = -,-). The limits of the first DO statement (DO 120 J = -,-,-) set the range of α's. Here $\alpha = (J-1)/10$.

Outputs: In both programs solution occurs when SUN goes through zero. SUN is the value of equation 67 for the overfed jet program and the value of equation 79 for the underfed jet program. PR stands for P_{cg}/p_{sg} and p for ξ. The value of PR when SUN goes through zero is the solution p_{cg}/p_{sg}. The last column of the overfed jet program gives the value of $5.0/k_3 t$. If this is greater than h/t, i.e. U, then the assumptions concerning the overfed jet theory may not be valid.

```
// JOB T
// FOR
*IOCS (CARD,TYPEWRITER,KEYBOARD,1132 PRINTER)
C       VISCOUS THEORY FOR OVERFED JET
C       YUCEL ERCAN  NOVEMBER 1967 M.I.T.
        U=2.0
        S=0.412
        RG=20000.0
        DGL1=1.70
        DGL2=1.70
        THETA=30.0
        SIN=0.5
        DO 120 J=1,6
        AT=J-1
        A=AT/10.0
        DO 110 I=45,80
        V=I
        PR=V/100.0
        P=SQRT(1.0-PR)
        R=1.0/P
        SU=1.0/S
        B=U*PR
        C=(P/(1.0-P))*(ALOG(R))
        PO=(S/(1.0-S))*(ALOG(SU))
        SOR=1.0/((SQRT(3.14159))*0.109)
        Q1=1.0
        Z1=(2.0*3.14159*(90.0+THETA))/(360.0*(1.0+SIN))
        XT2=Z1*(U-(1.0-A)*PO)
        IF (XT2-5.2) 50,50,51
   50   Q2=1.0+0.0400123*XT2
        GO TO 55
   51   Q2=0.5+0.5*(SQRT((2.0/SOR)*XT2))
   55   DUMMY=1.0
        Z2=(2.0*3.14159*(90.0-THETA))/(360.0*(1.0-SIN))
        X1T1A=Z2*(U*(1.0-S)-A*(ALOG(SU)))
        X1T1B=1.0-S-S*((SU**(1.0-A))-1.0)
        X1T1=X1T1A/X1T1B
        IF (X1T1-5.2) 2,2,300
    2   V1=1.0
        GO TO 4
  300   V1=SQRT(SOR/X1T1)
    4   DUMMY=1.0
        X2T2A=Z1*(U*(1.0-S)-(1.0-A)*S*(ALOG(SU)))
        X2T2B=S*((SU**(1.0-A))-1.0)
        X2T2=X2T2A/X2T2B
        IF (X2T2-5.2) 5,5,6
    5   V2=1.0
        GO TO 75
    6   V2=SQRT(SOR/X2T2)
   75   DUMMY=1.0
        K=1
```

```
  7 CONTINUE
    RT1=(A*S*DGL1*(ALOG(SU))*RG)/(2.0*(1.0-S))
    IF (41000.0-RT1) 38,8,8
  8 DUMMY=1.0
    IF (5200.0-RT1) 9,9,10
  9 AG1=1.71-0.0486*(ALOG(RT1))
    GO TO 20
 10 DUMMY=1.0
    IF (1200.0-RT1) 11,11,12
 11 AG1=1.892-0.0695*(ALOG(RT1))
    GO TO 20
 12 DUMMY=1.0
    IF (380.0-RT1) 13,13,14
 13 AG1=1.981-0.082*(ALOG(RT1))
    GO TO 20
 14 DUMMY=1.0
    IF (150.0-RT1) 15,15,16
 15 AG1=2.106-0.102*(ALOG(RT1))
    GO TO 20
 16 DUMMY=1.0
    IF (33.0-RT1) 17,17,101
 17 AG1=2.26-0.132*(ALOG(RT1))
 20 CONTINUE
    DGL1=1.762-0.1325*(ALOG(AG1))
    K=K+1
    IF (K-1) 7,7,21
 21 DUMMY=1.0
    SM1=0.3333-0.183*(ALOG(AG1))
    GO TO 104
101 SM1=0.0
104 DUMMY=1.0
    N=1
 41 DUMMY=1.0
    RT2=((1.0-A)*DGL2*S*(ALOG(SU))*Q2*RG)/(2.0*(1.0-S))
    IF (41000.0-RT2) 38,22,22
 22 DUMMY=1.0
    IF (5200.0-RT2) 23,23,24
 23 AG2=1.71-0.0486*(ALOG(RT2))
    GO TO 40
 24 DUMMY=1.0
    IF (1200.0-RT2) 25,25,26
 25 AG2=1.892-0.0695*(ALOG(RT2))
    GO TO 40
 26 DUMMY=1.0
    IF (380.0-RT2) 27,27,28
 27 AG2=1.981-0.082*(ALOG(RT2))
    GO TO 40
 28 DUMMY=1.0
    IF (150.0-RT2) 29,29,31
 29 AG2=2.106-0.102*(ALOG(RT2))
    GO TO 40
 31 DUMMY=1.0
```

```
      IF (33.0-RT2) 32,32,38
   32 AG2=2.26-0.132*(ALOG(RT2))
   40 CONTINUE
      DGL2=1.762-0.1325*(ALOG(AG2))
      N=N+1
      IF (N-5) 41,41,42
   42 DUMMY=1.0
      SM2=0.3333-0.183*(ALOG(AG2))
      TK=(2.0*V1)/((A*(ALOG(R)))/(1.0-P))
      TUR=5.0/TK
      SUN=B-2.0*P*SIN-4.0*C*(SM2*V2*Q2*(1.0-A)-SM1*V1*Q1
     1*A*P)
      WRITE (3,99) SUN,PR,A,TUR
   99 FORMAT (4F10.6)
      DUMMY=1.0
  110 CONTINUE
      DUMMY=1.0
  120 CONTINUE
   38 DUMMY=1.0
      CALL EXIT
      END
```

```
// JOB T
// FOR
*IOCS (CARD, TYPEWRITER, KEYBOARD, 1132 PRINTER, DISK)
C       YUCEL ERCAN 1967
C       UNDERFED PERIPHERAL JET VISCOUS THEORY
        U=2.0
        S=0.412
        RG=20000.0
        DGL=1.70
        THETA=30.0
        SIN=0.5
        DO 120 J=1,5,2
        AT=J-1
        A=AT/10.0
        DO 110 I=1,99
        V=I
        PR=V/100.0
        P=SQRT(1.0-PR)
        R=1.0/P
        SU=1.0/S
        PS=1.0-S**2.0
        B=U*PR
        C=(P/(1.0-P))*(ALOG(R))
        Z=(2.0*3.14159*(90.0+THETA))/(360.0*(1.0+SIN))
        D=SQRT(PS+((A*S*(ALOG(SU)))/(U*(1.0-S)))**2.0)
        PO=(S/(1.0-S))*(ALOG(SU))
        X=Z*(U-PO*(1.0+(A/D)))
        SOR=1.0/((SQRT(3.14159))*0.109)
        IF (X-5.2) 88,88,89
   88   Q=1.0+0.0400123*X
        VIX=1.0
        GO TO 37
   89   Q=0.5+0.5*(SQRT((2.0/SOR)*X)
        VIX=SQRT(SOR/X)
   37   DUMMY=1.0
        K=1
    7   CONTINUE
        RT=(P*DGL*(ALOG(R))*Q*RG)/(2.0*(1.0-P))
        IF (41000.0-RT) 38,8,8
    8   DUMMY=1.0
        IF (5200.0-RT) 9,9,10
    9   AG=1.71-0.0486*(ALOG(RT))
        GO TO 20
   10   DUMMY=1.0
        IF (1200.0-RT) 11,11,12
   11   AG=1.892-0.0695*(ALOG(RT))
        GO TO 20
   12   DUMMY=1.0
        IF (380.0-RT) 13,13,14
```

```
 13 AG=1.981-0.082*(ALOG(RT))
    GO TO 20
 14 DUMMY=1.0
    IF (150.0-RT) 15,15,16
 15 AG=2.106-0.102*(ALOG(RT))
    GO TO 20
 16 DUMMY=1.0
    IF (33.0-RT) 17,17,101
 17 AG=2.26-0.132*(ALOG(RT))
 20 CONTINUE
    DGL=1.762-0.1325*(ALOG(AG))
    K=K+1
    IF (K-1) 7,7,21
 21 DUMMY=1.0
    SM=0.3333-0.183*(ALOG(AG))
    GO TO 3
101 SM=0.0
  3 RUN=((A**2.0)*P*S*(ALOG(R))*(ALOG(SU)))
   1/((1.0-P)*(1.0-S))
    SUN=B-2.0*P*SIN-4.0*SM*VIX*Q*C-2.0*A*C*D+(2.0*RUN)/U
    WRITE (3,99) SUN,PR,A
 99 FORMAT (3F10.6)
110 CONTINUE
    DUMMY=1.0
120 CONTINUE
 38 DUMMY=1.0
    CALL EXIT
    END
// XEQ
```